National Institute of Electricity and Electronics
INELEC BOUMERDES
Department of Resarch

THESIS

Presented in partial fulfilment of the requirements of the

DEGREE OF MAGISTER

in Electronic Systems Engineering

by

Mohamed KESRAOUI

Stability *Analysis of the Static Kramer Drive*

Defended on September 15, 1996 before the Jury :

President :	Dr. **N. LOUAM**	(Maitre de Conference -ENP)
Supervisor :	Dr. **L. REFOUFI**	(Maitre de Conference-INELEC)
Members :	Dr. **H. ZEROUG**	(Chargé de Cours-USTHB)
	Dr. **K. HARRICHE**	(Chargé de Cours-INELEC)

Registration number : 01/96.

DEDICATION

To my grand mother who was praying for me and who wished to attend the presentation of my work.

To my mother who has always been present when I need her.

To my father for help and supports .

To my sister & friend NORA for her aid and encouragement.

I can not forget my sister RADIA to whom I wish success.

To my sister NACERA , her Husband KHIREDDINE and her daughter ASMA.

To my brothers SAMIR and HAKIM.

To my uncle ABDELLAH, my taunt FATMA and all their family.

Without forgetting my cousin DJAMILA ROUAZ , her husband MAHIEDDINE and their family.

To my best friend DJAMEL BOURIB.

And to all my friends.

I dedicate this work.....

On sunday July 28 th , 1996
MOHAMED KESRAOUI

ACKNOWLEDGEMENT

I must express the gratitude I feel toward my supervisor Dr L. REFOUFI (M. C - INELEC) who laboured many hours correcting errors, strengthening weaknesses and discovering incongruities.

My sincere appreciation is due to the president of the Jury Dr N. LOUAM (M. C - Ecole Nationale Polytechnique, Alger) and the members of the Jury Dr H. ZEROUG (C. C - University des Sciences et de la Technologie de Houari Boumedien) and Dr K. HARICHE (C. C - Head of research department, INELEC) for their acceptance.

I am indebted to many people for suggestions, supports and aids, including all INELEC post-graduate department staff, particularly Dr H. BOURDOUCEN (M. C - INELEC) and Miss F. BOUZIDI (Department Secretary).

Special thanks are to : H. ZABOT, A. OUADI, S. DAHMANI, M. DEHMAS, A. ZITOUNI, M. CHAFAI, B. ESSERHAN, F. RAHMOUN, H. BENTARZI and T. ALMANSBA for their help and encouragement to the realisation of this project.

I would also like to thank the library staff, especially Mrs ZERARI and Miss S. LALAMI for providing the necessary documentation and help in the bibliographical research, without forgetting the reprography room for the material supports.

I am also grateful to Mr L. MERROUCHE, Mr A. BAFOU, all students I taught and the staff of INSFP MOHAMMADIA Alger , for their encouragement and moral help.

To those people I give credits for all the good parts of this thesis. The rest is reserved to myself.

ABSTRACT

The steady state analysis of the conventional static Kramer drive using three different types of models, namely the DC, AC and DQ models is developed in the first part of the thesis. The aim is to arrive at a correct prediction of the basic steady state characteristics of the drive through correlation of results of the different models used. This is motivated by the fact that most of the published work done on stability analysis of this drive relied on a wrong DQ steady state model. A correct DQ steady state model is established.

The stability analysis of the static Kramer drive is presented in the second part of the thesis. A set of nonlinear differential equations describing the dynamic and steady state behaviour of the system are developed and linearized about an operating point using small signal perturbation technique. The eigenvalues loci of the system are plotted for different operating points with the effects of system parameter changes on the drive stability investigated for three such drives of different power levels.

In support of analytical predictions, transient responses to a load torque step change have been obtained by solving the set of non linear equations representing the actual system.

Conclusions reached in this present investigation study show important differences with previous research work. It has been found that both the operating point and the power level of the drive are important factors influencing the drive stability.

TABLE OF CONTENTS

LIST OF SYMBOLS

H	: inertia constant.
$I_{d'}$	: rectifier output current,referred to stator.
I_{ds} , I_{qs}	: stator currents in the *d* and *q* circuits respectively
$I_{dr'}$,$I_{qr'}$	: rotor currents in the d and q circuits respectively (Referred to stator).
R_S	: per phase stator resistance .
$R_{r'}$	: per phase rotor resistance referred to stator .
T_e	: electromagnetic torque developed.
T_l	: load torque.
V_d	: rectifier output voltage.
V_i	: counter EMF of the inverter .
V_{ms}	: peak value of stator phase voltage .
$V_{mr'}$	: peak value of rotor phase voltage referred to stator.
$X_{d'}$,$R_{d'}$	: filter reactance at base frequency and resistance referred to stator respectively.
X_{ss} , $X_{rr'}$	: stator reactance and rotor reactance referred to stator at base frequency .(per phase).
X_m	: mutual reactance at base frequency.
α	: firing angle of the inverter.
ω	: base electrical angular frequency in rad/s.
ω_r	: rotor electrical angular frequency in rad/s.
s	: slip of the motor $1-(\omega_r/\omega)$.

INTRODUCTION

The static Kramer drive also known as the slip energy recovery drive or subsynchronous converter cascade is particularly well adapted to fan and pump drive applications where usually only a limited speed range is needed. It is of particular interest to loads whose torque is proportional to the square of the speed. For such cases, the speed variation needed is within a limited range below synchronous speed by usually 40%, allowing very substantial reductions in the rating of the recovery circuit components and in the drive reactive power requirements [1]. Such a type of loads typically represent more than 50 % of the total energy consumption in the industrial world and most of the developing countries [1].
A high efficiency and highly desirable torque speed characteristics similar to that of the separately excited dc motor in addition to a definite cost advantage against other drives technologies make it a very popular drive in high power applications. The only serious drawback is a poor overall power factor. This problem has however found adequate solutions through the use of various forms of recovery circuits [2,3,4,5].

The stability analysis of the drive has also been the object of some appreciable work. Mittle et al used a 5^{th} order model of the induction machine to derive the characteristics equation of the drive and determine its stability using the Routh Hurwitz criterion. In this work the motor leakage reactance was neglected. They report that the system shows instability under certain operating conditions for given values of system inertia, supply voltage and system parameters [6].

The experimental results shown were not fit to support analytical predictions as they correspond to stable conditions only.

The root loci theory developed for determining the transfer function and dynamic response of the squirrel cage induction motor [7,8,9] has been extended to the static Kramer drive by Lequesne and Miles [10]. The machine 5^{th} order model is used in the analysis with the motor leakage reactance taken into account. The switching of the power electronics in the diode bridge and inverter was assumed ideal and the influence of the harmonics negligible. The model suggests the possibility for the system to show instability. No experimental validation has been presented. A closed loop analysis has also been developed by the same authors along similar lines.

However, two of the three underlying assumptions pertaining to reference [10] seem to be mutually exclusive. The effect of motor leakage reactance, if taken into account, must invalidate the assumptions that switching in the diode bridge is ideal as overlap is then inevitable.

Vas et al have simplified the characteristic equation of the drive by using the so called collinearity transformation (whose main feature is to leave the roots of the characterisitic equations unchanged) but have done no stability analysis [11].

Subrahmanyam and Surendram have studied the drive stability using the eigenvalue method [12]. The leakage reactances were neglected. They dispute the validity of the results of [6] on the ground of numerical errors. Their conclusions are that the static Kramer drive can never go unstable under normal operating conditions. These conclusions are in apparent contradiction with those of references [7] and [10].

Furthermore and more importantly, Krause et al have pointed to an error in the machine 5^{th} order model that has been used in most of the work so far [13]. In the light of the above considerations, it appears that a detailed stability analysis of the static Kramer drive is warranted.

This is the object of the present thesis.

First, the steady state analysis of the drive is treated in detail in chapter two, with the main objective of further substantiating findings in [13] by alternative means.

In the third chapter a simplified stability analysis of the drive using second order transfer function model is presented and transient responses

obtained in view of investigating effect of parameter changes on system relative stability

Development of a linear model obtained from a drive DQ non linear model together with extensive stability study of the drive for three different power levels is the object of chapter four, where appear comprehensive sets of results together with non linear system response plots to support analytical predictions.

Lastly, a general conclusion with important differences with previous investigations, summarizes the findings of the work.

CHAPTER 2

STEADY STATE ANALYSIS OF THE STATIC KRAMER DRIVE

2.1 INTRODUCTION

Despite its simplicity a rigourous analysis of the Static Kramer Drive is not straightforward, mainly because of the interdependence between the rotor voltage and current waveforms. The diode bridge draws non sinusoidal currents, therefore inducing a high harmonic content in the rotor voltage which will in turn affect the rotor currents. Both rotor voltage and current are non sinusoidal and a rigourously exact model should take into account their non sinusoidal nature in addition to the overlap effect in the three phase diode bridge[5,14].

The drive steady state perfomance can nonetheless be predicted with accuracy sufficient for the purpose of basic investigation of system stability as well as for the design of controllers, through the use of simple models of varying complexity.

Two approaches are the so called DC and AC equivalent circuits which essentially consist of transferring drive parameters on to the dc and ac side of the rotor diode bridge [15,16,17]. DC and AC models are developed with improvements, along with a DQ model in order to predict the drive steady state behaviour.

These various steady state analyses are carried out in order to arrive at reliable, error free prediction of system performance through correlation of the results of the various models used.

This work is warranted by the fact that published work on stability analysis of the drive [6,12] is marred by serious errors ; the model on which stability analysis is based predicts erroneous torque-speed characteristics first pointed out by [13], the same sort of error can also be found in advanced reference text books [15].
The fundamental principles of the Static Kramer Drive are first described.

2.2 DRIVE DESCRIPTION

The slip energy recovery drive in its conventionl form is shown in fig.1.

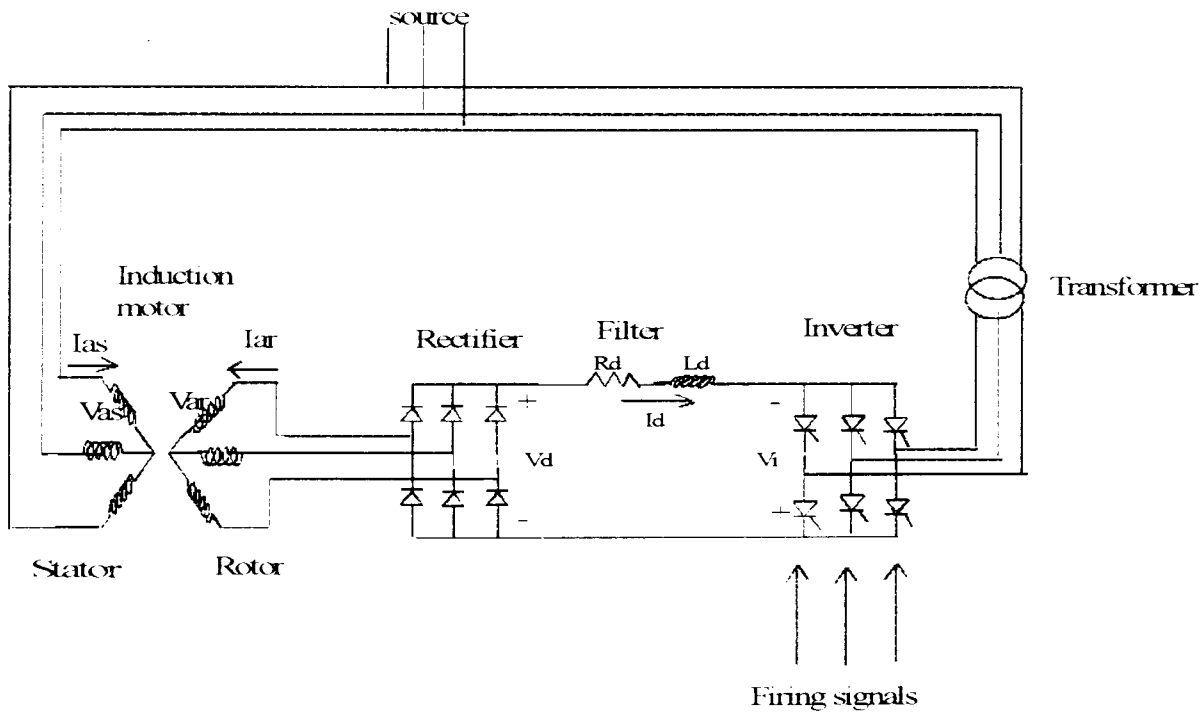

Fig 2.1 The Static Kramer Drive

It consists of a slip ring induction motor and a slip energy recovery circuit comprising a three phase diode bridge rectifier connected to the rotor winding terminals, a smoothing choke and a line commutated inverter connected to the AC supply usually via a step up transformer. The slip frequency rotor voltages are rectified by the diode bridge the resulting mean voltage V_d, essentially proportional to the slip, is countered by the inverter opposing voltage V_i which can be varied by adjusting the inverter firing angle α where normally it lies between 90° for maximum speed and

150° (instead of the theoretical 180° to avoid commutation failure) for minimum speed to control the DC link current I_d and hence the developed torque and speed. Slip power thus recovered and injected back into the AC supply through the inverter makes of the system a simple and efficient variable speed drive

In steady state operation, the slip rectified voltage V_d and the inverter voltage V_i will balance for a certain dc current I_d.

Neglecting the stator and rotor circuit drops, the rectifier output voltage V_d is given by :

$$V_d = \frac{1.35}{n_1} s V_l \qquad (2.1)$$

Where :

n_1 is the stator -to-rotor turns ratio of the machine.

V_l is the stator line -to-line rms voltage.

S is the per unit slip.

The inverter dc voltage V_i is given by :

$$V_i = \frac{1.35}{n_2} V_l \cos \alpha \qquad (2.2)$$

Where :

n_2 is the transformer line side-to-inverter ac side turns ratio.

α is the inverter firing angle in the range (90°-150°).

If losses are neglected, the following power equations can be written as :

$$sP_g = V_i I_d \qquad (2.3)$$

$$P_m = (1-s)P_g = T_e w_r = T_e w_e (1-s) \qquad (2.4)$$

Where P_g is the air gap power in Watts, P_m is the mechanical output power and w_e is the synchronous speed.

Combining the above equations 2.3 and 2.4 we get :

$$T_e = \frac{V_i \cdot I_d}{s \cdot w_e} \qquad (2.5)$$

Since ideally V_d and V_i must balance, equations (2.1) and (2.2) yield the expression of the no load slip

$$s = \frac{n_1}{n_2} \cos \alpha \qquad (2.6)$$

Indicating that the speed can be controlled by adjusting the firing angle α

Substituting eqns. (2.5) and (2.2) in eqn. (2.3) gives the torque as a function of the dc link current I_d

$$T_e = \left(\frac{1.35 V_l}{w_e n_1} \right) I_d \qquad (2.7)$$

The equation is similar to the torque equation of a separately excited motor. This shows that the torque is proportional to the dc link current I_d. For a higher load torque, the DC link current I_d will increase and for a fixed inverter voltage V_i, V_d should slightly increase to overcome the dc link drop indicating a speed drop like a DC machine.
We now proceed, in the coming sections, to analyse the performance of the drive using the DC, AC and DQ models.

2.3 DC EQUIVALENT CIRCUITS

The drive parameters are all referred to the dc side of the rotor diode bridge. An approximate dc equivalent circuit is first derived

2.3.1 DC APPROXIMATE CIRCUIT:

It is approximate because the magnetizing branch is assumed negligible. A per phase DC equivalent circuit is shown in Fig. 2.2. [15]

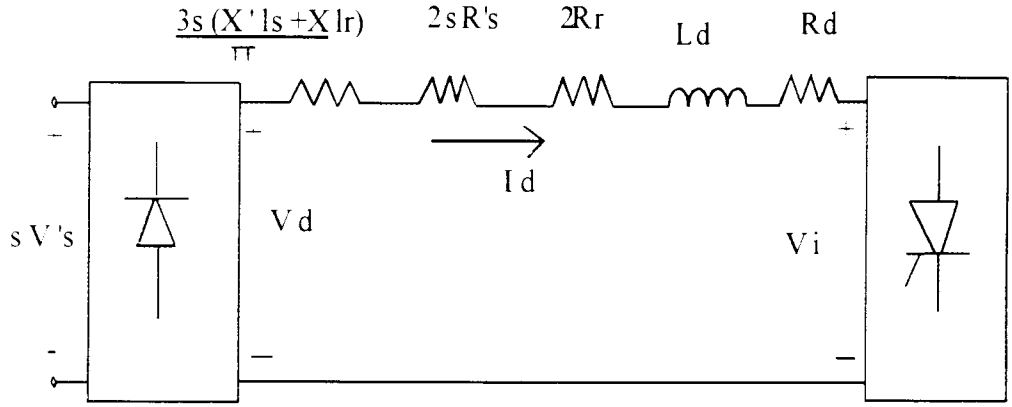

Fig 2.2 DC equivalent circuit

Where:

L_d , R_d : represent the inductance and the resistance of the dc link choke.

R_s', X_{ls}' : the rotor referred values of the stator resistance and leakage reactance respectively.

R_r , X_{lr} : are rotor resistance and leakage reactance, respectively.

The overlap effect is modelled as a dc voltage drop across the output three phase rectifier bridge. This is represented by a non dissipative resistance :

$$R_c = \frac{3\,s\,(X'_{ls}+X_{lr})}{\pi} \tag{2.8}$$

The presence of leakage inductances sX_{ls}' and sX_{lr} will cause commutation delay of the rectifier and as a result the DC output voltage will drop with current. The rectifier output voltage V_d is given as :

$$V_d = 1.35(\sqrt{3}\, s\, V_s') = s\, V_{d0} \tag{2.9}$$

Where :

$$V_{d0} = 1.35(\sqrt{3} V_s') \tag{2.10}$$

And :

$$V_s' = \frac{V_s}{n_1} \tag{2.11}$$

The dc link current I_d corresponding to the steady state operation condition of the system is given by :

$$I_d = \frac{V_d - V_t}{R} \tag{2.12}$$

Where :

$$R = \frac{3s(X'_{ls} + X'_{lr})}{\pi} + 2R_r + 2sR'_s + R_d \tag{2.13}$$

If we neglect ripple in the dc current I_d, the rotor circuit copper loss is given by :

$$P = V_d I_d - \frac{3s(X'_{ls} + X'_{lr})}{\pi} I_d^2 - 2sR'_s I_d^2 \tag{2.14}$$

Otherwise :

$$P = s\left(V_{d0} I_d - \left[\frac{3(X'_{ls} + X'_{lr})}{\pi} + 2R'_s\right] I_d^2\right) \tag{2.15}$$

The developed electromagnetic torque T_e at slip s, can be given as :

$$T_e = \frac{P}{sw_e} = (1/w_e)\left(V_{d0} I_d - \left[\frac{3(X'_{ls} + X'_{lr})}{\pi} + 2R'_s\right] I_d^2\right) \tag{2.16}$$

Eqn (2.16) shows that the developed torque at a given speed is a function of the dc link current I_d and if contribution of the second term is neglected, it is proportional to dc link current and eqn (2.16) in fact agrees with eqn (2.7). The torque-speed characteristic for different values of firing angles α is computed using eqn (2.16) and shown in Fig 2.3.

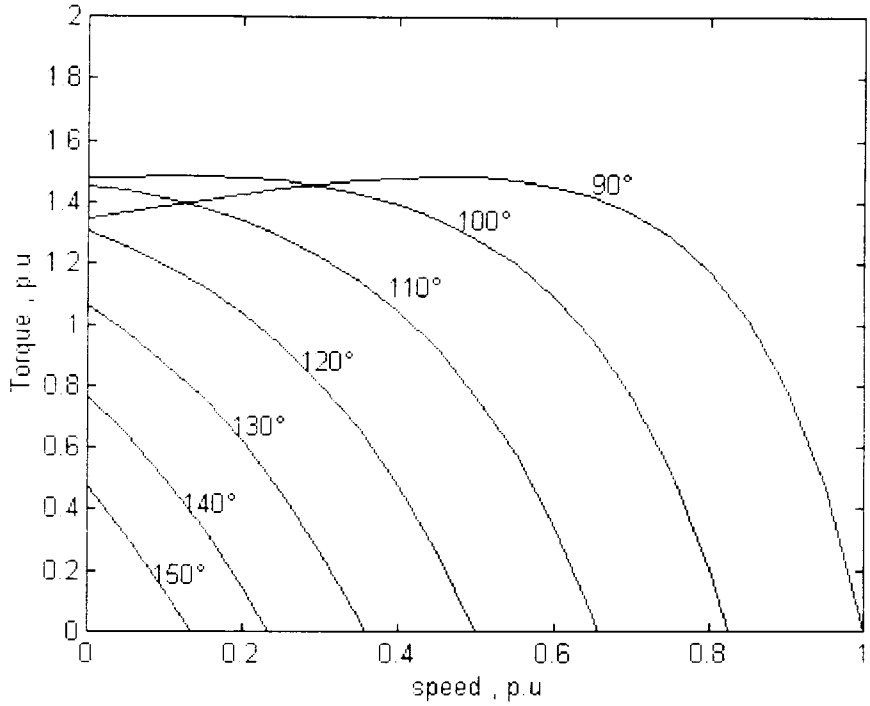

Fig. 2.3 DC model torque versus speed characteristics

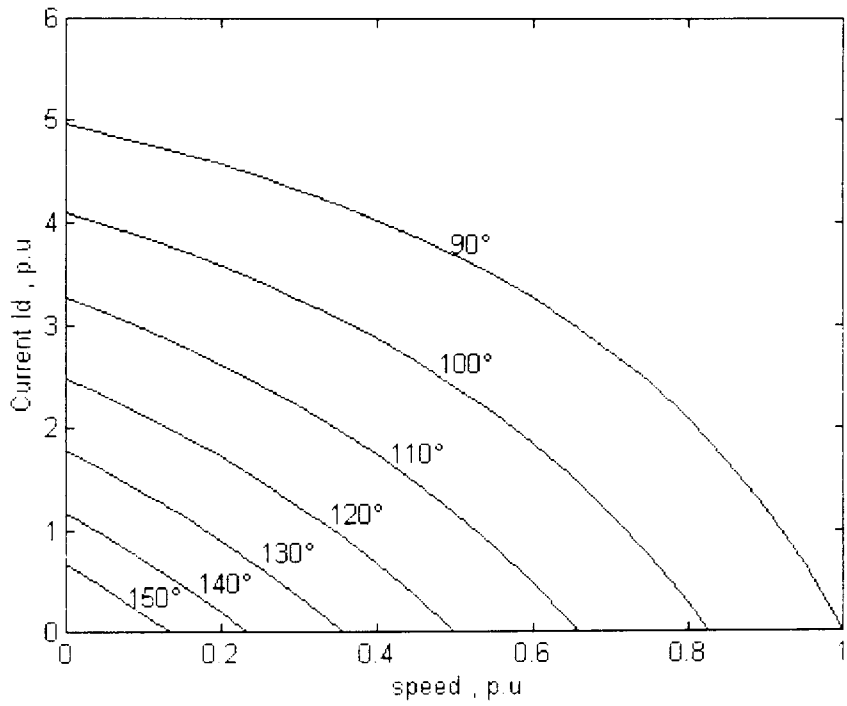

Fig. 2.4 DC link current versus speed characteristics

The maximum or pull out torque is of the same irrespective of the firing angle α and is equal to 1.5 p.u. It is not reached within the normal speed range for firing angles α greater than 110°.

2.3.2 EXACT DC CIRCUIT :

Now the magnetizing branch placed after the primary resistance and reactance as shown in Fig. 2.5 (a) is taken into account. The thevenized equivalent circuit is shown in Fig. 2.5 (b). The resulting exact dc equivalent circuit appears in Fig. 2.5 (c), where the parameters of figure 2.5 (b) are referred to the dc side [15].

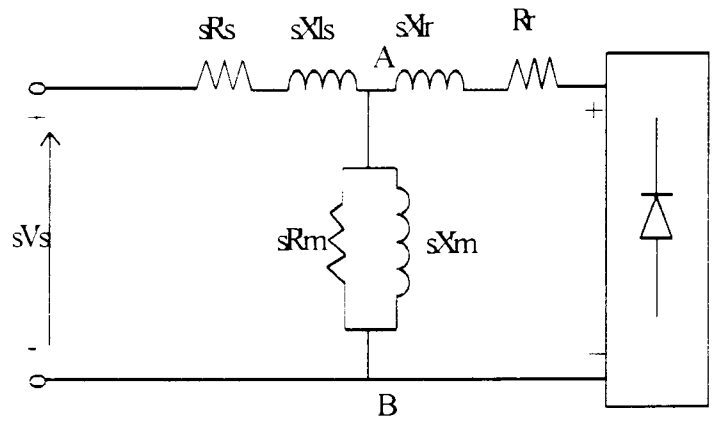

Fig. 2.5 (a) Exact per phase equivalent circuit

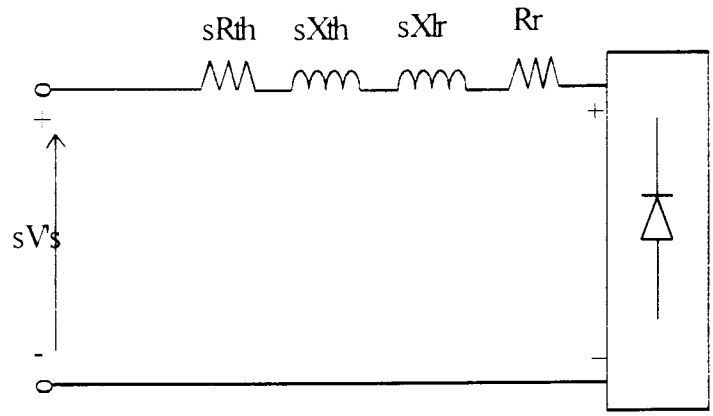

Fig. 2.5 (b) Thevenized per phase motor equivalent circuit

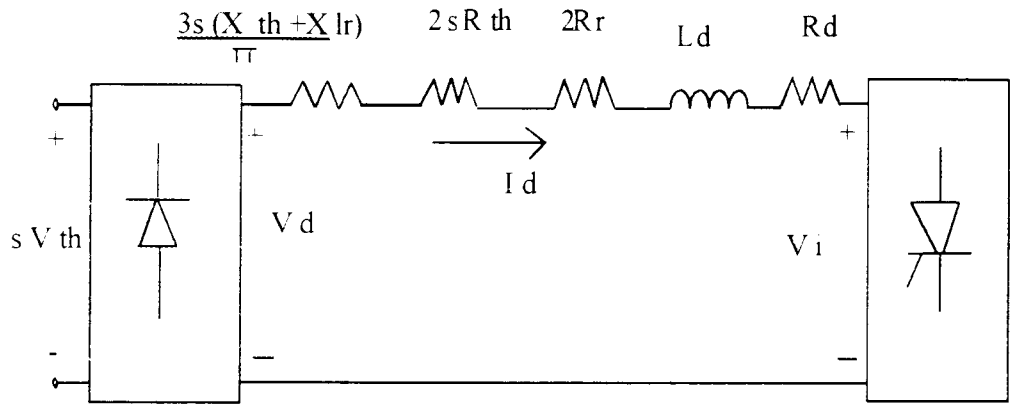

Fig 2.5 (c) Resulting exact dc equivalent circuit

Where

$$V_{th} = \frac{Z_m}{Z_m + Z_s} \, s V_s' \tag{2.17}$$

$$Z_{th} = Z_m // Z_s \tag{2.18 a}$$

$$Z_{th} = R_{th} + j X_{th} \tag{2.18 b}$$

$$Z_m = \frac{R_m X^2_m}{R^2_m + X^2_m} + j \frac{R^2_m X_m}{R^2_m + X^2_m} \tag{2.19}$$

$$Z_s = sR_s + j\, sX_{ls} \tag{2.20}$$

The steady state torque-speed and dc link current characteristics of the exact dc equivalent circuit are shown in Fig. 2.6 and Fig. 2.7.

The effect of neglecting the magnetizing branch on the torque-speed characteristics causes an optimistic prediction of pull out or maximum torque by approximately 8 %. The difference is important.

In the case of the dc link current the difference is of the order of 4 %. In general, the effect of the magnetizing branch is expected to decrease as the power rating of the machine increases.

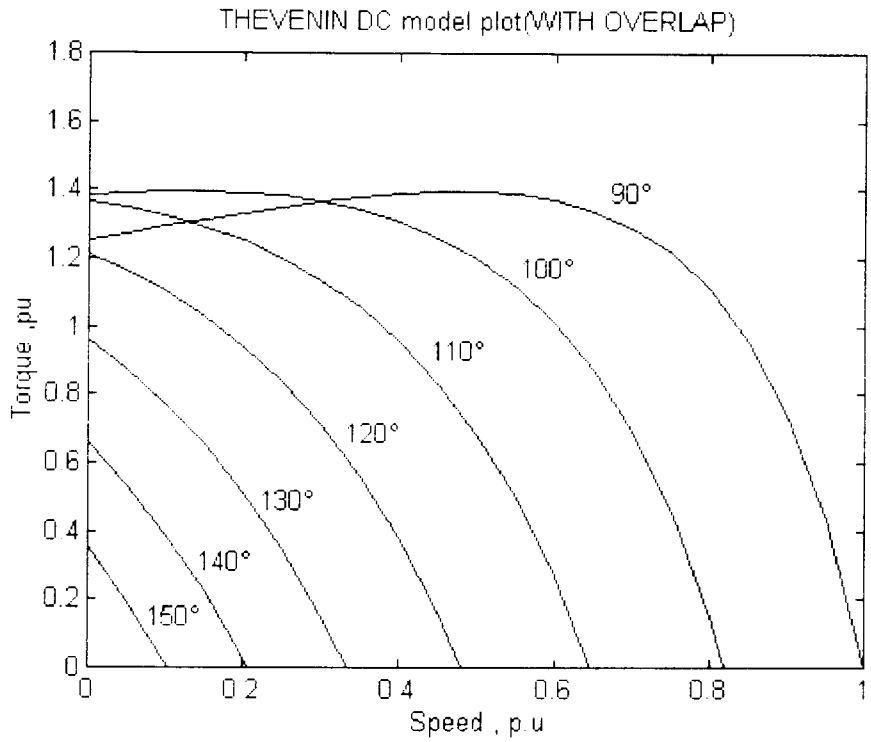

Fig. 2.6 Torque-speed characteristics

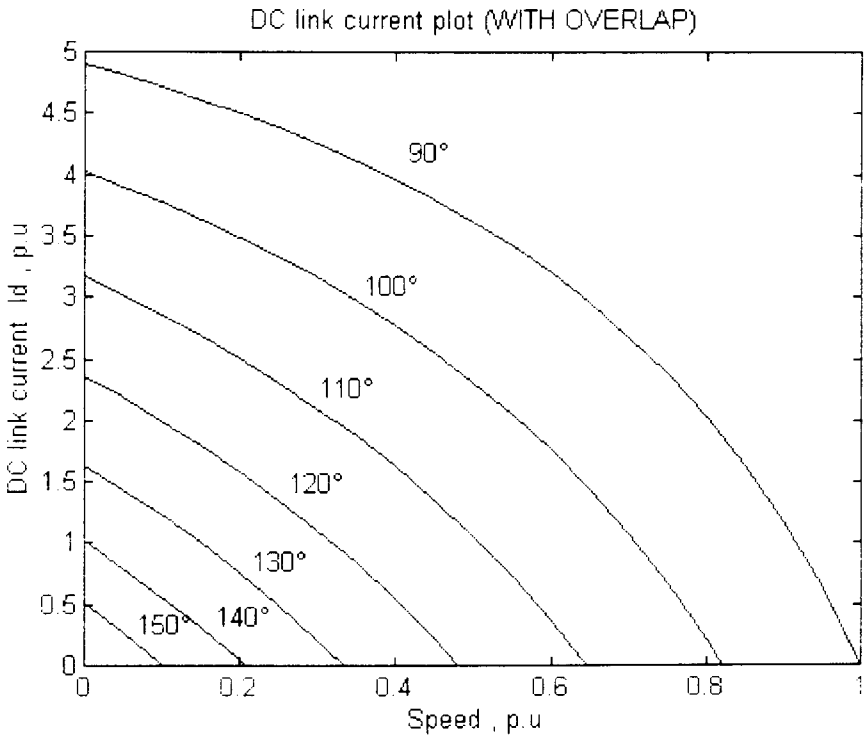

Fig. 2.7 DC link current I_d versus speed characteristics

2.4 AC EQUIVALENT CIRCUIT

An approximate per phase AC equivalent circuit followed by an exact one are now developed with the intent of finding out any effect of simplifying assumptions on the torque-speed characteristics of the drive.

2.4.1 APPROXIMATE AC EQUIVALENT CIRCUIT

An approximate per phase AC equivalent circuit of the drive with respect to the rotor where the magnetizing branch is placed across the input is shown in Fig. 2.8 [15]

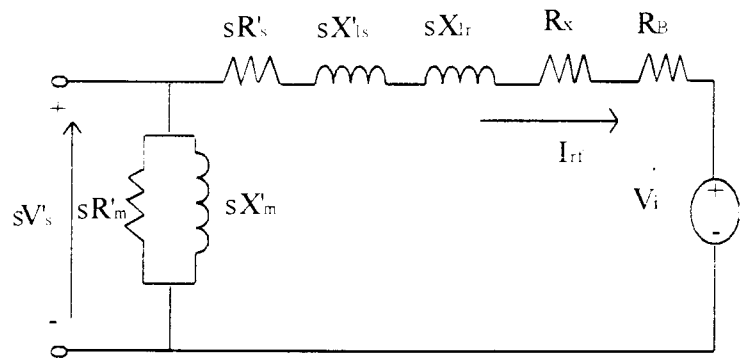

Fig. 2.8 Approximate drive AC equivalent circuit with respect to rotor

Where :

$$R_B = \left(\frac{R_r + 0.5R_d}{S} \right) \tag{2.21}$$

$$R_X = \left(\frac{\pi^2}{9} - 1 \right)(R_r + 0.5R_d) \tag{2.22}$$

$$V_i = \frac{V_s}{sn_2} \cos \alpha \tag{2.23}$$

R'_s , X'_{ls} represent the stator resistance and leakage reactance referred to the rotor.

R'_m , X'_m are the core loss and magnetizing reactance referred to the rotor.

R_X is a resistance representing additional harmonic power loss due to harmonic currents caused by the diode bridge rectifier.

The average torque developed by the machine is given by the fundamental air gap power divided by the synchronous speed. The expression in terms of the passive equivalent circuit parameters is given by :

$$T_e = \frac{1}{w_s}\left(3I^2_{rf}\frac{R_A}{S}\right) \qquad (2.24)$$

Where R_A represents the total circuit resistance and is given by :

$$R_A = (R_s + 0.5R_d) + \frac{\pi}{3\sqrt{6}}\frac{1.35V_l}{n_2 I_{rf}}\cos\alpha \qquad (2.25)$$

The fundamental component of the rotor current I_{rf} is given by :

$$I_{rf} = \frac{SV'_s}{\sqrt{\left((SR'_s + R_A)^2 + (SX'_{ls} + SX_{lr})^2\right)}} \qquad (2.26)$$

2.4.1.1 Steady state characteristics :

Equations (2.22), (2.23), (2.24), (2.25) and (2.26) have been used to plot the electromagnetic torque T_e and the alternating current I_{rf}. By substituting the expression of R_A in that of I_{rf} a second order algebric equation is obtained :

$$aI^2_{rf} + bI_{rf} + c = 0 \qquad (2.22)$$

The equation is numerically solved for different values of slip S and firing angle α and the computed electromagnetic torque T_e plotted.
Torque-speed and fundamental rotor current I_{rf} versus speed characteristics are shown in Fig. 2.9 and Fig. 2.10 :

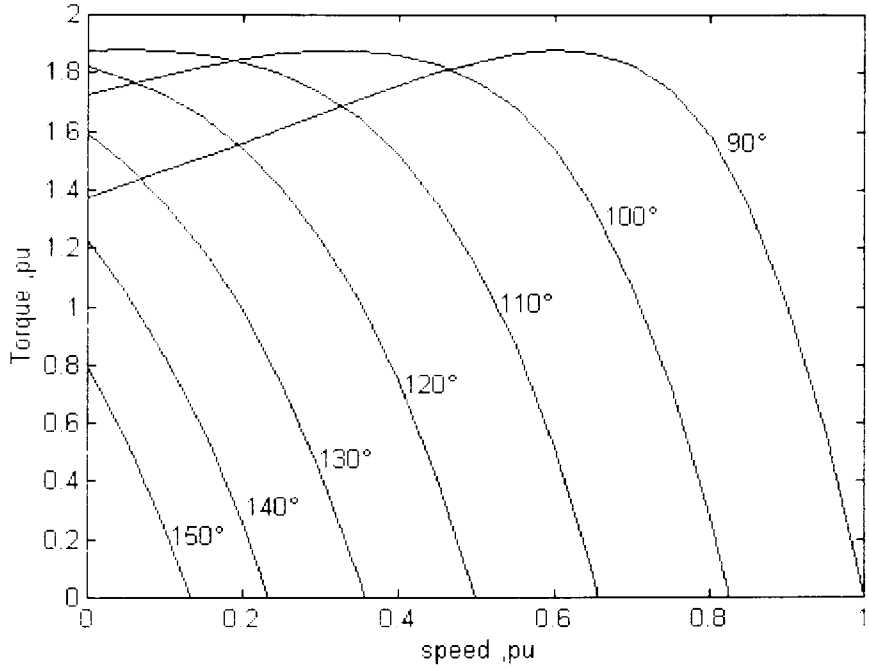

Fig. 2.9 AC model torque-speed characteristics

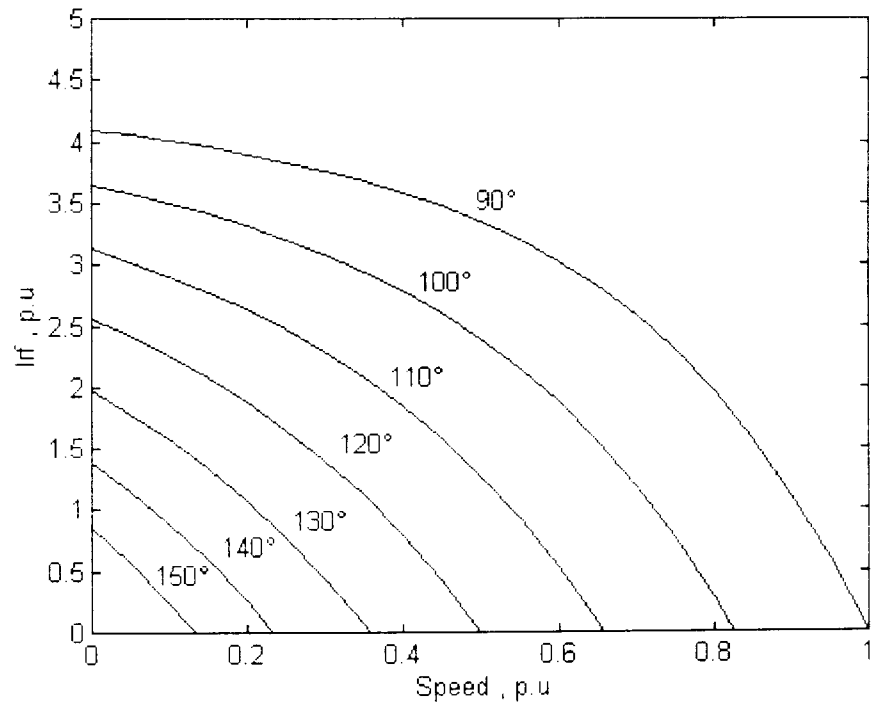

Fig. 2.10 I_{rf} current versus speed

2.4.2 EXACT EQUIVALENT CIRCUIT

An exact AC equivalent circuit is now described. The magnetizing branch is inserted in its correct place as shown in Fig. 2.11 and a Thevenin equivalent circuit across points A and B is obtained [15]

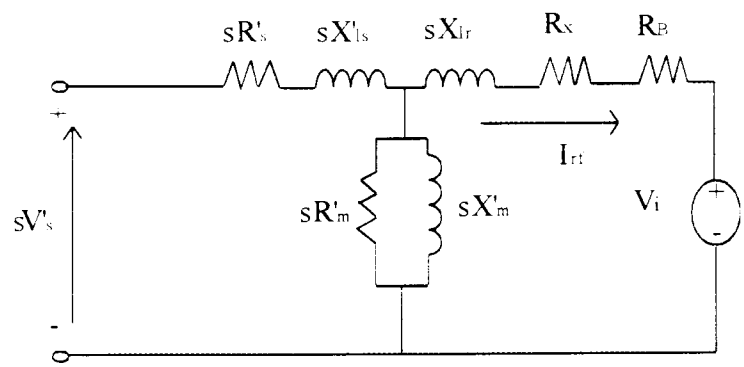

Fig. 2.11 Exact ac per phase equivalent circuit

The Thevenin equivalent circuit is

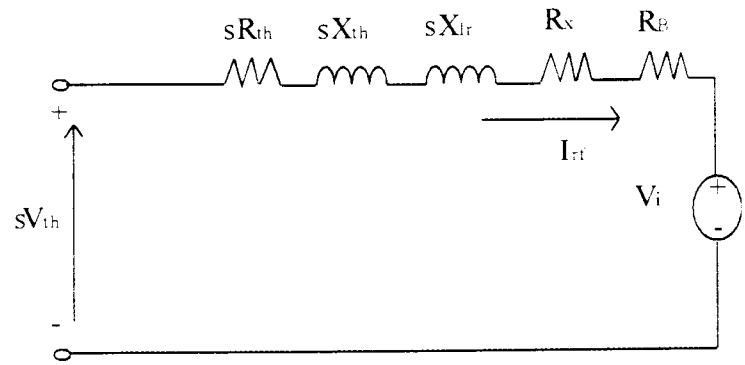

Fig. 2.12 Thevenized AC per phase equivalent circuit

Where V_{th}, R_{th} and X_{th}, given in eqns. (2.17) to (2.20), are the Thevenin equivalent voltage, resistance and reactance respectively.

The steady state torque versus speed and the fundamental rotor current versus speed characteristics are plotted using the same system parameters as those used in the DC and AC approximate equivalent circuit and shown

in Fig 2.13 and Fig. 2.14 Commutation ovelap effect is not taken into account .

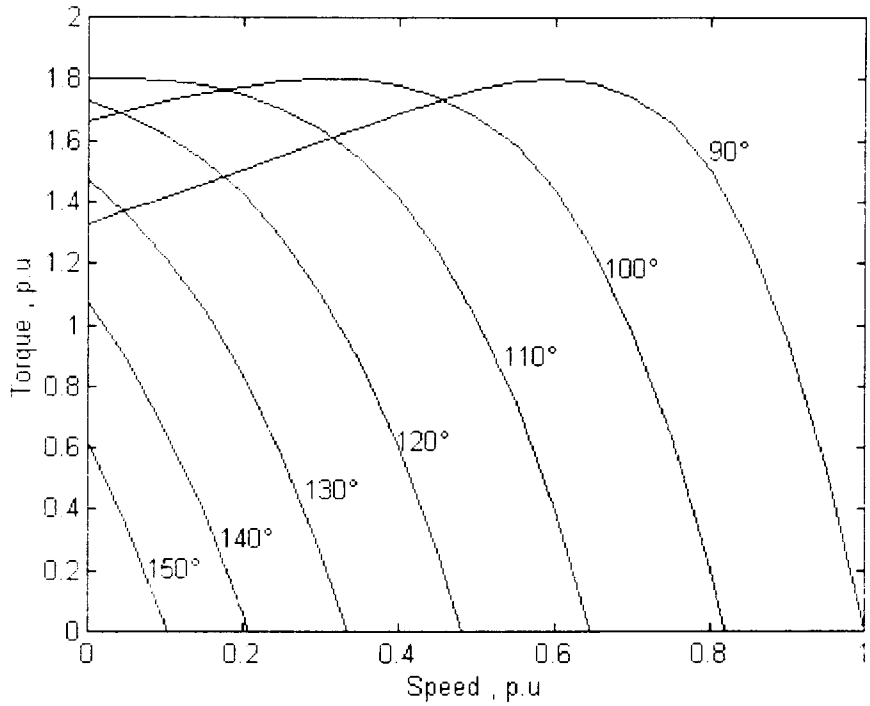

Fig. 2.13 Torque-speed characteristics of exact AC model (No overlap).

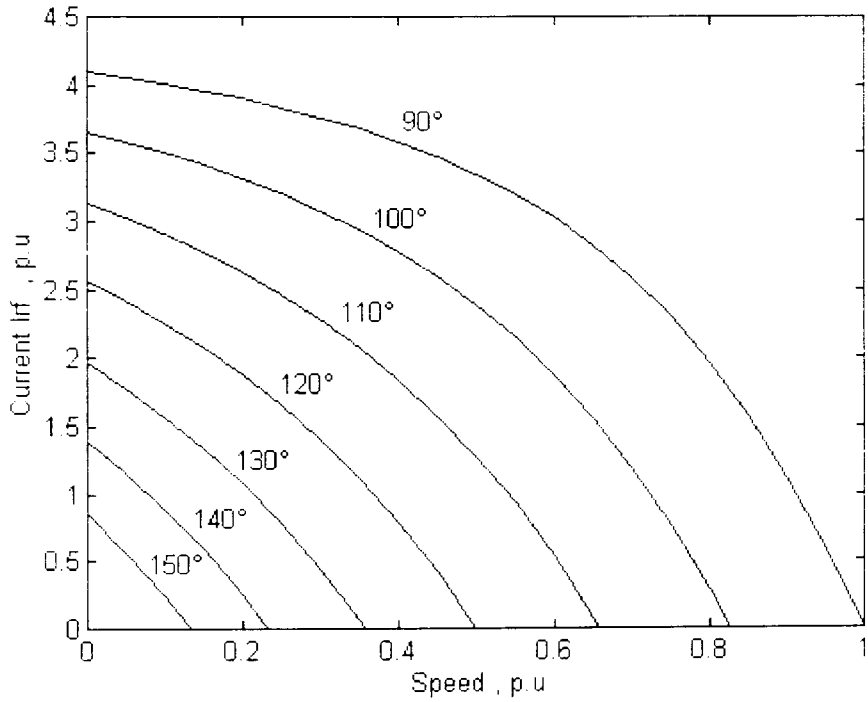

Fig 2.14 Fundamental rotor current I_{rf} versus speed characteristics

The curves show very good agreement with those obtained by Krause [13]. The more accurate AC equivalent circuit predicts a torque reduction of approximately 10 %. This is due to the magnetizing branch effect which is normally important as already mentioned.

2.5 DQ MODEL

In this section a DQ model for the drive is developed and its steady state behaviour computed. The underlying assumptions of the model are:

(1). Ideal and symmetric induction machine.
(2). The effects on the drive stability of the harmonics due to the bridge rectifier on the ac and the dc side are negligible. The torques induced by harmonics are comparatively small [1,23]. Predicted effects of some harmonic at specific slips has proved not to actually take place [5].
(3). The commutation in the rectifier as well as in the line commutated inverter are instantaneous, i.e., overlap effect is neglected.
(4). The dc link current ripple is negligible.
(5). The diodes and thyristors are ideal.

Regarding assumption (3), the commutation overlap in the inverter from a practical standpoint is not usually important to justify its inclusion in the model. On the other hand the commutation overlap in the diode bridge can be substantial, especially at higher speeds under heavy loads [14]. The slip ring induction motor, the filter and the converters of the recovery circuits are modelled in the following sections.

2.5.1 The induction machine :

The voltage equations of the three phase induction motor in the synchronously rotating reference frame may be expressed as [13]:

$$\begin{bmatrix} V_{qs} \\ V_{ds} \\ V'_{qr} \\ V'_{dr} \end{bmatrix} = \begin{bmatrix} R_s + \frac{X_{ss}}{\omega} p & X_{ss} & \frac{X_m}{\omega} p & X_m \\ -X_{ss} & R_s + \frac{X_{ss}}{\omega} p & -X_m & \frac{X_m}{\omega} p \\ \frac{X_m}{\omega} p & sX_m & R'_r + \frac{X'_{rr}}{\omega} p & sX'_{rr} \\ -sX_m & \frac{X_m}{\omega} p & -sX'_{rr} & R_r + \frac{X'_{rr}}{\omega} p \end{bmatrix} \begin{bmatrix} I_{qs} \\ I_{ds} \\ I'_{qr} \\ I'_{dr} \end{bmatrix} \qquad (2.27)$$

R_m, R_s and R_r represents the core loss, stator and rotor resistances respectivelly.

The electromagnetic torque, positive for motor action, may be expressed in per unit as :

$$T_e = X_m(I_{qs}I'_{dr} - I_{ds}I'_{qr}) \tag{2.28}$$

2.5.2 The filter

The voltage equation for the filter circuit is :

$$V_d = R'_d I_d + \frac{X'_d}{\omega} pI_d - V_i \tag{2.29}$$

Where X'_d and R'_d are the filter reactance and resistance respectively (referred to stator). I_d is the dc link current, V_i and V_d represents the dc side inverter voltage and rectifier output voltage respectively.

2.5.3 The converters:

Neglecting the commutating inductance, the average output voltage of a full wave converter with balanced AC voltages may be expressed as :

$$V_d = V_{d0}\cos\alpha \tag{2.30}$$

Where α is the firing angle. For the bridge rectifier α is zero . So the voltage V_{d0} is :

$$V_{d0} = \frac{3\sqrt{3}}{\pi} V_p \tag{2.31}$$

Where Vp is the peak value of the ac phase voltages (rotor phases for the rectifier and the stator phases for the inverter).

2.5.4 Physical DQ model :

If the rotor harmonic components of the rotor variables are neglected then the rotor phase voltages will be sinusoidal [13]

Important assumption :
If the q-axis is positioned so that it always coincides with the maximum or peak positive value of V_{ar} then [13]

$$\begin{aligned} V'_{qr} &= V_{mr} \\ V'_{dr} &= 0 \end{aligned} \tag{2.32}$$

Where V_{mr} is the peak value of the rotor phase voltages refered to the stator windings by the appropriate turns ratio.
If the commutation of the rectifier is neglected and since $\alpha = 0$, the rectifier voltage may be expressed from equ. 2.30 as :

$$V_d = \frac{3\sqrt{3}}{\pi} V_{mr} \tag{2.33}$$

With the commutation in the rectifier neglected, the fundamental rotor currents into the rectifier are in phase with the input rotor voltages.
Since the q-axis is assumed always positioned at the peak value of V_{ar} then I_{dr} must be zero.
The commutation effect in the inverter being negligible, the inverter dc side output voltage is given by :

$$V_i = \frac{3\sqrt{3}}{\pi} V_{ms} \cos \alpha \tag{2.34}$$

Where α is the inverter firing angle varying from 90° to 150° and V_{ms} is the peak value of the stator phase voltages.

Note that if a transformer is connected between the source and inverter (which is usually the case), its turns ratio must be appropriately taken into account.

Using eqn. (2.27), (2.30) through to (2.34), the resulting final equation of the system is given by :

$$\begin{bmatrix} V_{qs} \\ V_{ds} \\ -V_{ms}\cos\alpha \\ 0 \end{bmatrix} = \begin{bmatrix} R_s - \frac{X_{ss}}{\omega}p & X_{ss} & \frac{X_m}{\omega}p & \\ -X_{ss} & R_s + \frac{X_{ss}}{\omega}p & -X_m & \\ \frac{X_m}{\omega}p & sX_m & R'_r + \frac{\pi^2}{18}R'_d + \frac{(X'_{rr} + \frac{\pi^2}{18}X'_d)}{\omega}p & \\ -sX_m & \frac{X_m}{\omega}p & -sX'_{rr} & \end{bmatrix} \begin{bmatrix} I_{qs} \\ I_{ds} \\ I'_{qr} \end{bmatrix} \quad (2.35)$$

The prime notation indicates referring to stator circuit. With I'_{dr} equal to zero, the per unit electromagnetic torque may be expressed as :

$$T_e = -X_m I_{ds} I'_{qr} \quad (2.36)$$

The q-axis is positioned so that it always coincides with the peak value of V_{ar}. Hence, for a given machine, the values of V_{qs} and V_{ds} will be determined by the amplitude of the source voltage and the system operating conditions. That is, V_{qs} and V_{ds} are related to V_{ms} as [13] :

$$V_{ms}^2 = V_{qs}^2 + V_{ds}^2 \quad (2.37)$$

Torque may be related to rotor speed w_r as :

$$T_e = 2H\frac{d(\frac{w_r}{w})}{dt} + T_L \quad (2.38)$$

Where H is the inertia constantin seconds and T_L is the load torque expressed in per unit.

2.5.5 THE STEADY STATE MODEL

The steady state model is obtained from eqn. (2.35), by putting the variation in time of the system variables to zero, that is, p( ) = 0. The steady state DQ model of the drive is then obtained :

$$\begin{bmatrix} V_{qs0} \\ V_{ds0} \\ -V_{ms}\cos\alpha \\ 0 \end{bmatrix} = \begin{bmatrix} R_s & X_{ss} & 0 \\ -X_{ss} & R_s & -X_m \\ 0 & sX_m & R'_r + \frac{\pi^2}{18} R'_d \\ -sX_m & 0 & -sX'_{rr} \end{bmatrix} \begin{bmatrix} I_{qs0} \\ I_{ds0} \\ I'_{qr0} \end{bmatrix} \qquad (2.39)$$

Where the steady state variables are denoted by a subscript 0 .

2.5.6 Steady state characteristics :

The steady state electromagnetic torque, dc link current I_{dc} and the direct and quadratic voltages and currents versus speed characteristics for values of firing angles α, ranging from 90° to 150° and for system parameters given in appendix A.1, are shown in figures 2.15, 2.16, 2.17, 2.18, 2.19 2.20, 2.21 and 2.22 :

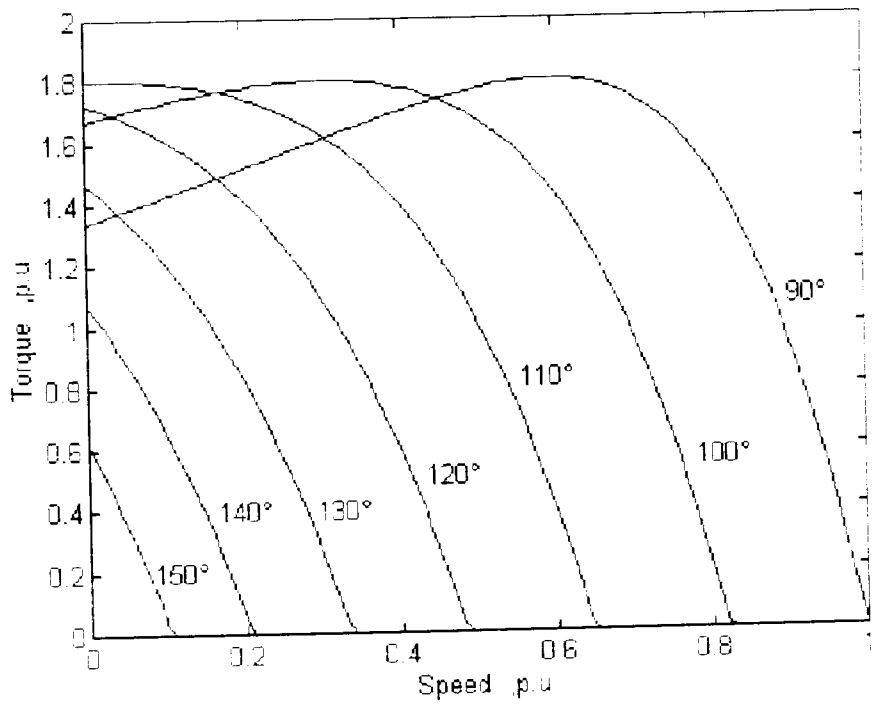

Fig. 2.15 Developed electromagnetic torque versus speed

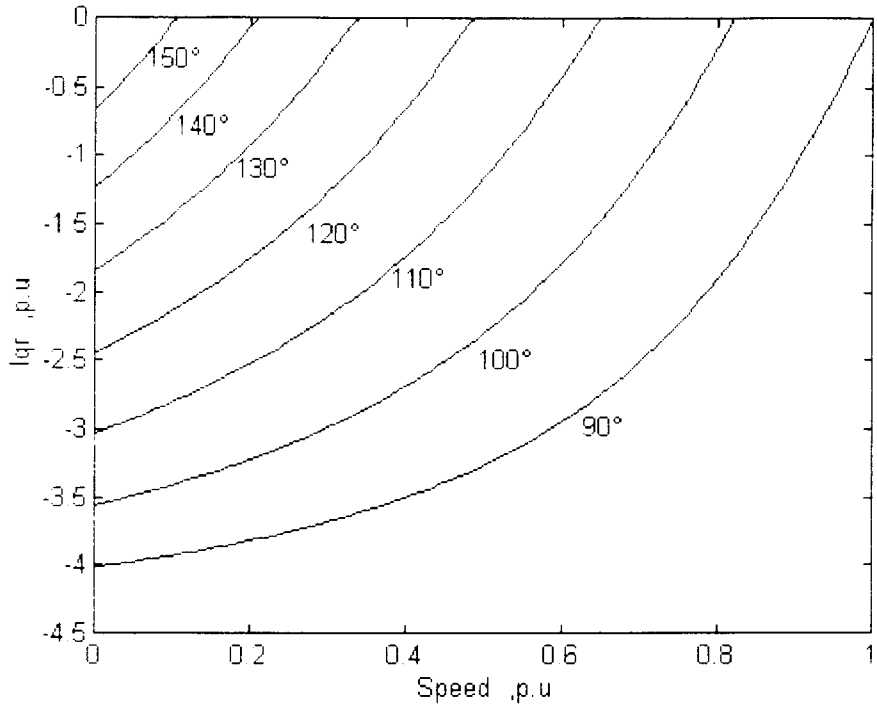

Fig. 2 16 Quadratic current I_{qr} versus speed

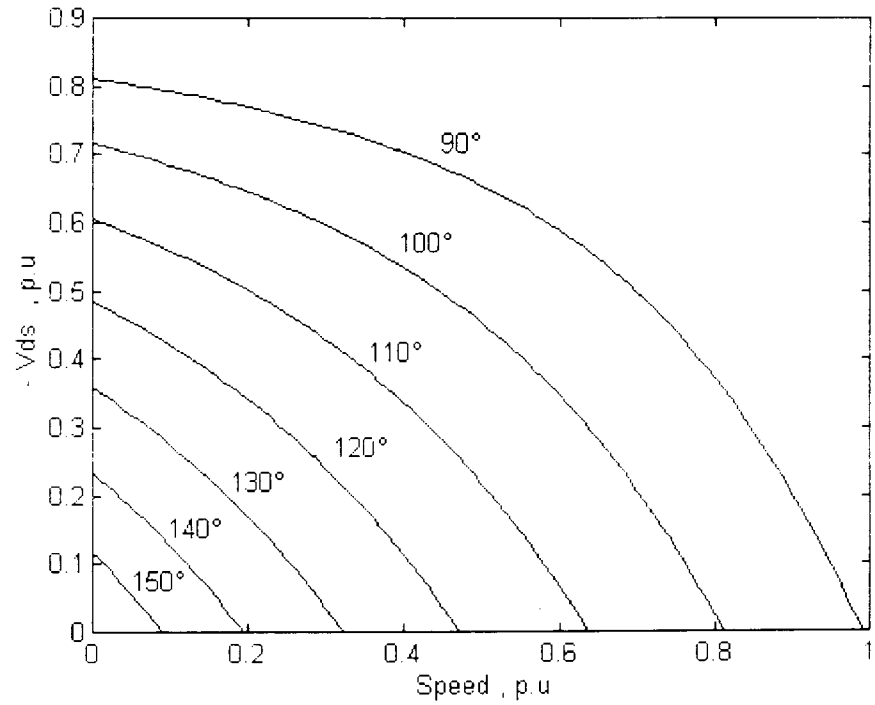

Fig. 2 17 Direct voltage V_{ds} versus speed

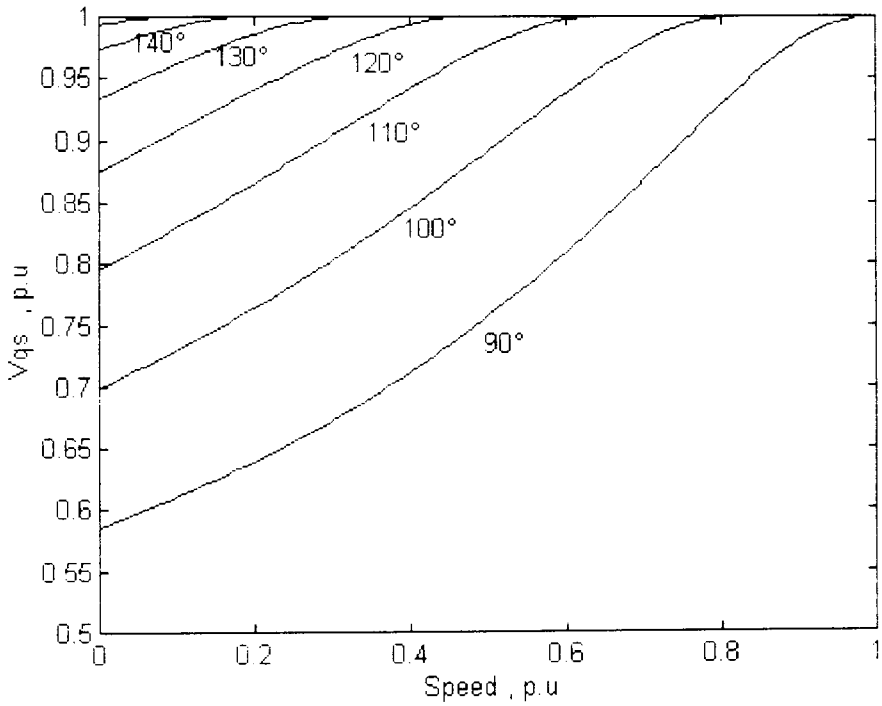

Fig. 2.18 Quadratic voltage V_{qs} versus speed

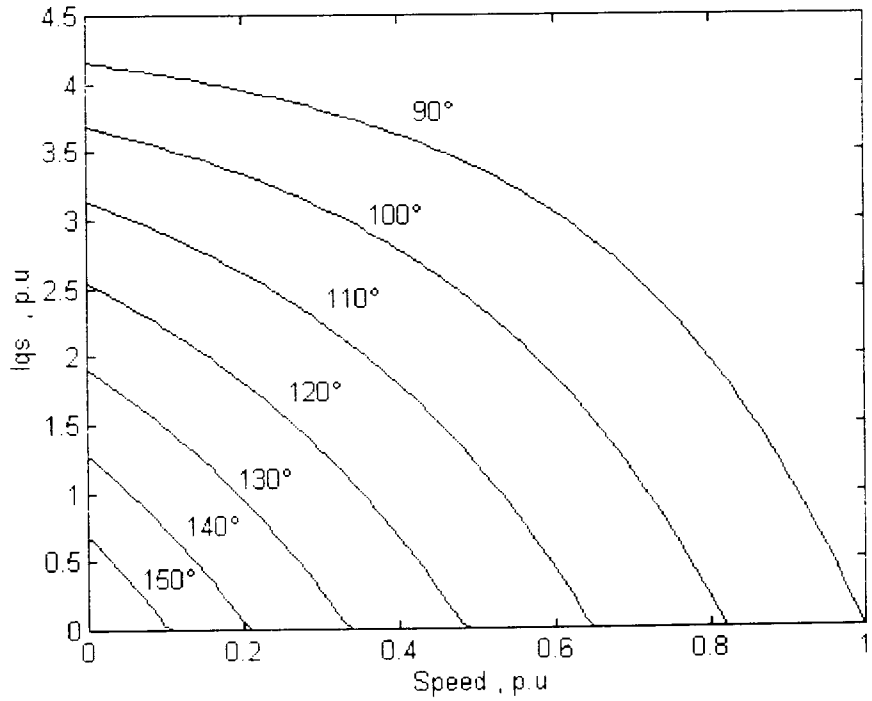

Fig. 2.19 Quadratic current I_{qs} versus speed

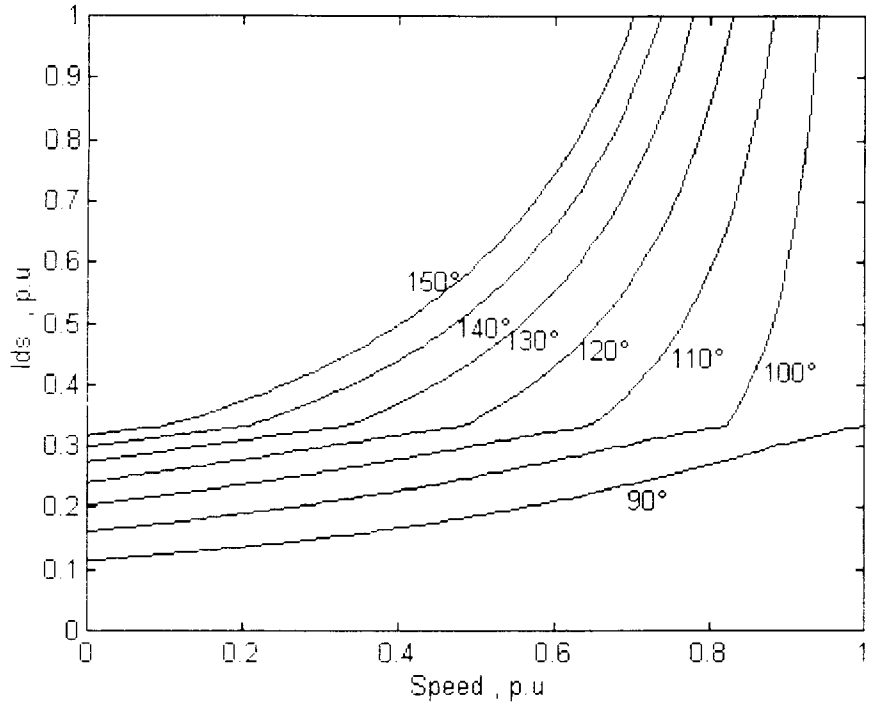

Fig. 2.20 Direct current I_{ds} versus speed

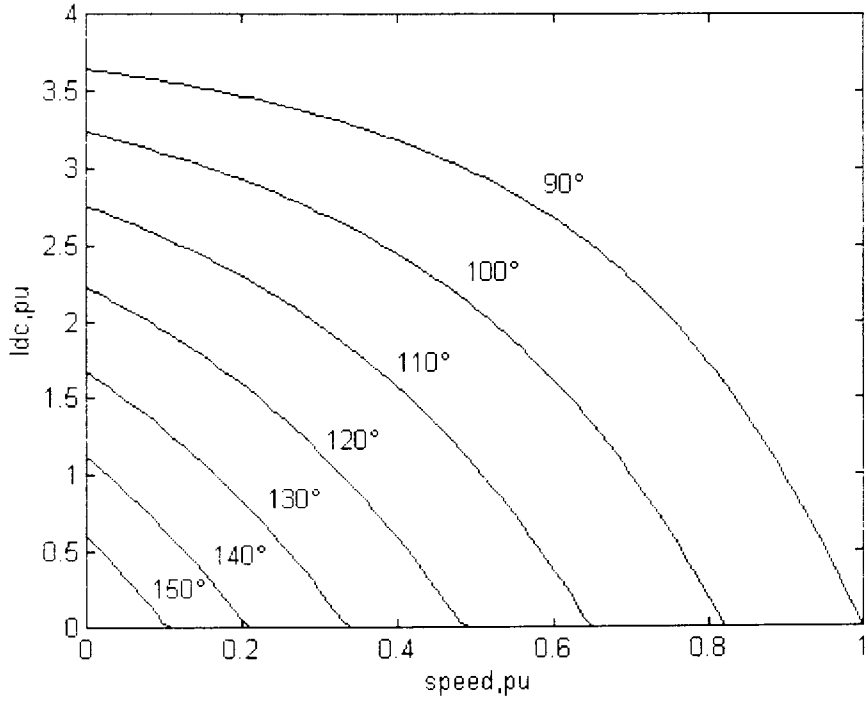

Fig. 2.21 DC link current I_{dc} versus speed

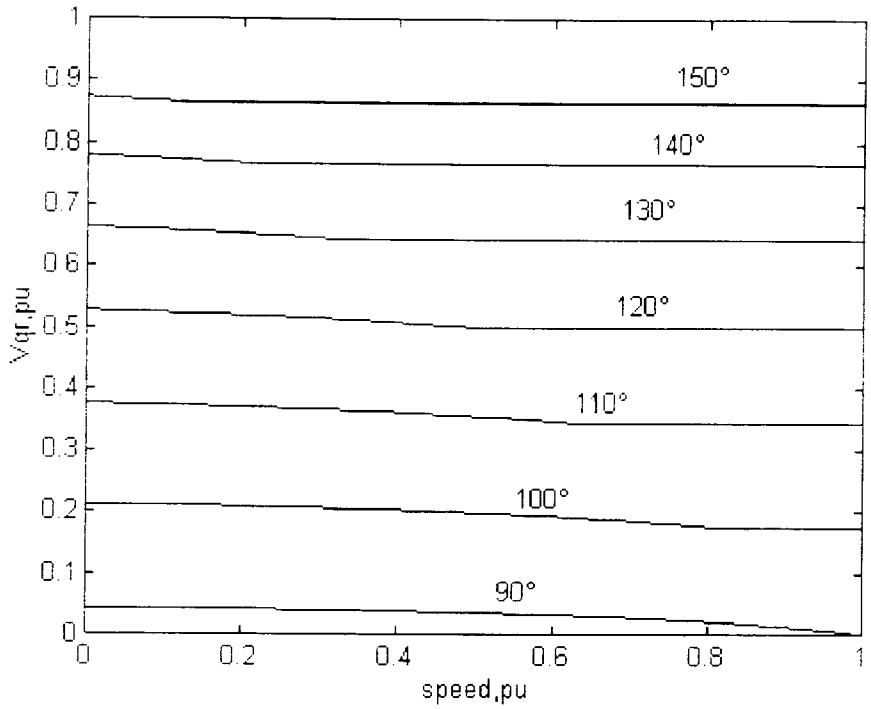

Fig. 2.22 Quadratic rotor voltage V_{qr} versus speed

2.5.7 CONCLUSION AND COMMENTS

The steady state electromagnetic torque T_e and dc link current I_{dc} versus speed characteristics of the system have been predicted using three different models : the DC model, an improved version of the AC model, and a synchronously rotating reference frame DQ model .

On the one hand, we notice that the predicted steady state behaviour by the AC and the DQ models show excellent agreement. On the other hand the electromagnetic torque-speed characteristics predicted by the DC model fundamentally agree with the other simulation results except that computed pull-out torque is now approximately 15 % less than the pull-out torque predicted through the AC and DQ models.

This is due to the overlap effect that has been taken into account in the DC model but neglected in the first two. A 15 % electromagnetic torque reduction due to the overlap effect represents a typical percentage figure estimations mesure made by other authors [5,13,14].

The erroneous assumptions in previous DQ models :

Authors of references [6,12] have made the following simultaneous assumptions :

$$\begin{cases} V_{qs} = V_{ms} \\ V_{ds} = 0 \end{cases} \tag{2.40}$$

$$\begin{cases} V_{qs} = V_{ms} \\ V_{ds} = 0 \end{cases} \tag{2.41}$$

In the process of deducing the voltage forcing functions, they have in fact assumed that the q-axis of the transformed voltage equations is simultaneously positioned at the peak values of the stator and rotor voltages Vas and Var respectively.

If the first set of the assumptions eqn. (2.40) is legitimate, it is however incorrect to assume at the same time the second set eqn. (2.41) to be simultaneously true. Both sets of assumptions can not go hand in hand. They are valid together only if V_{as} and V_{ar} are in phase which is not the case

To clarify the point further, consider the standstill condition under which $w_r = 0$ and slip s = 1.

The stator and rotor frequencies are the same ; stator and rotor voltages V_{as} and V_{ar} have the same frequency, and in order for the q-axis of the transformed equation to be simultaneously positioned at the peak values of V_{as} and V_{ar}, these two voltages must necessarily be in phase. Because of finite primary leakage inductances and magnetizing reactances this can not be normally the case.

The electromagnetic torque T_e plotted as a function of speed is shown in Fig. 2.23 for firing angles ranging from 90° to 150°.

The same drive parameters are used (Appendix A.1). The torque speed characteristics is clearly different. In fact one can notice a fundamental flaw: the theoritical pull out (maximum) torque which must be of a given constant value irrespective of firing angle α is not constant. It is considerably different from one firing angle to another eventhough overlap effect has been neglected. Even in the presence of overlap, the maximum torque that the motor would develop can not show such a wild difference. It is excessively magnified at α = 90°.

This is in clear contrast with plots obtained using various models described in this chapter. In particular, is worth mentioning the perfect agreement between the improved AC model and the DQ model using the correct assumptions (Fig. 2.13 and 2.15)

The fundamental underlying assumptions on which a previous steady state model is based are in fact wrong as noticed by [13] and as further made clear in this chapter. From this incorrect model has been deduced a set of small signal displacement equations representing a linearized version of the system in order to carry out a stability study [6, 10].

Conclusions drawn in these references regarding the Static Kramer Drive stability are therefore questionable.

The stage is now set to develop a linearized model using the small signal perturbation method to study the drive stability.

This will be the object of the coming chapter.

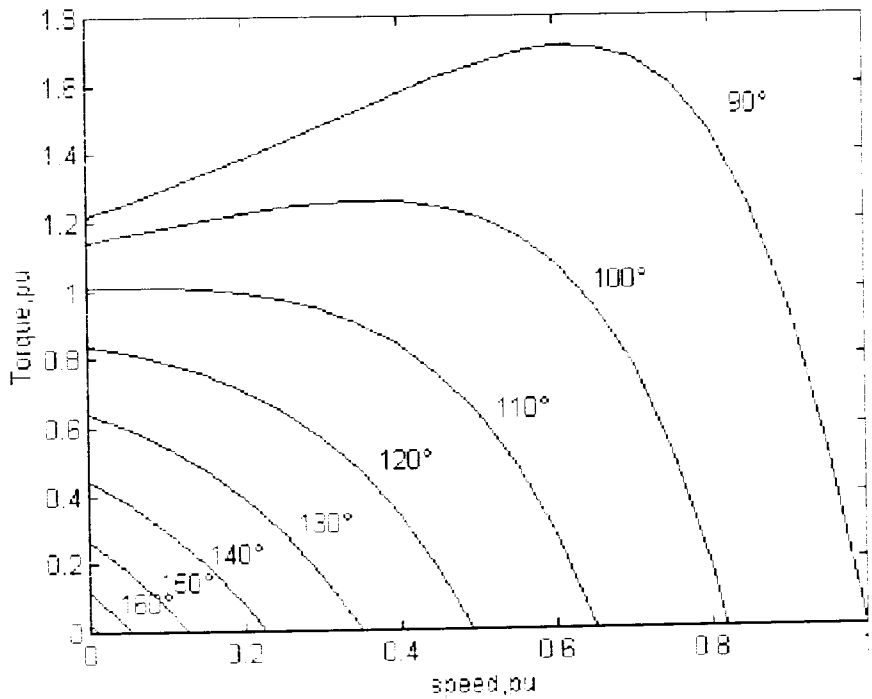

Fig. 2.23 Previous authors torque-speed characteristics

Chapter 3

SIMPLIFIED STABILITY ANALYSIS OF THE STATIC KRAMER DRIVE

3.1.INTRODUCTION

The prediction of the steady state behaviour of the static Kramer drive through the use of the DC and AC equivalent circuits together with a DQ model has proved very satisfactory. Computed characteristics of the drive using the various models have shown very good agreements.

It seems therefore fitting to conduct some stability investigation of the system using a state space model deduced from the DC equivalent circuit before developing a more rigorous model to be presented in chapter 4. The objective is to investigate the effects of some parameters on the system overall relative stability.

One must say that the system model is of the second order. It is well to mention also that controller design for the drive based on the second order model has proved satisfactory [18,19].

A second order state space model deduced from the DC equivalent circuit is first presented. Its linearization together with a root locus analysis are carried out with systematic variation of some specific parameters to study their effects on the drive relative stability. A transfer function of the entire drive in its open loop configuration is then established and commented.

3.2 TRANSFER FUNCTION OF THE DC MODEL

The transfer function valid for small variation around an operating point can be determined , with the following simplifying assumptions :

- The harmonics effects due to the rotor diode bridge are negligible .
- The dc link current is assumed perfectly smooth .

The commutation overlap is included in the system equivalent circuit and is represented by a fictious inductance, same as eqn. (2.8) and given by :

$$R_c = \frac{3\,S\,(X_{ls}' + X_{lr})}{\pi} \qquad (3.1\,a)$$

Where X_{ls}' and X_{lr} are leakage reactances of the stator (referred to rotor) and rotor respectivelly.

The dc equivalent circuit adopted in Fig. 2.2 can be rearranged in order to get the circuit in Fig. 3.1 :

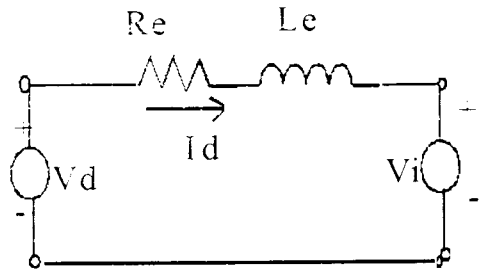

Fig 3.1 DC equivalent circuit of the drive

Where V_d and V_i are the rectifier and inverter output voltages respectivelly, I_d is the dc link current.

R_e is the circuit equivalent resistance given by:

$$R_e = R + SR_1 \qquad (3.1\,b)$$

Where :

$$R = 2R_r + R_d' \qquad (3.1\,c)$$

$$R_1 = 2R_s' + R_c \qquad (3.1\,d)$$

And L_e the circuit equivalent inductance given by :

$$L_e = 2(L_s' + L_r) + L_d' \qquad (3.1\,e)$$

R_r, R_d' and R_s' are resistance of the rotor, filter and stator referred to rotor respectively. L'_s, L_r and L'_d inductance of the stator, rotor and filter respectively.

$$V_d = 1.35SV \tag{3.1.f}$$

$$V_d = 1.35V\cos\alpha \tag{3.1.g}$$

The per unit slip is given by : $S = (w_S - w_r)/w_S$

V is the stator RMS line voltage, w_r the rotor speed (radian/sec) and w_S synchronous speed (radian/sec)

3.2.1 The electrical circuit equation :

The application of the basic voltage Kirchoff's law to the circuit of Fig 2.8 gives the following equation :

$$V_d = R_e I_d + L_e \frac{dI_d}{dt} + V_i \tag{3.2}$$

Or in Laplace notation :

$$SV_{d0} = (R_e + L_e s) I_d + V_i \tag{3.3}$$

Where V_{do} is the standstill rectified rotor voltage and s the Laplace variable.

A small variation around the operating point in the preceding equation gives :

$$\Delta SV_{d01} = (R_{e0} + L_e s)\Delta I_d + \Delta V_i \tag{3.4}$$

Where : $R_{e0} = R - R_1 S_0$

And $V_{d01} = V_{d0} - R_1 I_{d0}$

Where S_0 is the steady state slip.

The steady state dc link current is given by :

$$I_{d0} = \frac{S_0 V_{d0} - V_i}{R + R_1 S_0} \tag{3.5}$$

Note that steady state variables are represented with a subscript 0. And since for small variation of the slip around a steady state value of slip, we obtain :

$$\Delta S = -\frac{\Delta w_r}{w_s} \tag{3.6}$$

Substituting (3.6) in (3.4):

$$-\frac{\Delta w_r}{w_s} V_{d01} = (R_{e0} + L_e s)\Delta I_d + \Delta V_i \tag{3.7}$$

That is:

$$\Delta I_d = \left[-\frac{\Delta w_r}{w_s} V_{d01} - \Delta V_i \right] \frac{1}{(R_{e0} + L_e s)} \tag{3.8}$$

Hence in Laplace transform notation :

$$\Delta I_d(s) = \left[-\frac{\Delta w_r(s)}{w_s} V_{d01} - \Delta V_i(s) \right] \frac{1}{(R_{e0} + L_e s)} \tag{3.9}$$

3.2.2 The mechanical equation of the system :

The drive mechanical equation is given by [19]

$$T_e - T_l = J\frac{dw_r}{dt} + Bw_r \tag{3.10}$$

A small variation around an operating point will yield the following relation:

$$\Delta T_e - \Delta T_l = J\frac{d\Delta w_r}{dt} + B\Delta w_r \qquad (3.11)$$

Where

T_e : The electromagnetic torque [N m]

T_l : The load torque [N m]

B : Friction coefficient or damping coefficient [N m sec/rd]

J : Moment of inertia of complete system [Kg m^2]

In terms of Laplace transform, we have :

$$\Delta w_r(s) = \frac{1}{(B + Js)}\left[\Delta T_e(s) - \Delta T_l(s)\right] \qquad (3.12)$$

Since the electromagnetic torque T_e is approximately proportional to the dc link current I_d, this is given by eqn. 2.5 of chapter 2 :

$$T_e = \frac{V_{d0}}{w_s} I_d \qquad (3.13)$$

For small variations about a steady state operating point we obtain :

$$\Delta T_e(s) = \frac{V_{d0}}{w_s}\Delta I_d(s) \qquad (3.14)$$

3.2.3 The inverter transfer function :

The inverter can be modeled as an amplifier represented by a gain G and a dead time T_i. This is achieved by the following transfer function [19]

$$\frac{\Delta V_i}{\Delta V_c} = \frac{G}{1 + T_i s} \qquad (3.15)$$

Where

V_i : inverter output voltage

G : Amplification factor (negative)

T_i : Inverter time constant.

V_c : control signal that corresponds to a given firing angle

3.2.3.1 The inverter dead time T_i :

The three phase bridge inverter consists of six thyristors. Each one is made to conduct by means of triggering pulses from the triggering unit or drive unit. The position of the triggering pulse with respect to the natural conduction point of an untriggered rectifier or diode is called the triggering delay angle or firing angle α.

The input control voltage V_c to the triggering unit, determines the firing angle α. This voltage is taken to be the input variable and the inverter dc voltage V_i is the output variable.

In the process of varying the firing angle α, that is the inverter voltage V_i by varying the triggering control voltage V_c, the following extreme cases can arise :

a) If a change of firing angle α is called for just before the new triggering angle occurs, then the change will take place immediatly without any delay.

b) If now a change in α is called for just after the new triggering angle has passed, then approximately one sixth of a cycle will elapse before the new value of α can begin to operate. In this case we have a dead time behaviour.

In general the inverter dead time T_i is given by the following statistical mean value [20] :

$$T_i = \frac{1}{2} \frac{\text{Period duration}}{\text{Number of pulses per cycle}} \qquad (3.16)$$

With a 50 Hz mains supply, T_i = 1.67 ms for a six pulse thyristor three-phase bridge.

3.2.4 System block diagram and transfer functions :

The substitution of eqn (3.15) into eqn (3.9) gives the following equation :

$$\Delta I_d(s) = \left[\frac{G}{1+T_i s} \Delta V_c(s) - \frac{\Delta w_r(s)}{w_s} V_{d01} \right] \frac{1}{(R_{e0} + L_e s)} \qquad (3.17)$$

An approximate linear model of the Static Kramer drive is obtained by using equations (3.12), (3.14), (3.15) and (3.17).

Using the preceding equations, the block diagram of the static Kramer drive in its DC model is drawn and shown below in Fig. (3.2).

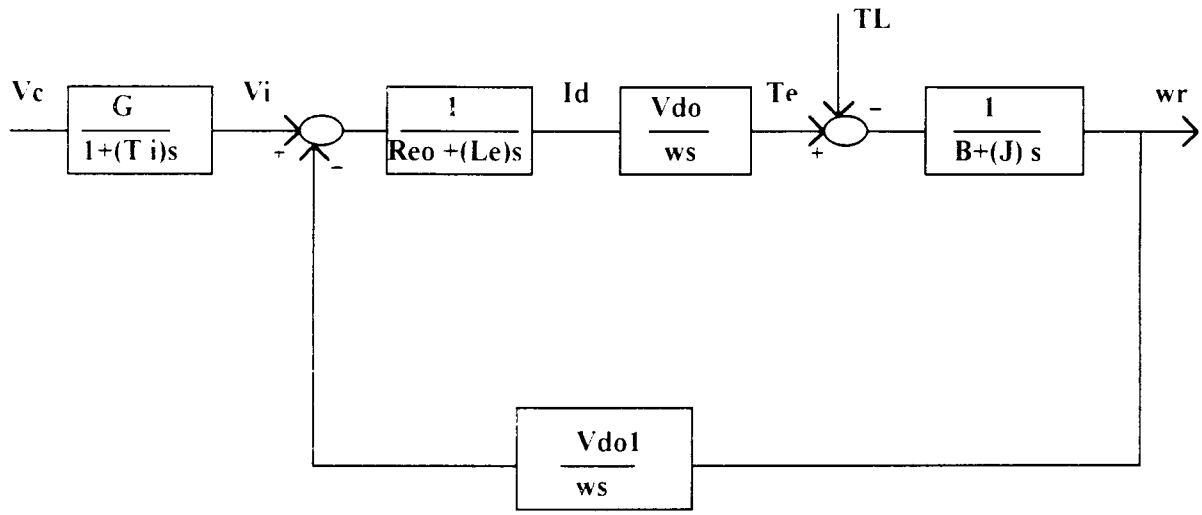

Fig 3.2 DC model block diagram of the Static Kramer Drive

The determination of the transfer function of the system is done for the following two cases

- Constant load torque T_L that is $\Delta T_L = 0$
- Constant firing angle α, i.e., $\Delta V_c = 0$

a) Transfer function at constant load torque : (ΔT_L =0).

Substitution of equations (3.12), (3.14) and (3.15) into equation (3.17) for the constant load torque case, obtained by putting $\Delta T_L = 0$, gives the following transfer function relating the control votage ΔV_c as an input to the rotor speed Δw_r as the output

$$\Delta w_r(s) = \frac{G\dfrac{V_{d0}}{w_s}}{BR_{e0}\left[(1+T_E s)(1+T_m s)+\dfrac{V_{d0}V_{d01}}{BR_{e0}w_s^2}\right](1+T_l s)}\Delta V_c \qquad (3.18)$$

Where

$$T_E = \frac{L_e}{R_{e0}} \qquad (3.19\ a)$$

$$T_m = \frac{J}{B} \qquad (3.19\ b)$$

T_m , T_E are the mechanical and electrical time constants respectivelly. The gain G. of the thyristor inverter and the parameters T_E, T_m ,etc. are not strictly constant and vary with the operating point. They can be assumed to be constant for small variations about the operating point.
The mechanical time constant T_m can be neglected. if it is much larger than the electrical one T_E. This is usually true for higher power machines.
The inverter dead time are particularly small in comparison with usual time constant. it can therefore be neglected to simplify the analysis.

b) Transfer function at constant firing angle α : ($\Delta V_c = 0$)

Substitution of eqns (3.12), (3.14) and (3.15) in eqn (3.17), at constant firing angle α that is at constant voltage control signal V_c, gives a transfer function where the input is the load torque variation ΔT_L and the output is the variation of the rotor speed Δw_r :

$$\Delta w_r(s) = -\frac{(1+T_E s)}{B\left[(1+T_E s)(1+T_m s)+\dfrac{V_{d0}V_{d01}}{BR_{e0}w_s^{\,2}}\right]}\Delta T_l(s) \qquad (3.20)$$

3.3 STABILITY ANALYSIS :

Using the transfer function established in eqn (3.20), the effect of parameter changes on system damping are investigated through plots of roots loci. This is preceded by relevant step response plots pertaining to overlap effect. the parameters chosen are :

(1) Commutation overlap.
(2) Inertia constant H.
(3) Filter inductance L_d (L_d +/- 0.5 Ld nominal value).

The results obtained are presented in the following sections.

3.3.1 The effect of commutation overlap :

System response to step changes in load torque of ΔT_L for different operating points are computed and plotted. The operating point chosen are T_L = 0.1 p.u and 0.6 p.u for firing angles α = 90°, 110° and 130°.
For the first set of operating points, that is, T_L = 0.1 p.u and α = 90°, 110° and 130° the plots are shown in figures 3.11, 3.12 and 3.13. The step responses of the second set are given in Figs. 3.14 , 3.15 and 3.16.
In order to put in evidence the effect of commutation overlap on system relative stability (system damping), each figure corresponds to one operating point for two cases :

- The commutation overlap is taken into account, that is considering the fictious inductance R_c.
- The overlap effect is neglected, this done by putting R_c = 0.

The drive parameters used are in Appendix A.1.

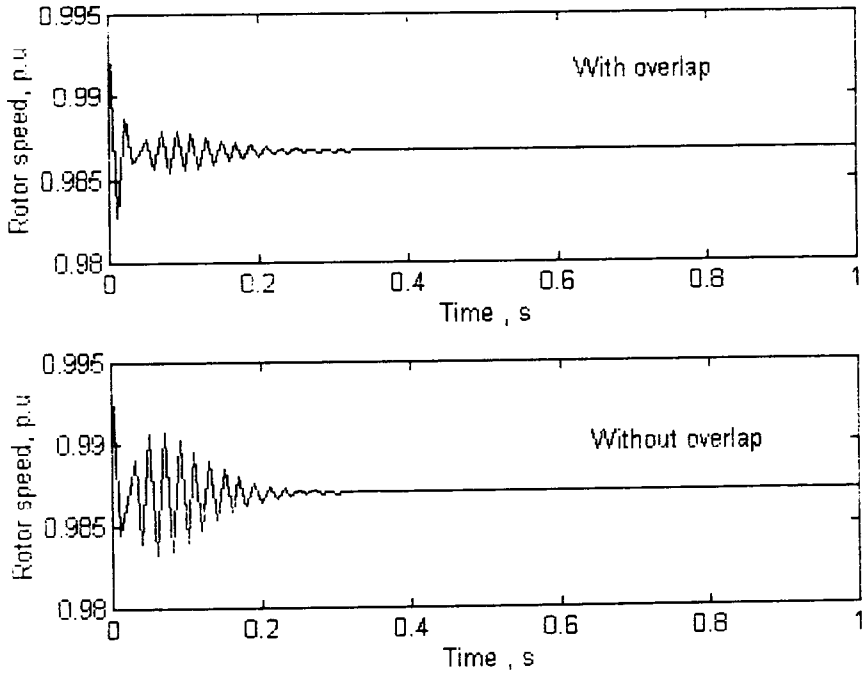

Fig. 3.11 Step responses of the system by ΔT_L = 0.1 p.u
(α = 90° & T_L = 0.1 p.u)

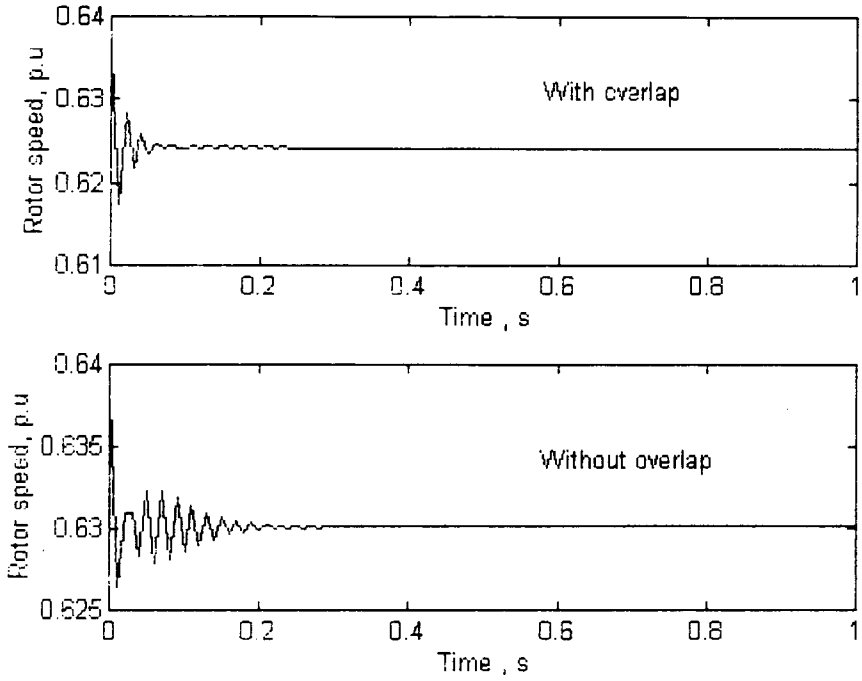

Fig. 3.12 Step Responses of the system by $\Delta T_L = 0.1$ p.u
($\alpha = 110°$ & $T_L = 0.1$ p.u)

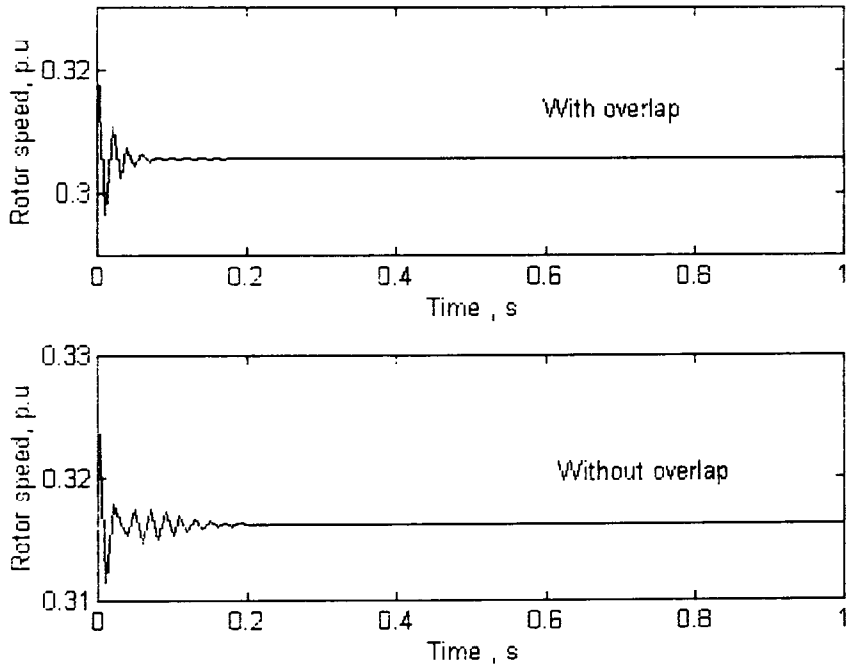

Fig. 3.13 Step responses of the system by $\Delta T_L = 0.1$ p.u
($\alpha = 130°$ & $T_L = 0.1$ p.u)

The change of the initial operating point is investigated with a new initial load torque T_L=0 6 p u. The results obtained are given in Fig 3.14, 3 15 and 3 16.

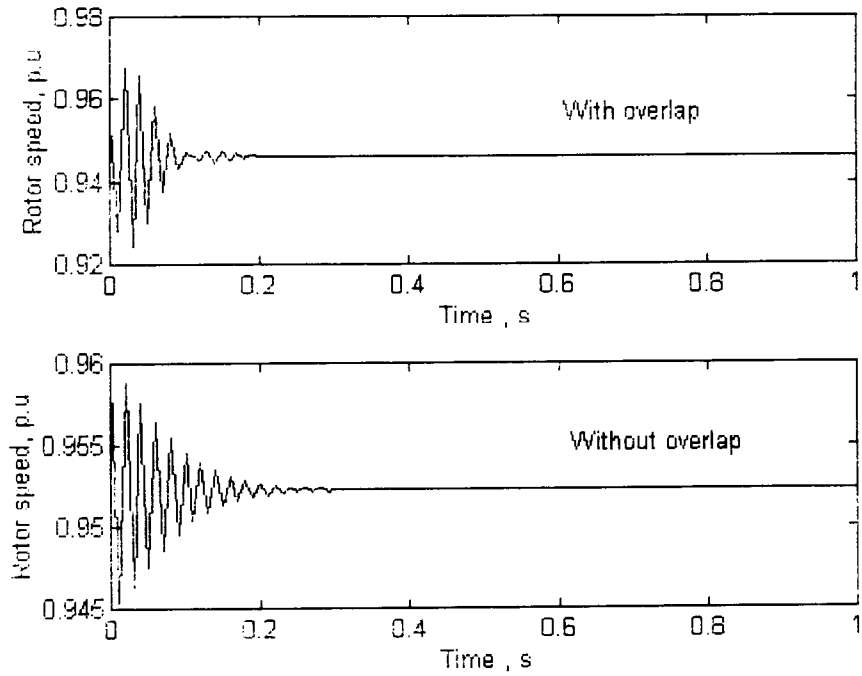

Fig. 3.14 System responses to step change in load torque ΔT_L = 0.1 p u (α = 90° & T_L = 0.6 p.u)

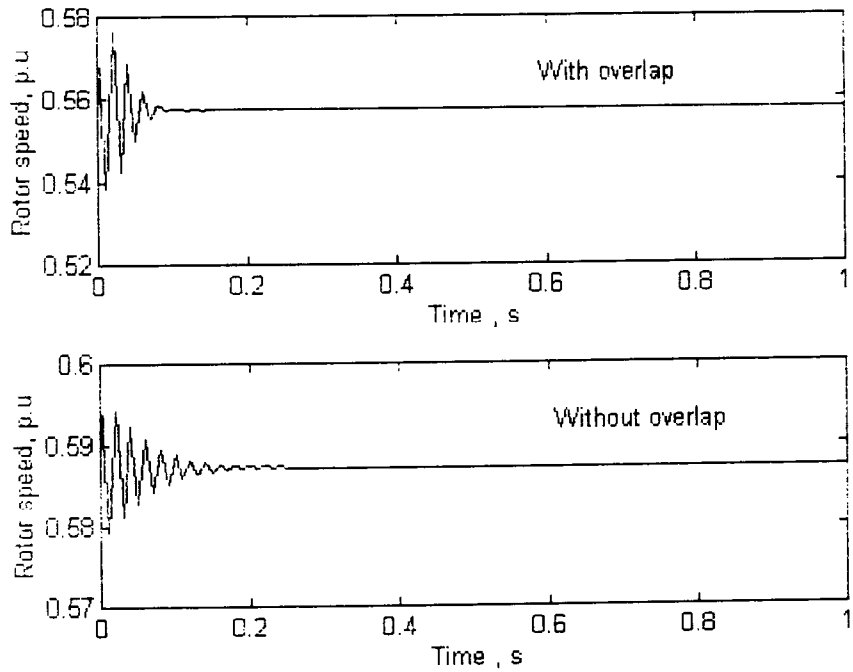

Fig. 3.15 Responses to step change in load torque ΔT_L = 0.1 p u (α = 110° & T_L = 0 6 p u)

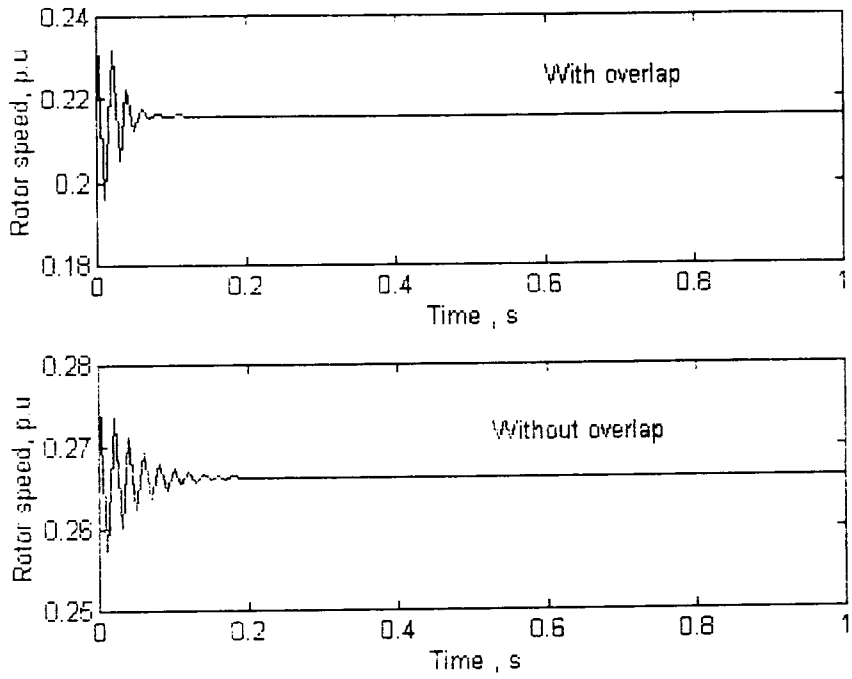

Fig. 3.16 Responses to step change in load torque ΔT_L = 0.1 p.u (α = 130° & T_L = 0.6 p.u)

The commutation overlap if taken into account will increase system stability. This is an important consideration, when the stability of the system is investigated, because neglecting overlap will simplify the analysis on the one hand, and make predictions more pessimistic, hence "safer" on the other.

3.3.2 Effect of inertia constant H variation :

The effect of variation of the inertia constant H, is investigated by varying it within a practical range of values, that is from 0.01 s to 0.5 s and see the effect on the drive relative stability. This is done by plotting the loci of the eigenvalues of the system for each value of the inertia constant H, in the s- plane, for operating points corresponding to a load torque T_L = 0.1 p.u at firing angles α =90°, 100, 110° and 120°. Results are shown in Fig. 3.17.

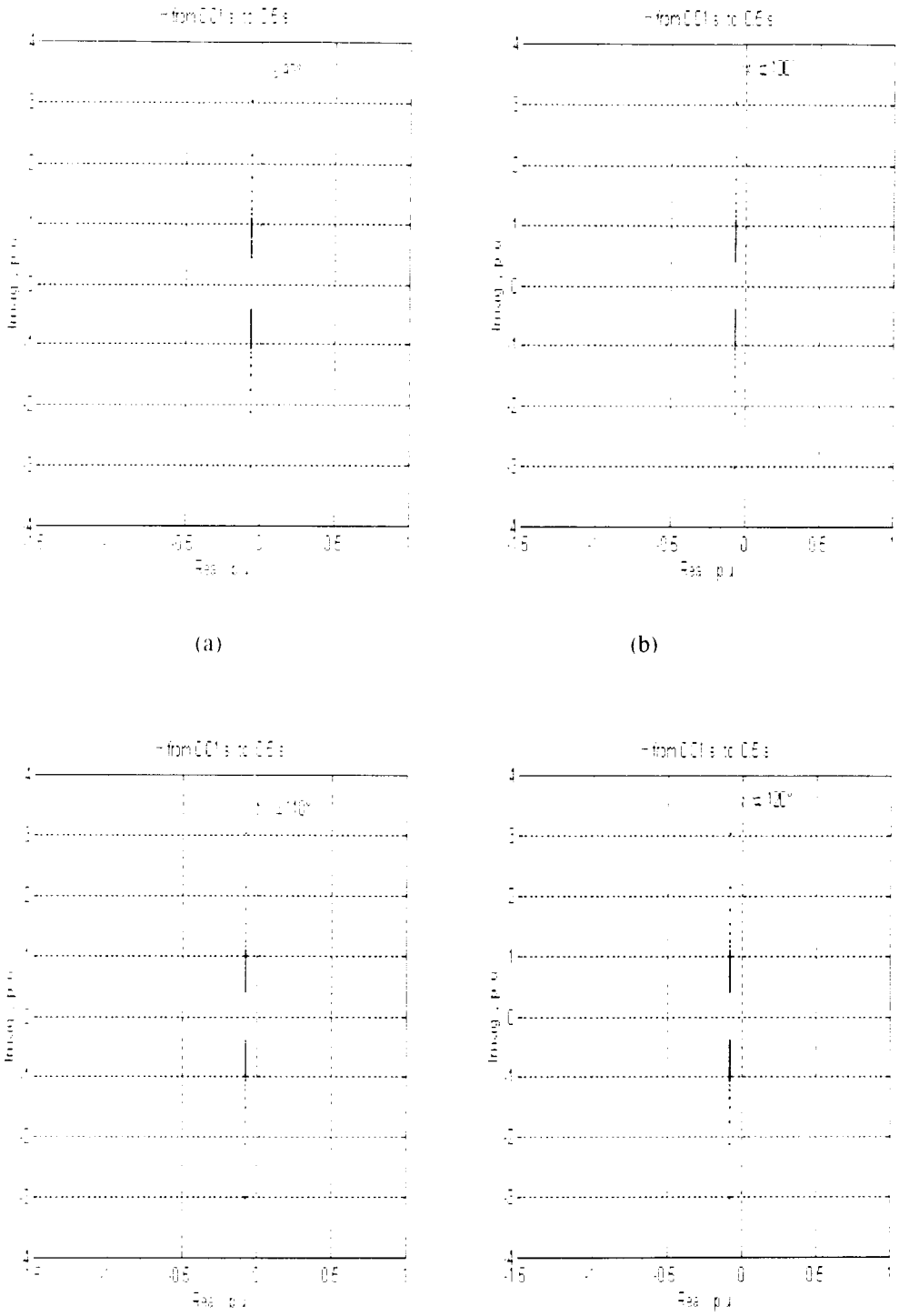

(a) (b)

(c) (d)

Fig. 3.17 Roots loci for H variation (T_L = 0.1 p u)

3.3.3 Effect of filter inductance L_d variation :

The effect of varying the filter inductance L_d on system stability is also studied by varying it from its nominal value (1 p.u) to 10 p.u.
That is done for firing angles α = 90°, 110° and 130° for small variation of the load torque ΔT_L = 0.1 p.u. The plots are shown in figure 3.18 (a), (b), (c) and (d).
From plots of figure 3.18, it can be seen that any increase in the filter inductance L_d will decrease system relative stability (less damping).
Also, as the firing angle α decreases, system relative stability decreases.
The drive remains stable irrespective of parameter changes.
An interesting case to consider is that when the filter inductance gets infinitely large, i.e., L_d varying from 1 p.u to 1000 p.u., for α = 90°.
The system gets limitedly or marginally stable as shown in Fig. 3.18 (d).

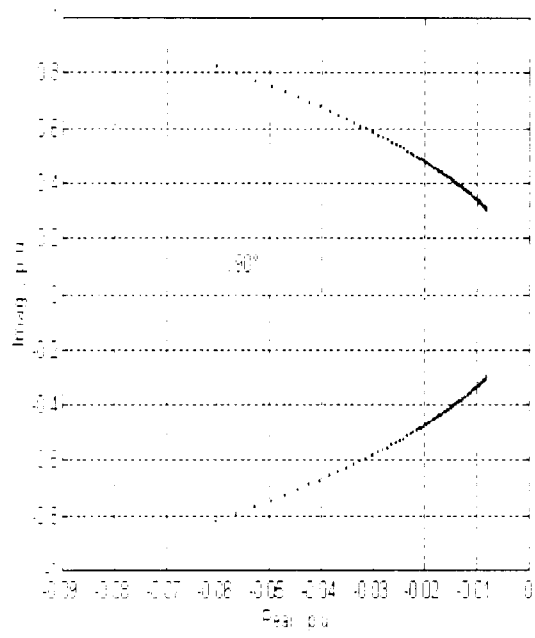

(a)

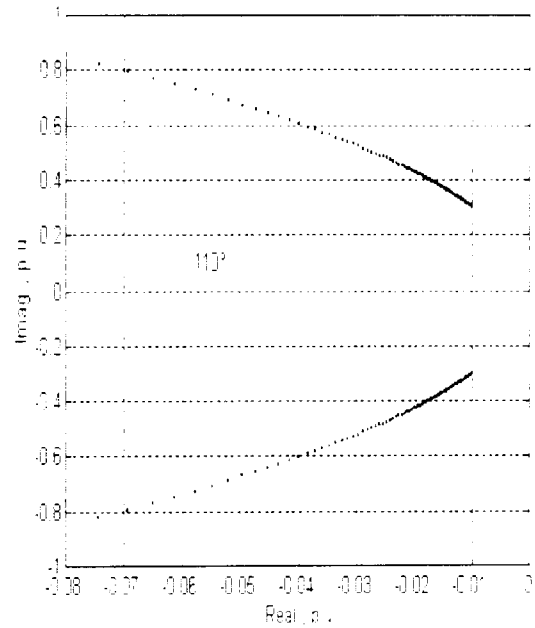

(b)

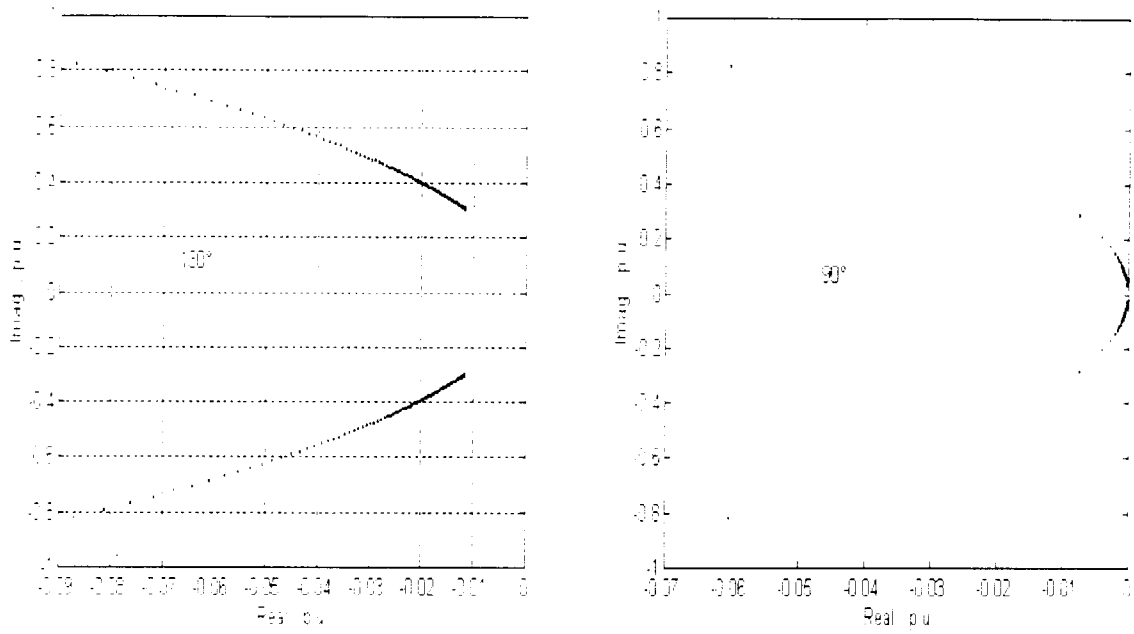

(c) (d)

Fig. 3.18 Eigenvalues loci for variation of L_d (T_L = 0.1 p.u.)

3.4 CONCLUSION

The effects of commutation overlap and variations of the system inertia constant H and dc link choke inductance L_d have been investigated with the simplified second order model of the static Kramer drive.

Any increase in the system filter inductance L_d will decrease the system relative stability. In contrast, if the inertia constant H is increased the drive the stability is not affected.

When commutation overlap is taken into account, the system response to any step change in load torque is less oscillatory, that is more damped as shown in Fig. 3.11 through to Fig. 3.16, than if it is neglected.

Thus according to the preceding simulations, neglecting the commutation overlap in the stability analysis of the drive, will effectively correspond to the worst case condition.

Chapter 4

STABILITY ANALYSIS OF THE STATIC KRAMER DRIVE

4.1 INTRODUCTION

The equations describing the behaviour of the drive are non linear and can therefore only be solved numerically with the help of a computer. However, considerable physical insight into the system can be gained when considering its small displacement behaviour obtained from a linearized version of the non linear equations describing the real system. Small displacement method is extensively used in machine stability investigation [6,12,21,22].

It should however be stressed that for non linear systems, such as the static Kramer drive, the behaviour for small deviations about an equilibrum point may well be different from that for large deviations. In other words, local stability does not imply global stability; that is, stability in the overall state plane. The two concepts should be considered separately.

General conclusions reached about the system (local) stability using a linearized version of the system equations can be usefully compared with results obtained by solving the system non linear equations for small (and large) deviations.

Linearisation of the system of equations can be carried out by applying the small signal perturbation method. The resulting set of linear time invariant differential equations will describe the dynamic behaviour for small excursions about an operating point; the drive can be treated as a linear system so long as it is subjected to small disturbance where upon the powerful linear theory can be applied to calculate eigenvalues and useful conclusions can be deduced regarding the open loop stability of the system.

Furthermore, in practical systems, it is not sufficient to know that the system is stable or not, but a stable system should meet specifications on relative stability, a quantitative measure of how fast transients die out in the system following a disturbance.

Relative stability can be measured by the settling times of each root or pair of roots (eigenvalues). It is also a measure of system damping. As these roots move further away to the left from the j-axis, the relative stability of the system improves, i.e., settling times are shorter, the amount of damping is greater.

The object of this chapter is the development of a linearized DQ model of the static Kramer drive expressed in the synchronously rotating reference frame. This is followed by a comprehensive eigenvalue stability analysis of the linearized model for several operating points together with computed non linear system responses.

4.2 THE LINEARIZED MODEL

The non linear DQ model of the static Kramer drive in its state space form obtained by combining eqns. (2.35), (2.36), (2.37) and (2.38), where the state vector is defined by : (I_{qs}, I_{ds}, I_{qr} , w_r/w), is given by :

$$\begin{cases} \left(\frac{1}{w}\right) pI_{qs} = X_m V_{ms}\cos\alpha + \frac{ZV_{qs}}{K} - \frac{ZR_s}{K} I_{qs} - \frac{(ZX_{ss} - sX^2_m)}{K} I_{ds} + \frac{RX_m}{K} I'_{qr} \\ \left(\frac{1}{w}\right) pI_{ds} = sI_{qs} + s\frac{X'_{rr}}{X_m} I'_{qr} \\ \left(\frac{1}{w}\right) pI'_{qr} = -\frac{X_{ss} V_{ms}\cos\alpha}{K} - \frac{X_m}{K} V_{qs} + \frac{R_s X_m}{K} I_{qs} + \frac{X_m X_{ss}(1-s)}{K} I_{ds} - \frac{RX_{ss}}{K} I'_{qr} \\ \left(\frac{1}{w}\right) p\left(\frac{w_r}{w}\right) = -\frac{X_m}{2wH} I_{ds} I'_{qr} - \frac{T_L}{2wH} \end{cases} \quad (4.1.a)$$

And :

$$s = 1 - \frac{w_r}{w} \quad (4.1.b)$$

$$V_{ds} = X_{ss}(s-1) I_{qs} + R_s I_{ds} + \frac{(sX'_{rr} X_{ss} - X^2_m)}{X_m} I'_{qr} \quad (4.1.c)$$

$$V^2_{ms} = V^2_{qs} + V^2_{ds} \quad (4.1.d)$$

Where :

$$Z = X'_{rr} + X'_{d}\frac{\pi^2}{18}$$

$$R = R'_{r} + R'_{d}\frac{\pi^2}{18}$$

$$K = Z X_{ss} - X_{m}^2$$

The small signal perturbation method and eigenvalue analysis will now be used, to study the stability of static Kramer drive. In this method all variables are allowed to change by a small amount about a steady-state operating point. All system variables except the firing angle α and supply voltage V_{ms}, are expressed in the form $f_i = f_{io} + \Delta f_i$, where f_{io} is the steady state value of the variable and Δf_i is the small excursion of this variable about its steady state value. The terms which describe the steady-state peration are eliminated. Higher-order incremental terms are neglected. The resulting set of state space linear differential equations of the static Kramer drive is then obtained (See Appendix. C, for details):

$$\dot{X} = AX + BU \tag{4.2}$$

Where: X= (ΔI_{qs}, ΔI_{ds}, ΔI_{qr} , $\Delta(w_r/w)$) and U the input vector.

$$A = \begin{bmatrix} A_{11} & A_{12} & A_{13} & A_{14} \\ A_{21} & 0 & A_{23} & A_{24} \\ A_{31} & A_{32} & A_{33} & A_{34} \\ 0 & A_{42} & A_{43} & 0 \end{bmatrix} \tag{4.3}$$

$$B = \begin{bmatrix} 0 \\ 0 \\ 0 \\ -\dfrac{T_l}{2\omega H} \end{bmatrix} \tag{4.4}$$

With:

$$A_{11} = \frac{Z(b_0 - R_s)}{K} \quad ; \quad A_{12} = \frac{a_0 Z - Z X_{ss} + S_0 X_m^2}{K} \quad ; \quad A_{13} = \frac{Z c_0 + X_m R}{K} \quad ;$$

$$A_{14} = \frac{Z d_0 - X_m^2 I_{ds0}}{K}$$

$$A_{21} = S_0 \; ; \; A_{23} = \frac{S_0 X'_{rr}}{X_m} \; ; \; A_{24} = -\frac{I_{qs0} X_m + X'_{rr} I_{qr0}}{X_m} \; ;$$

$$A_{31} = \frac{(R_s - b_0) X_m}{K} \; ; \; A_{32} = \frac{X_m X_{ss}(1 - S_0) - a_0 X_m}{K} \; ; \; A_{33} = -\frac{R X_{ss} + c_0 X_m}{K}$$

$$A_{34} = \frac{I_{ds0} X_m X_{ss} - d_0 X_m}{K}$$

$$A_{42} = -\frac{X_m I_{qr0}}{2\omega H} \; ; A_{43} = -\frac{X_m I_{ds0}}{2\omega H}$$

$$m_0 = \frac{I_{ds0}}{I_{qs0}} \; ; a_0 = -m_0 a \; ; \; b_0 = m_0 b \; ; \; c_0 = m_0 c \; ; \; d_0 = m_0 d \; ;$$

$$a = R_s \; ; \; b = X_{ss}(S_0 - 1) \; ; \; c = \frac{S_0 X'_{rr} X_{ss} - X_m^2}{X_m} \; ; \; d = -\frac{X_{ss}(X_m I_{qs0} + X'_{rr} I_{qr0})}{X_m} \; ;$$

$$S_0 = 1 - \frac{\omega_{r0}}{\omega}$$

4.3 EIGENVALUES ANALYSIS

The study of the system is accomplished by the evaluation of matrix A in the complete operating region at different values of slip ranging from minimum to maximum values ,fixing the firing angle of the inverter in the range 90°-150°.

The eigenvalues of matrix A decide the stability of the system .The system is stable if all the eigenvalues have negative real parts. The system is unstable even if one eigenvalue has positive real part. The effect of the system parameters can be studied by repeating the above procedure for each value of the parameter, then plotting the loci of the eigenvalues in the s-plane. If one eigenvalue is located in the right hand side of the s-plane the system is unstable.When located on the j-axis it is limitedly stable and stable if it is in the left hand side of the s-plane.

The eigenvalue loci investigation carried out for several operating points. An operating point (or equilibrium point) is determined on the torque-speed plane by the intersection of the electromagnetic torque Te and the load torque T_L for a given firing angle α, thus dictating the value of the speed. Conversely, the speed and load torque can be fixed and the required firing angle for this operating point deduced.

In this study, the firing angle α and the load torque T_L are fixed for a specific operating point and the speed (or slip) then deduced. In this manner all relevant operating points are considered.

Using the parameter values in per unit of the drives listed in appendix A the system is studied for four operating points, corresponding to the following p.u load torques : T_L = 0.1, 0.4, 0.6 and 0.9 p.u .

The system will contain four poles, but attention is only focused on the dominant ones, i.e., those closest to the j-axis , because they are the first poles that may cross the j-axis in case of parameter changes, and therefore to decide upon the stability of the system. For any operating point , the effect of the system parameters variation on system stability can be studied by computing the eigenvalues of the matrix A for each value of the parameter taken as an independent variable.The parameters varied in our case are the inertia constant H, the dc link filter reactance X_d , the stator resistance R_S, rotor resistance R_r and finally the supply voltage V_{ms}.

Eigenvalues loci are computed for given system parameter variations within some relevant practical range.

Support of analytical predictions is afterward, sought through plots of transient responses of the drive to step changes in load torque obtained by numerical integration.

Finally, Some startup transients are given at loaded conditions. During a switching operation or some other changes in the operating conditions, the drive experiences transient torques, the instantaneous of which may reach several times the steady state value. Although, this condition may persist only for a few short time, the transient torques may impose undue strain on the mechanical parts and shaft failure may result. The most important transients from electromechanical point of view are those of the electromagnetic torque and speed [24]. The study is applied to three static Kramer drives of different power levels, 5 hp, 500 hp and 2250 hp.

4.4 5 hp machine drive

4.4.1. Eigenvalues loci

4.4.1.1 Effect of the inertia constant H variation :(from 0.01 to 0.5 s)

The loci of the eigenvalues of the system matrix A when the inertia constant H is varied at the following firing angles a α= 90° , 100° , 110° and 120° for load torques T_L = 0.1 , 0.4 ,0.6 and 0.9 p.u are shown in Fig. 4.1 through to Fig. 4.4 .

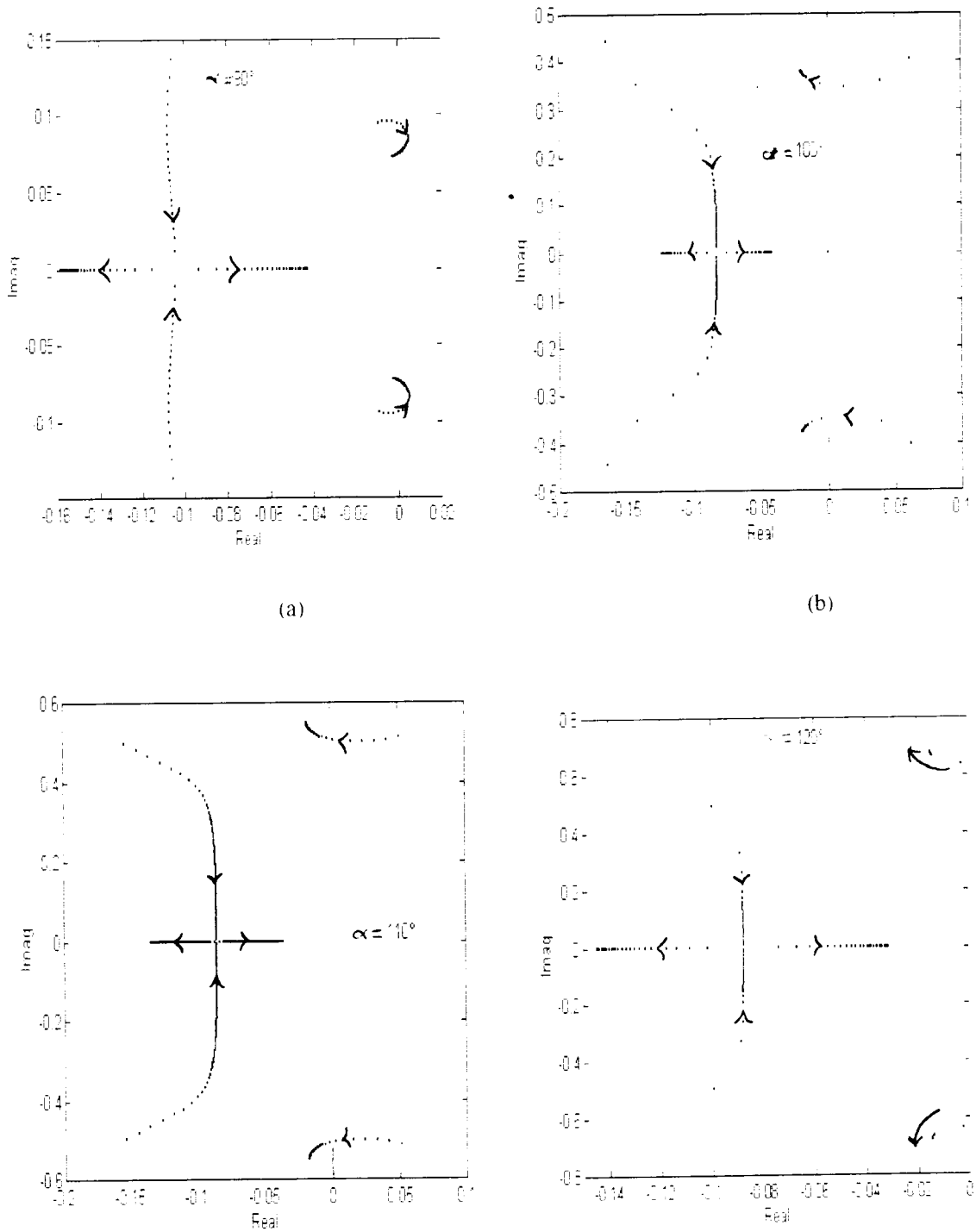

Fig. 4.1 Eigenvalues loci for load torque T_L = 0.1 p.u

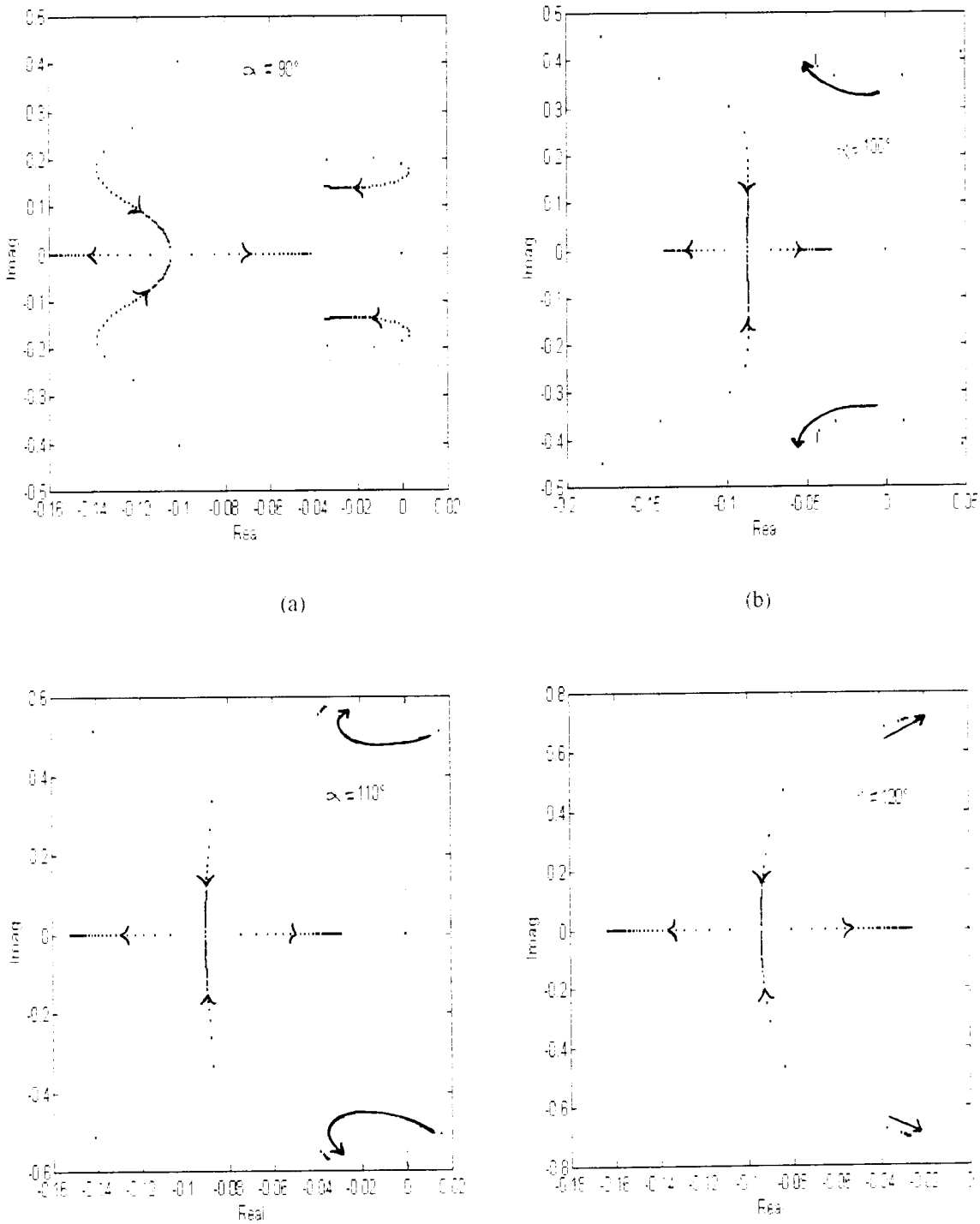

Fig. 4.2 Eigenvalues loci for H variation (T_L = 0.4 p.u)

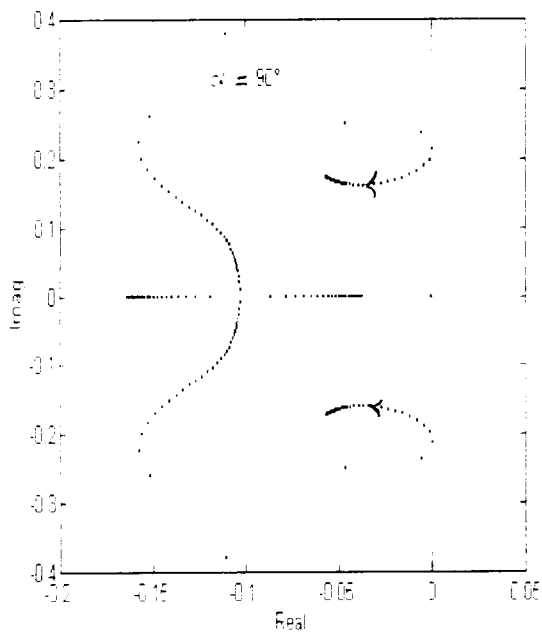

(a)

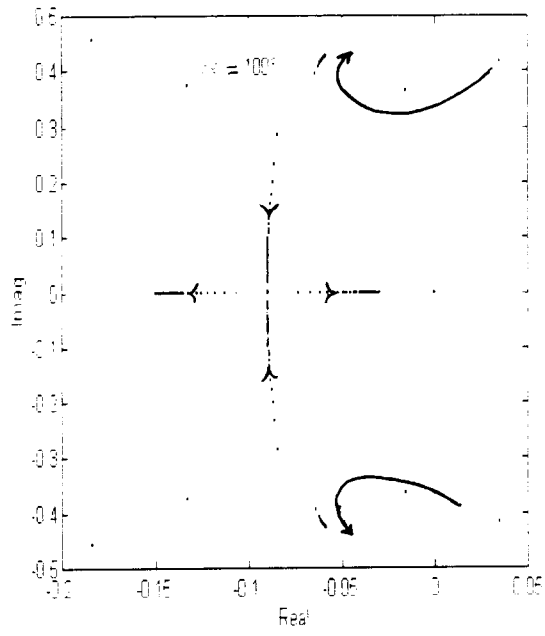

(b)

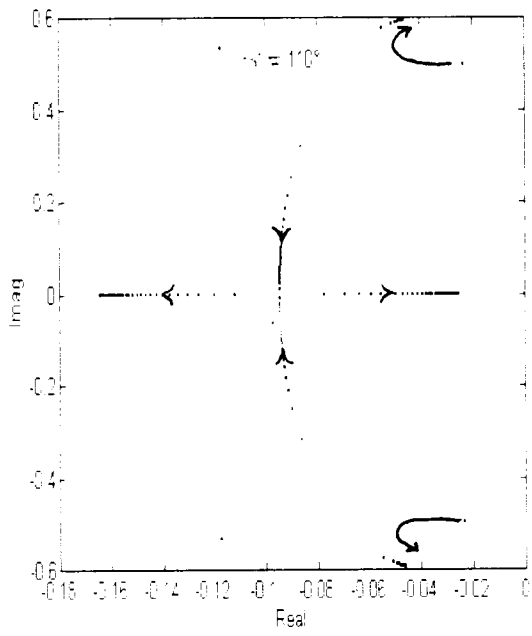

(c)

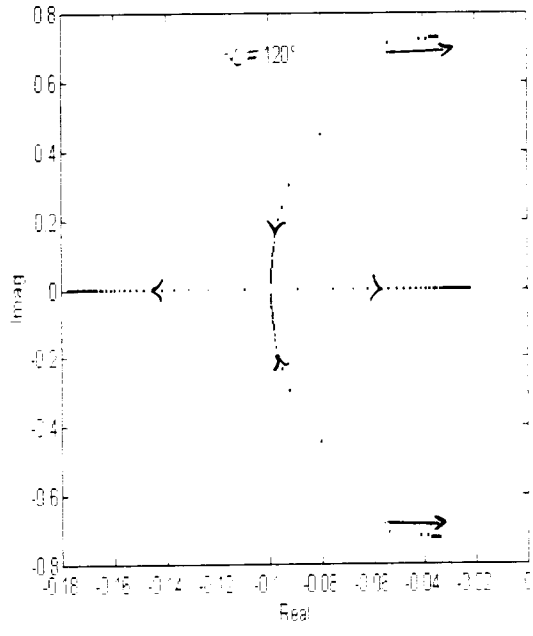

(d)

Fig. 4.3 Eigenvalues loci for H variation (T_L = 0.6 p.u)

At load torque T_L = 0.1 p.u :

For a firing angle α = 90°, as H is increased from 0.01 to 0.05 s, the system relative stablilty decreases. The drive is unstable for H between 0.06 and 0.36 s. As H is bigger or equal to 0.36 s the system becomes marginally stable and then stable.

For α = 100° the drive is unstable for a range of the inertia constant H between 0.01 s to 0.03 s. But as H is made greater than 0.04 s the system relative stability is enhanced.

For α = 110°, if H = 0.01 s the drive is unstable. When H is greater than 0.02 s the system relative stability is increased.

For α = 120°, instability is possible only for inertia constants less than 0.008 s which is not practical, i.e., for the applicable range of variation of H, the system relative stability is enhanced as H is increased.

At T_L = 0.4 p.u :

For α = 90°, the relative stability decreases for H varying between 0.01 and 0.03 s. The system is unstable for H between 0.04 s and 0.07 s and gains in relative stability for H bigger or equal to 0.08 s.

For α = 100°, instability of the drive is possible for H between 0.01 s and 0.02 s. The relative stability increases as H increases from 0.03 s and decreases from 0.1 s.

For α = 110°, instability occurs if H=0.01 s. When H is greater than 0.02 s the drive relative stability is better. But for H greater than 0.1 s, it is worsened.

For α = 120°, The system relative stability decreases as H increases. But the drive remains always stable.

At T_L = 0.6 p.u :

For α = 90°, the system relative stability decreases when H goes from 0.01 to 0.02 s, instability occurs at H = 0.03 s Finally, the relative stability increases as H increases from 0.04 s and decreases from 0.3 s onwards
For α = 100° , the system is unstable for H = 0.01 s, and its relative stability decreases as H increases from 0.02 s onwards.
For α = 110° and 120° the system relative stablilty decreases as H increases, but it remains always stable.

At T_L = 0.9 p.u :

For α = 90°, the drive relative stability decreases as H varies from 0.01 to 0.02 s, increases for H between 0.03 to 0.29 s and decreases from 0.3 s onwards. For α = 100°, if H = 0.01 s the drive is unstable, from 0.02 to 0.04 s its relative stablilty increases and it decreases for H from 0.05 s onwards. For α = 110° and 120°, the system relative stability decreases as H increases.

4.4.1.2 Effect of filter reactance X_d variation :(from 0.5 to 1.5 p.u)

The loci of the eigenvalues of the system matrix A when the filter reactance is varied for the following firing angles:α=90°,100°,110° and 120°, for load torques T_L= 0.1, 0.4 and 0.9 p.u are shown in Fig. 4.5 through to Fig. 4.7 .

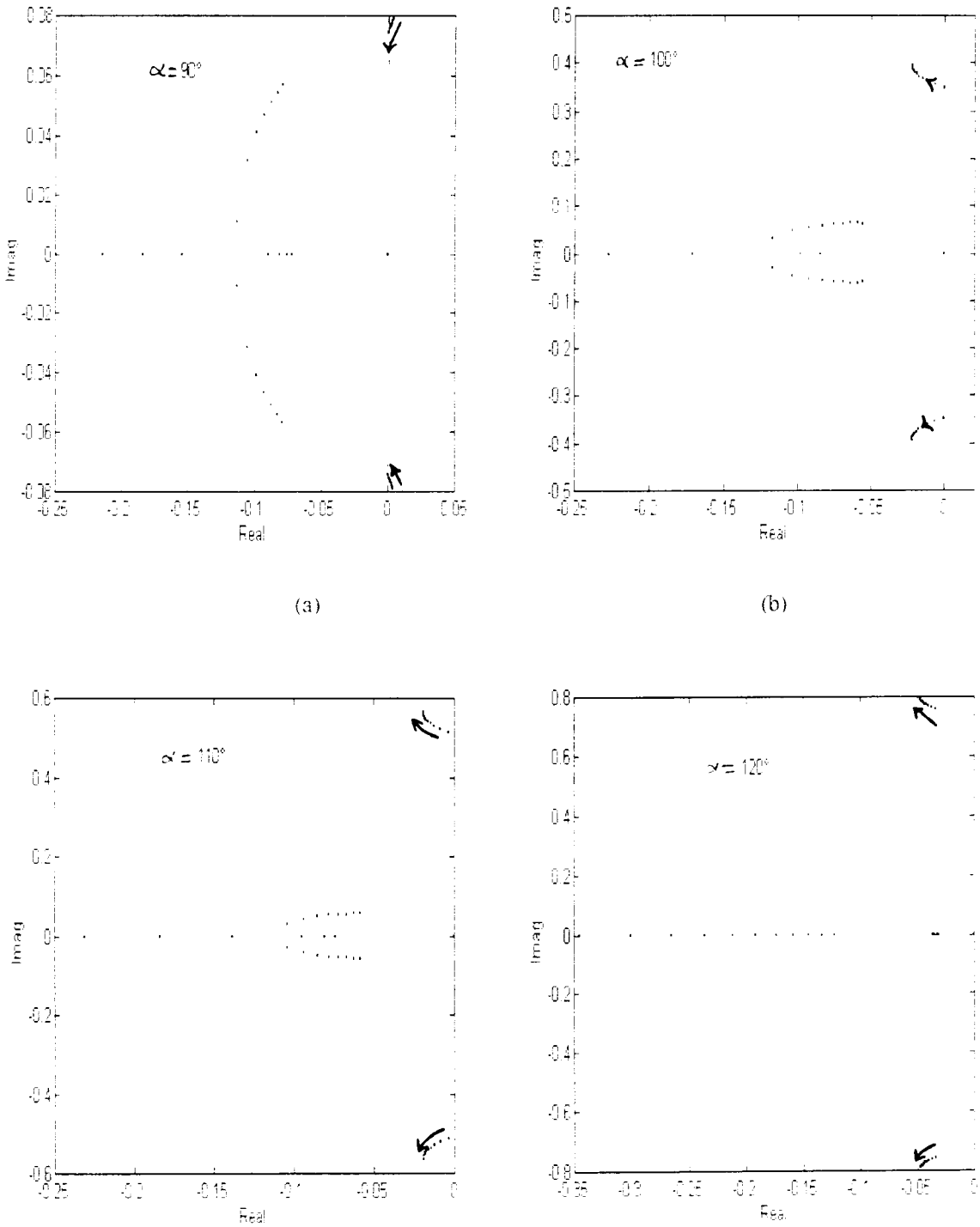

Fig. 4.5 Eigenvalues loci for X_d variation (T_L = 0.1 p u)

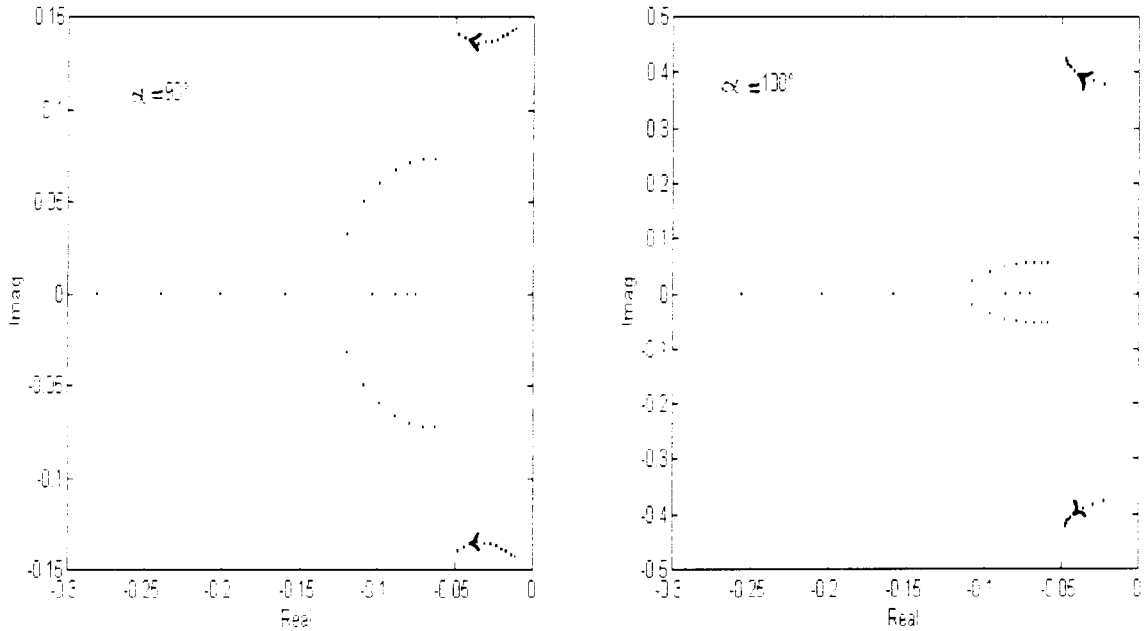

(a) (b)

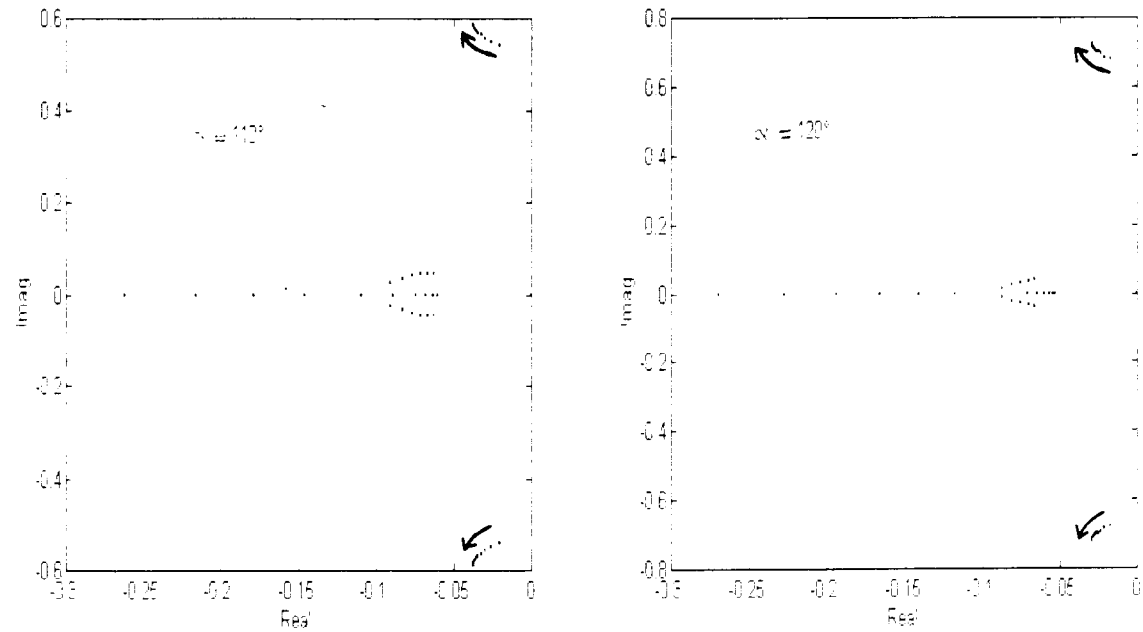

(c) (d)

Fig. 4.6 Eigenvalues loci for X_d variation (T_L = 0.4 p.u)

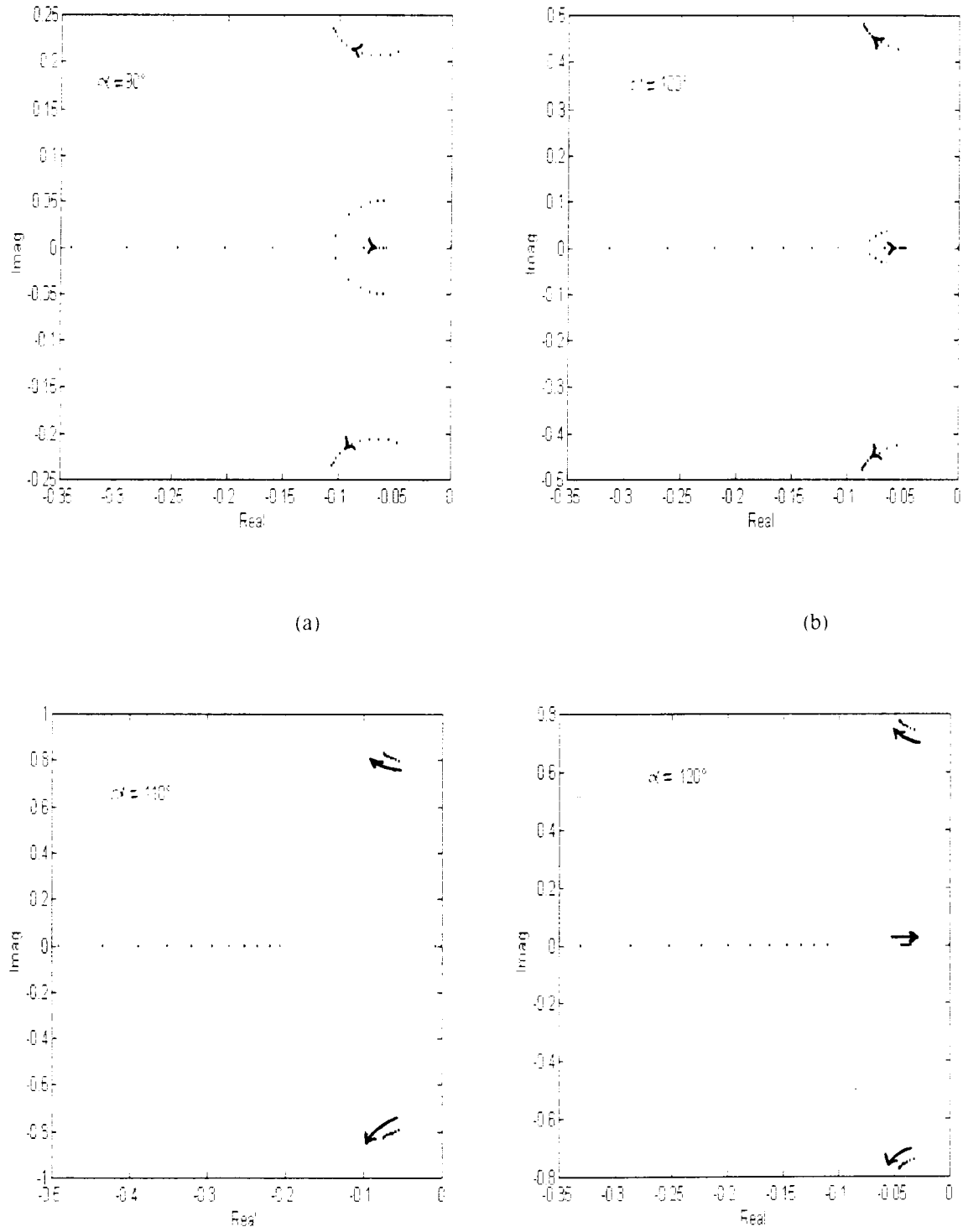

Fig. 4.7 Eigenvalues loci for X_d variation (T_L = 0.9 p.u)

At T_L = 0.1 p.u :

The system is unstable (H = 0.25 s) but its eigenvalues are pushed tothe left hand side of the s-plane as X_d is increased. Increase in X_d help stabilize the drive.

At T_L = 0.4 p.u and 0.6 p.u :

The relative stability increases as X_d increases for all the firing angles.

At T_L = 0.9 p.u :

For α = 90°, 100°, 110° and 120°, the relative stability decreases for any variation of X_d around 1.1 p.u, 1.2 p.u , 1.3 p.u and 1.5 p.u respectively.

4.4 .1.3 Effect of stator resistance R_s variation :

The effect of the stator resistance R_s variation is investigated by varying R_s by 50 % more or less its nominal value R_s = 0.058 p.u, at operating points T_L = 0.1 and 0.9 p.u. This is shown in Fig. 4.8 and 4.9

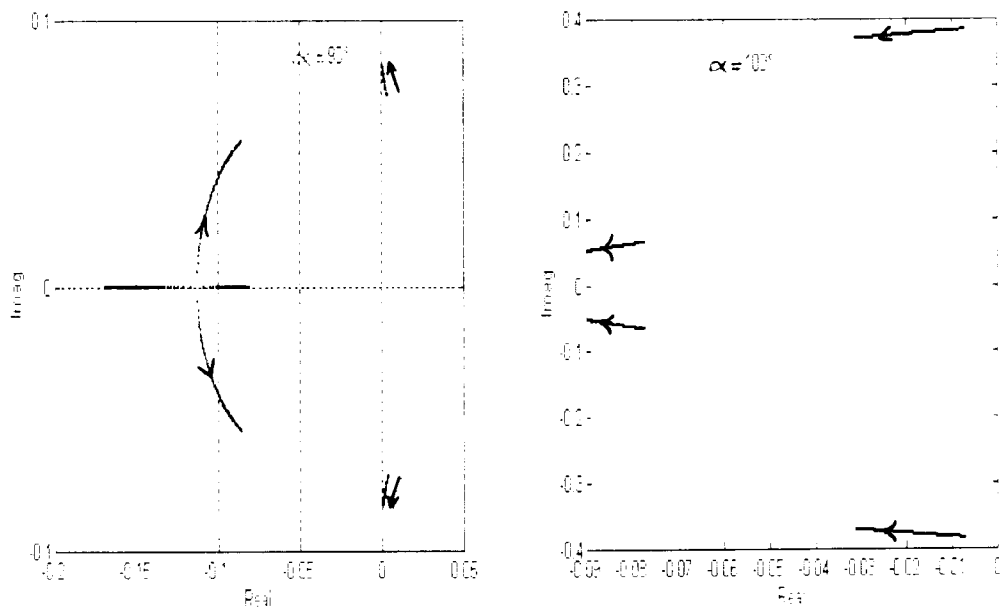

(a) (b)

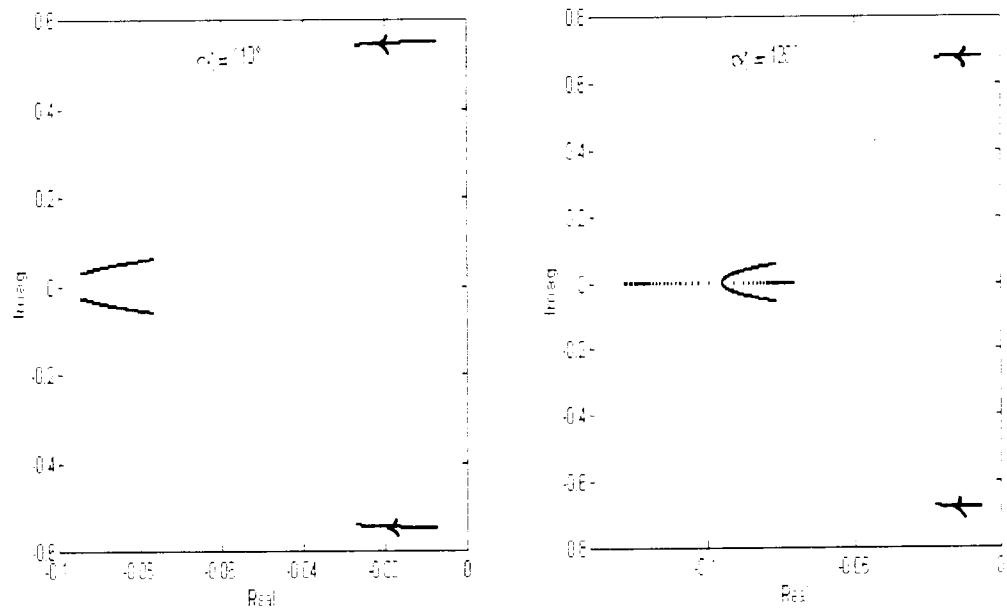

(c) (d)

Fig. 4.8 Eigenvalues loci for R_S variation (T_L = 0.1 p u)

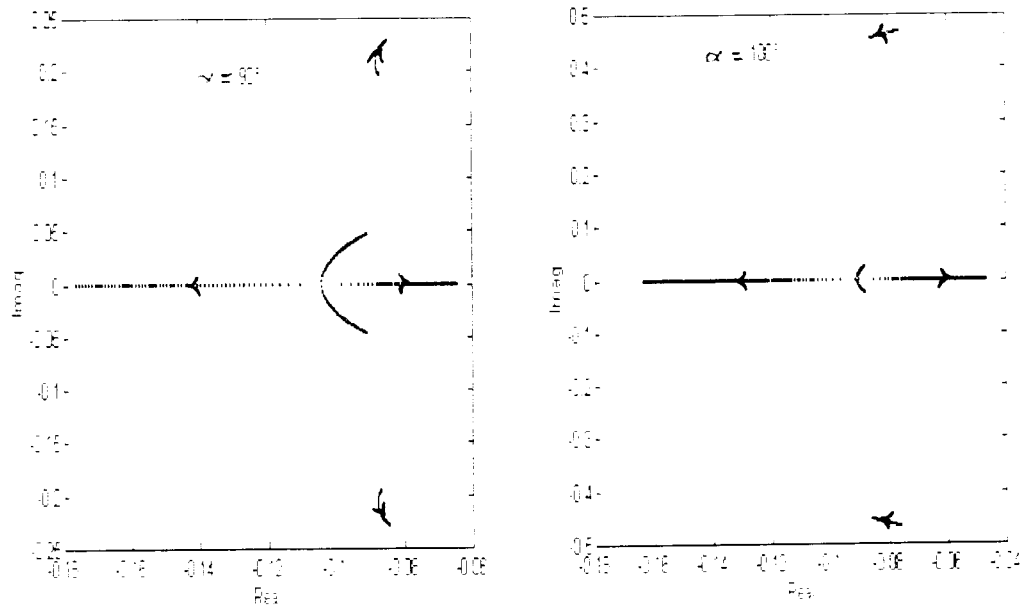

(a) (b)

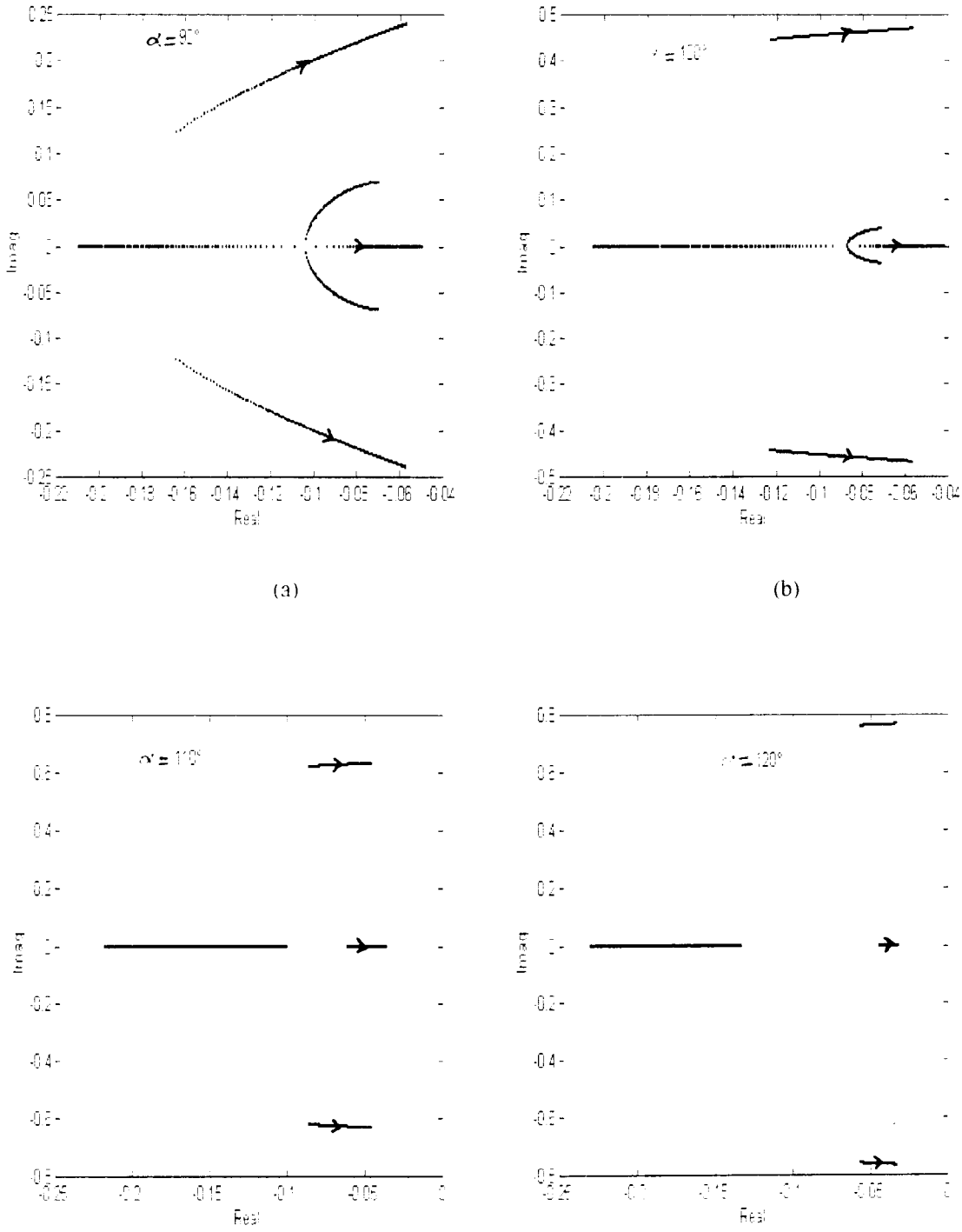

Fig. 4.11 Eigenvalues loci for R_r variation (T_L = 0.9 p.u)

For the load torques considered (0.1 and 0.9 p.u) and firing angles (90° 100°, 110° and 120°), the increase of the rotor resistance R_r decreases the drive relative stability.

4.4.1.5 Effect of supply voltage V_{ms} variation:

The effect of supply voltage V_{ms} variation, is investigated by plotting the loci of the eigenvalues, with V_{ms} varying from 0.9 p.u to 1.5 p.u. This is shown at load torques T_L = 0.1 and 0.9 p.u, in Fig. 4.12 and 4.13.

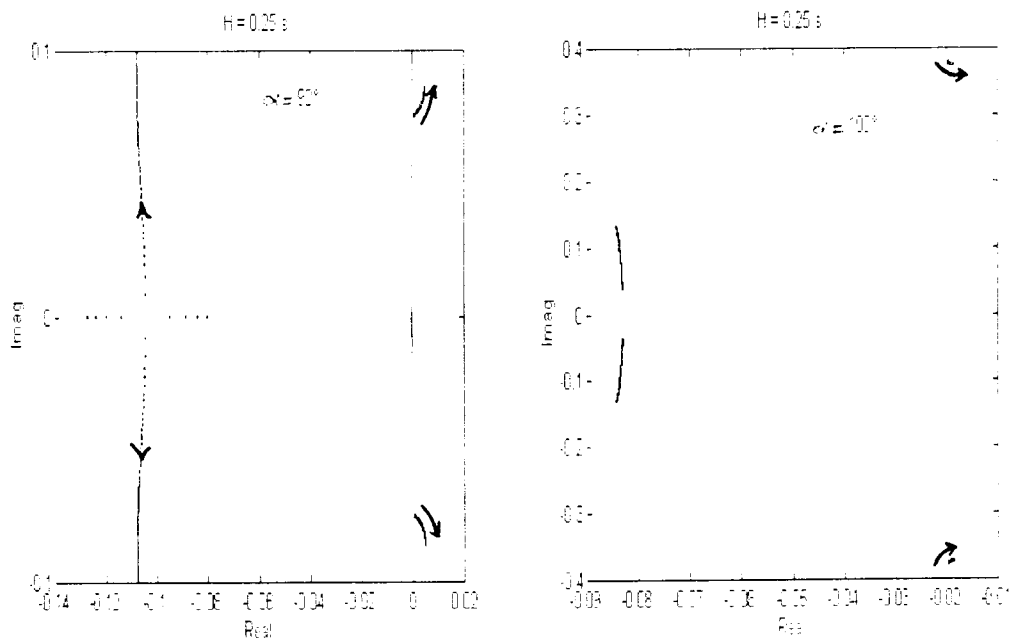

(a) (b)

Fig. 4.12 Eigenvalues loci in V_{ms} variation (T_L = 0.1 p.u)

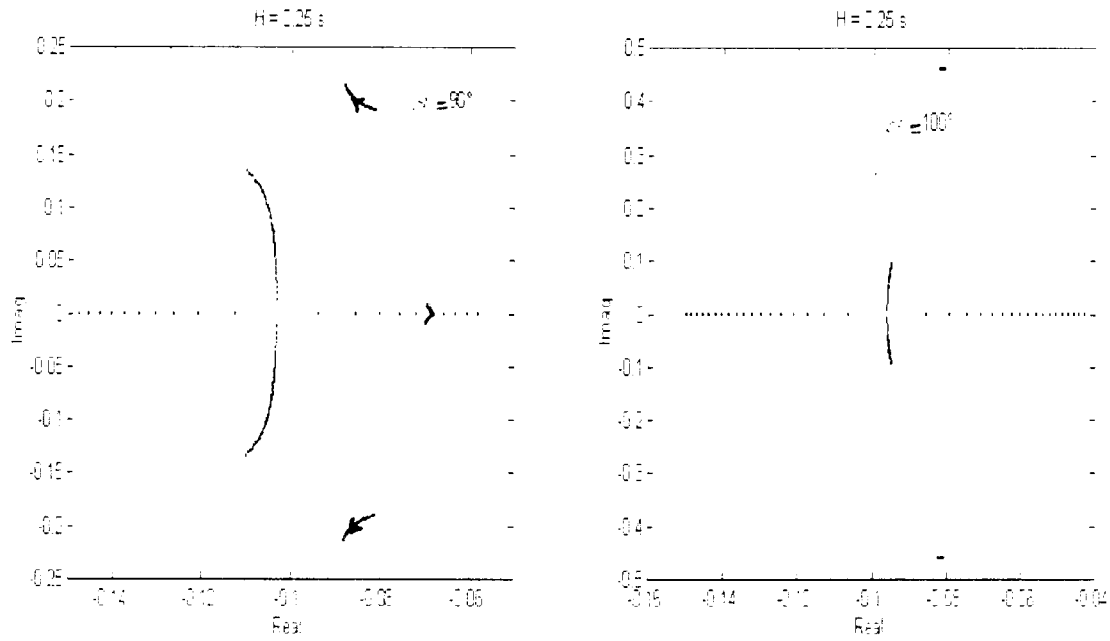

(a) (b)

Fig. 4.13 Eigenvalues loci in V_{ms} variation (T_L = 0.9 p.u)

At T_L = 0.1 p.u :

An increase in V_{ms} has a negative effect on the drive stability. For α = 90°, as V_{ms} increases, the system being alreadyunstable (H = 0.25 s) sees its eigenvalues pushed to the right hand side of the s-plane. For the other firing angles, an increase in V_{ms} decreases system relative stability, as indicated in Fig. 4.12.

At T_L = 0.9 p.u :

For α = 90°, the drive relative stability decreases when V_{ms} is increased or decreased around 1 p.u. In contrast, for the other firing angles, it is enhanced, when V_{ms} is increased, as indicated in Fig. 4.13.

4.4.2 TRANSIENTS

To support the results of eigenvalues loci study, transient responses of the system to step changes in load torque by a step of ΔT_L = 0.1 p.u, are obtained by numerical integration of the eqns. 13, 14, 15 and 16, the plots are shown in Fig. 4.14 through to Fig. 4.18.

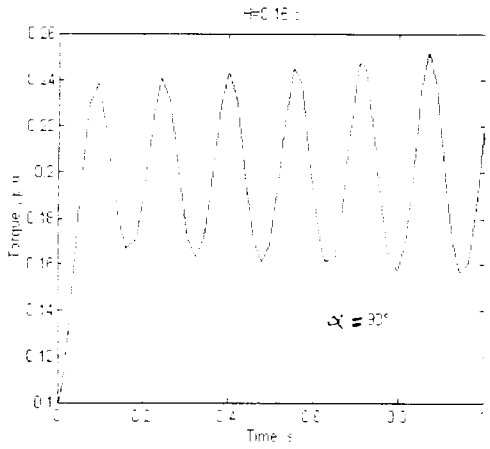

(a)

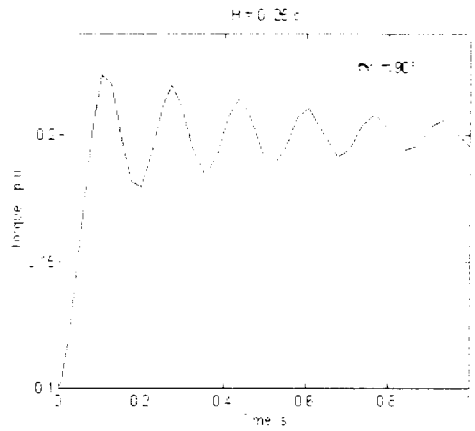

(b)

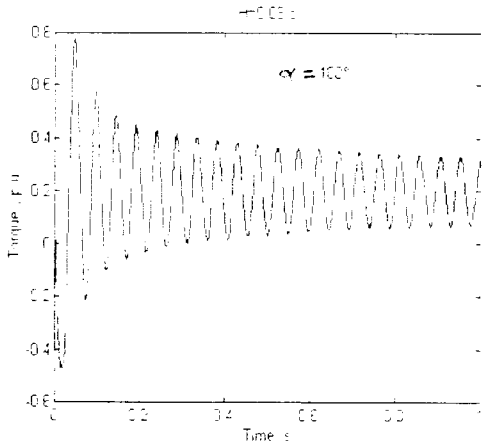

(c)

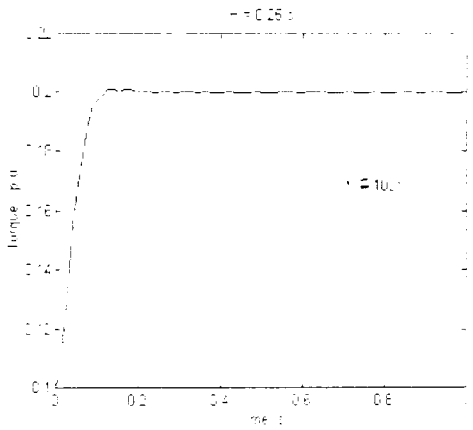

(d)

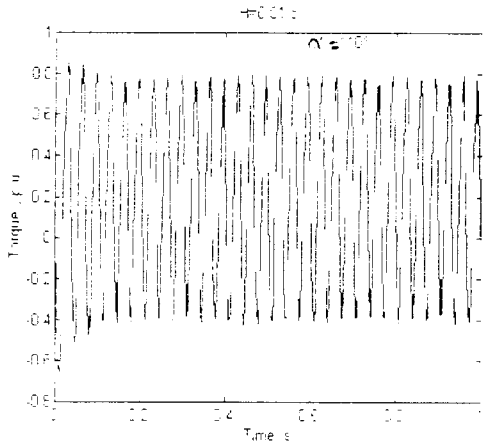

(e)

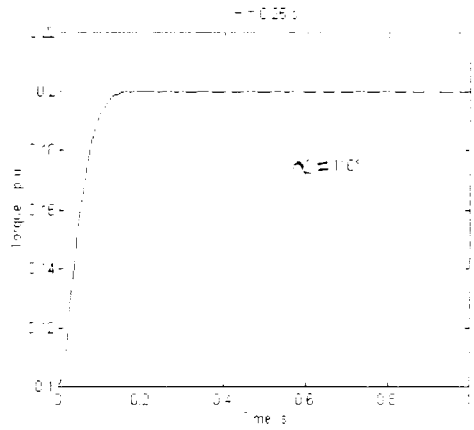

(f)

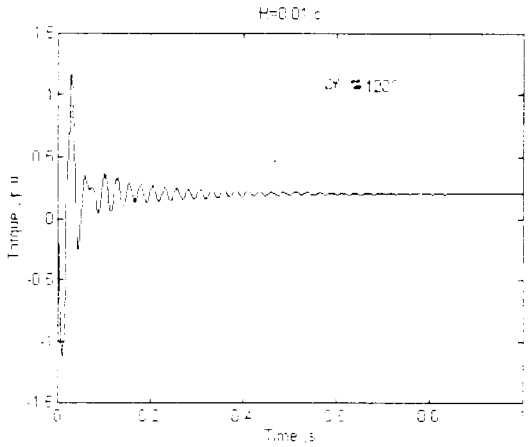

(g)

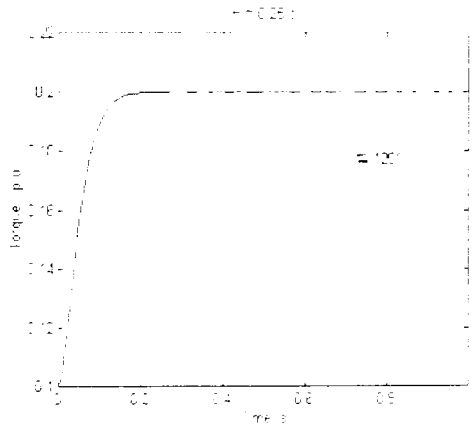

(h)

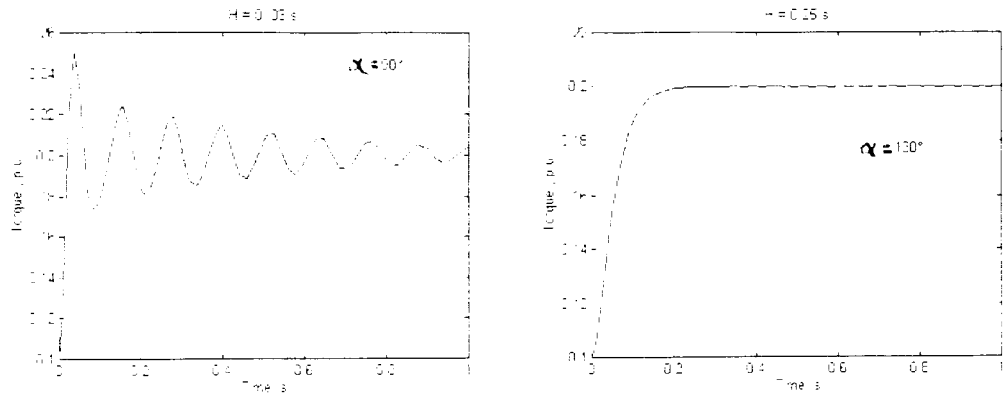

(i) (j)

Fig. 4.14 Response of the system to step changeof ΔT_L = 0.1 p.u in load torque
(Initial torque is T_L = 0.1 p.u)

At T_L = 0.1 p.u :

For firing angle α = 90°, the value of H is first chosen in the range of instability given by the eigenvalues loci study, that is H = 0.15 s.

Fig. 4.14 (a) shows that the torque oscillations are negatively damped, thus causing instability of the drive.

It is shown in Fig. 4.14 (b,i) that when H = 0.03 s and 0.25 s, the torque oscillations are positively damped, hence the system is stable. In fact there exists an inertia constant H bounded range of instability .

For α = 100°, 110° and 120°, if the inertia constant H increases the torque oscillations are more damped, so the drive relative stability is enhanced. As the firing angle increases, the torque oscillations are more damped.

The results agree with those of the eigenvalues loci analysis.

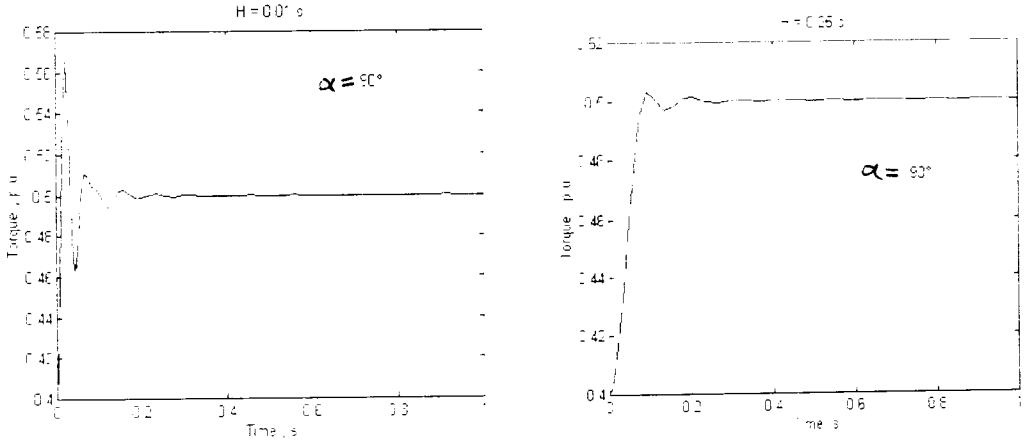

(a) (b)

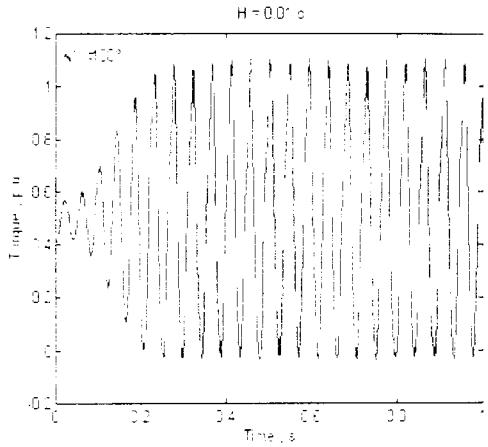

(c)

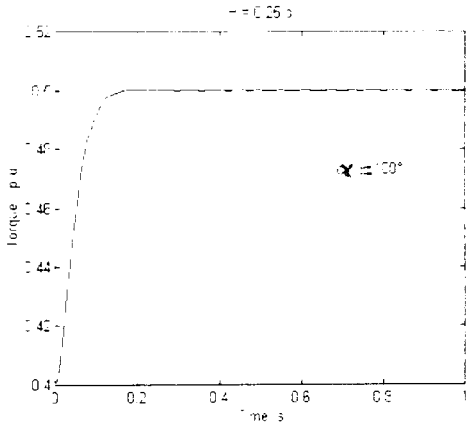

(d)

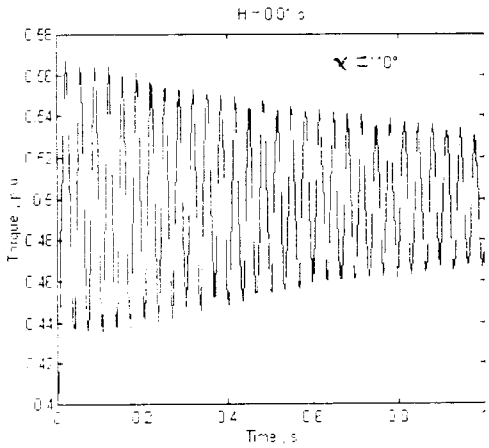

(e)

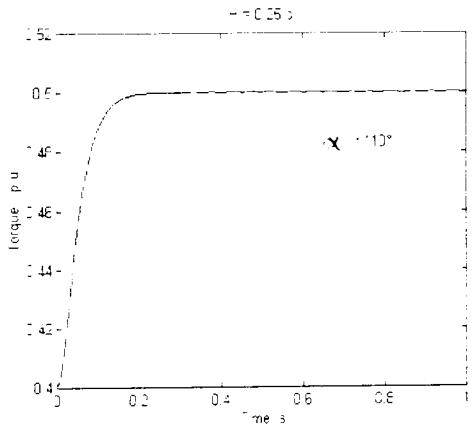

(f)

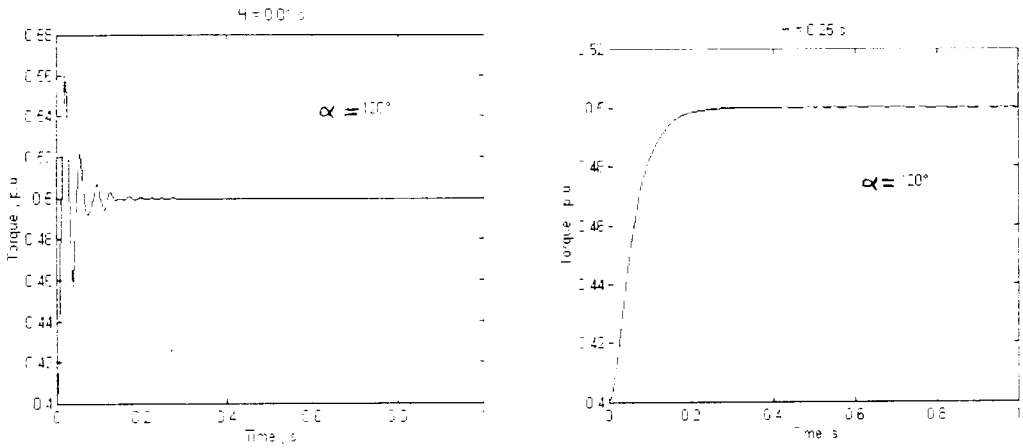

(g) (h)

Fig. 4.15 Response of the system to step change in load torque of ΔT_L = 0.1 p.u
(Initial torque is T_L = 0.4 p.u)

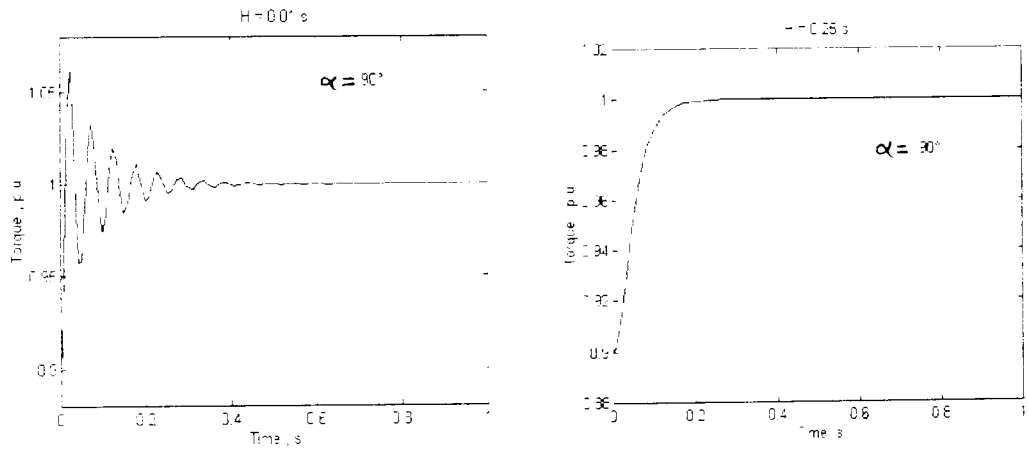

(a) (b)

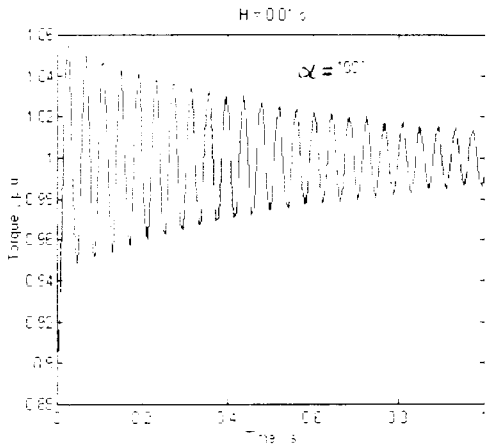

(c)

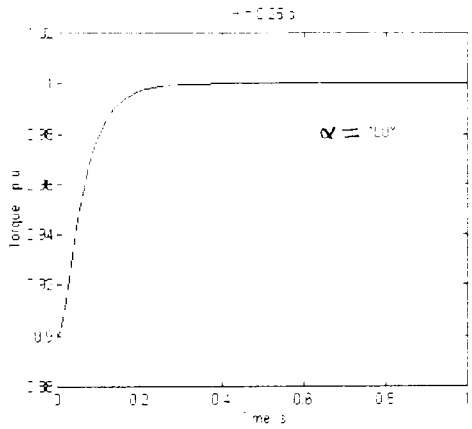

(d)

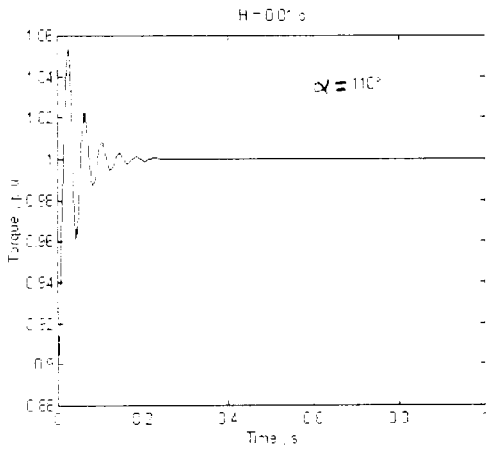

(e)

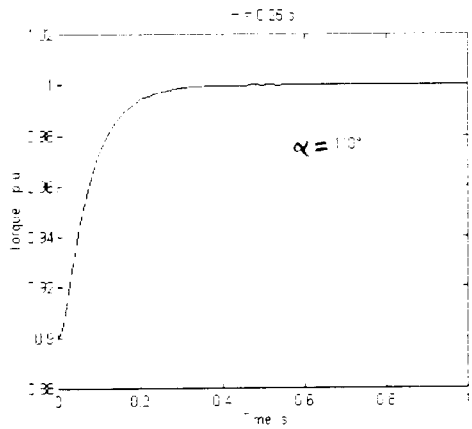

(f)

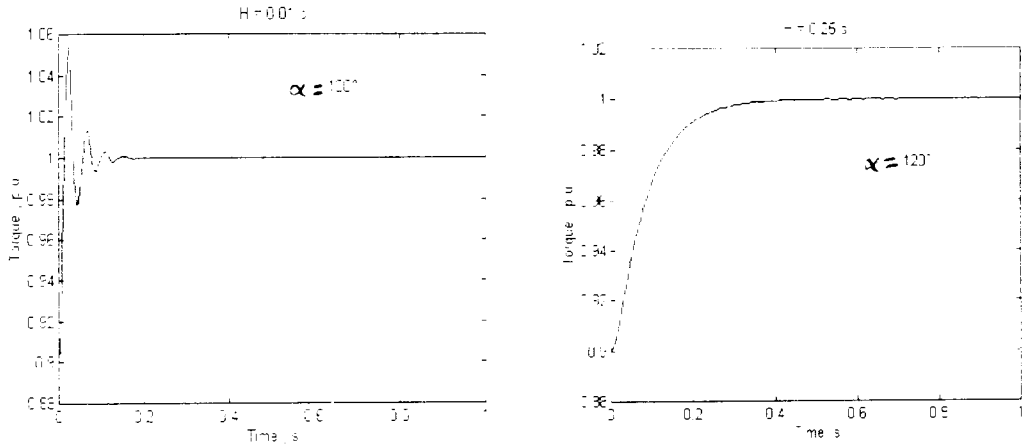

(g) (h)

Fig. 4.16 Response of the system to step change in load torque of ΔT_L = 0.1 p.u
(Initial torque is T_L = 0.9 p.u)

At T_L = 0.4 p.u and 0.9 p.u :

For firing angle α = 90°, the torque oscillations are less damped as the load torque increases. For the same load torque, as the firing angle increases the system shows a tendency to stability, since the overshoot and rise time decrease.

For α = 100°, 110° and 120°, the drive reaches the steady state torque more smoothly, that is the torque oscillations are more damped, as the load torque increases. For a given load torque T_L, the drive gets more stable as α increases.

The torque transient responses support the conclusions of the eigenvalues loci analysis, by confirming that any increase in the inertia constant H increases the drive stability.

4.4.3 STARTUP TORQUE TRANSIENTS

The electromagnetic torque transients during start up of the drive for firing angles α = 90° and 120° at load torques T_L = 0.1 and 0.9 p.u are shown in Fig. 4.17 and Fig. 4.18.

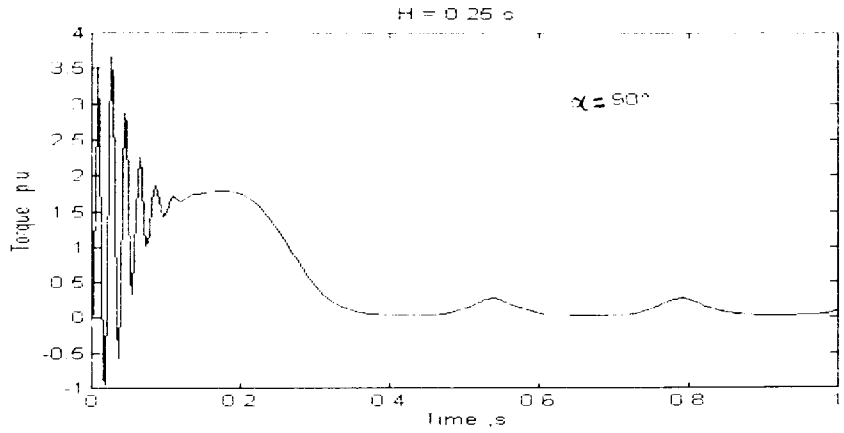

(a)

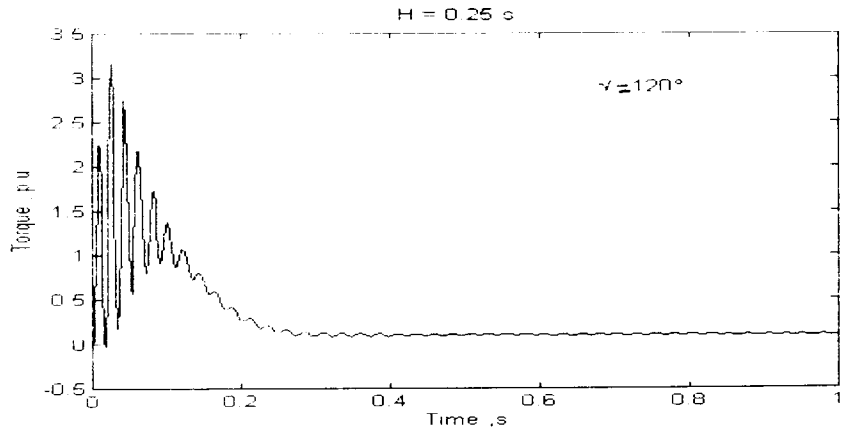

(b)

Fig. 4.17 Torque transients during start up (T_L = 0.1 p.u)

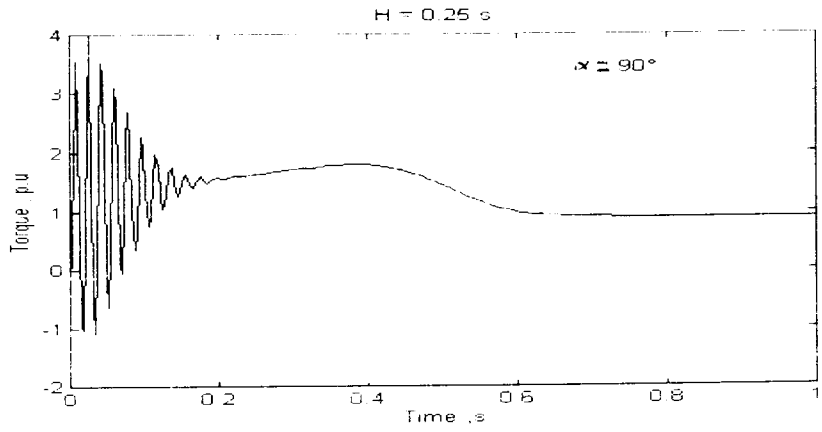

(a)

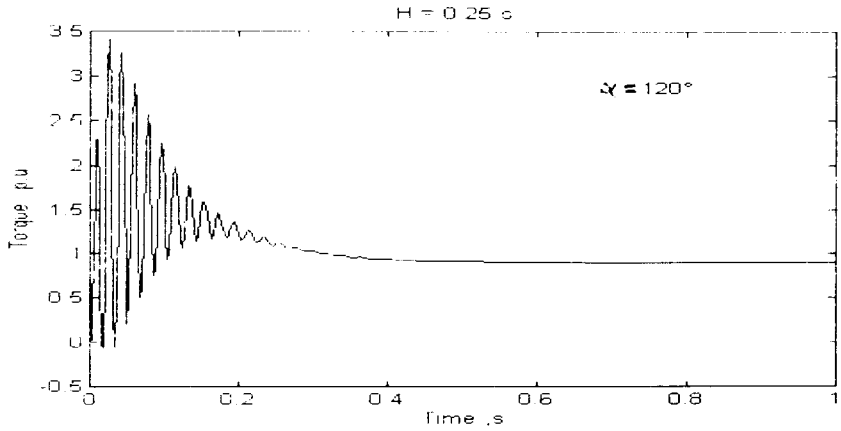

(b)

Fig. 4.18 Torque transients during start up (T_L = 0.9 p.u)

The run-up time decreases as the firing angle α increases and the steady state torque is reached more fastly in load condition T_L = 0.1 p.u than in T_L = 0.9 p.u.

For the same firing angle the magnitude of the peaks is not affected by a change in load torque.

For a given load torque, the torque oscillations are relatively less oscillatory for any increase in the firing angle α.

4.5 500 hp machine drive

4.5.1 Eigenvalues loci

4.5.1.1 Effect of inertia constant H variation :

The inertia constant H is varied from 0.1 s to 2* H_m, that is 0.55 s since H_m = 0.26 s, by steps of 0.05 s. The loci of the four eigenvalues are shown in Fig. 4.19 through to Fig. 4.22.

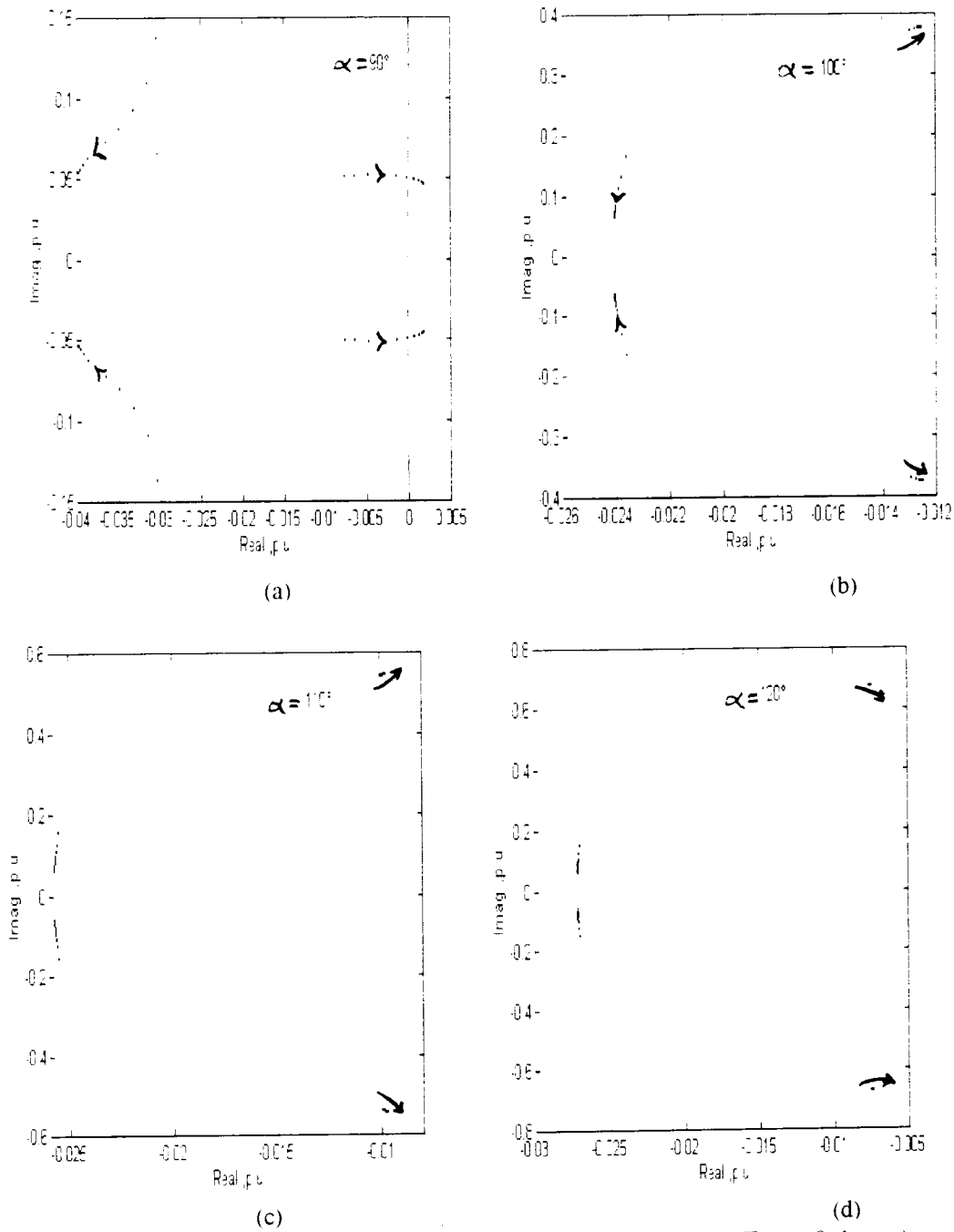

Fig. 4.19 Eigenvalues loci for H variation (T_L = 0.1 p.u)

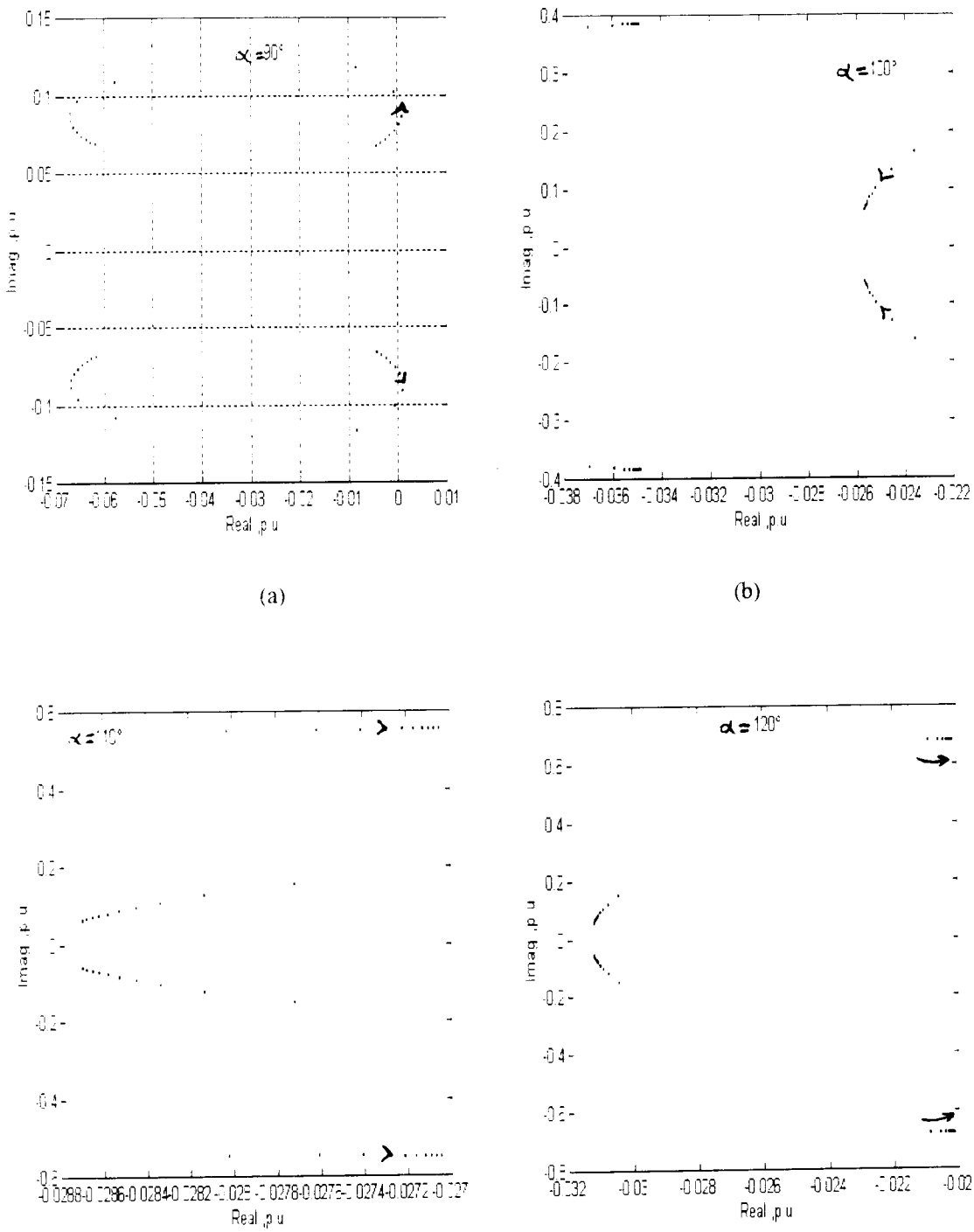

(a) (b)

(c) (d)

Fig. 4.20 Eigenvalues loci for H variation (T_L = 0.4 p.u)

For α = 110°, any variation of X_d around 0.9 p.u decreases the system relative stability. For α = 120°, the relative stability is decreased for variation of X_d around 1.1 p.u.

At T_L = 0.9 p.u :

For α = 90°, the drive relative stability is enhanced as X_d is increased. For α = 100° and 110 °, the relative stability deteriorates as X_d is increased. For α = 120°, any variation of X_d around 0.9 p.u decreases the drive relative stability.

4.5.1.3 Effect of stator resistance R_S variation :

The effect of the stator resistance R_S variation is investigated by varying R_S by 50 % more or less its nominal value R_S = 0.0185 p.u. This is done for only two load torques T_L = 0.1 and 0.9 p.u, and shown in Fig. 4.27 and 4.28.

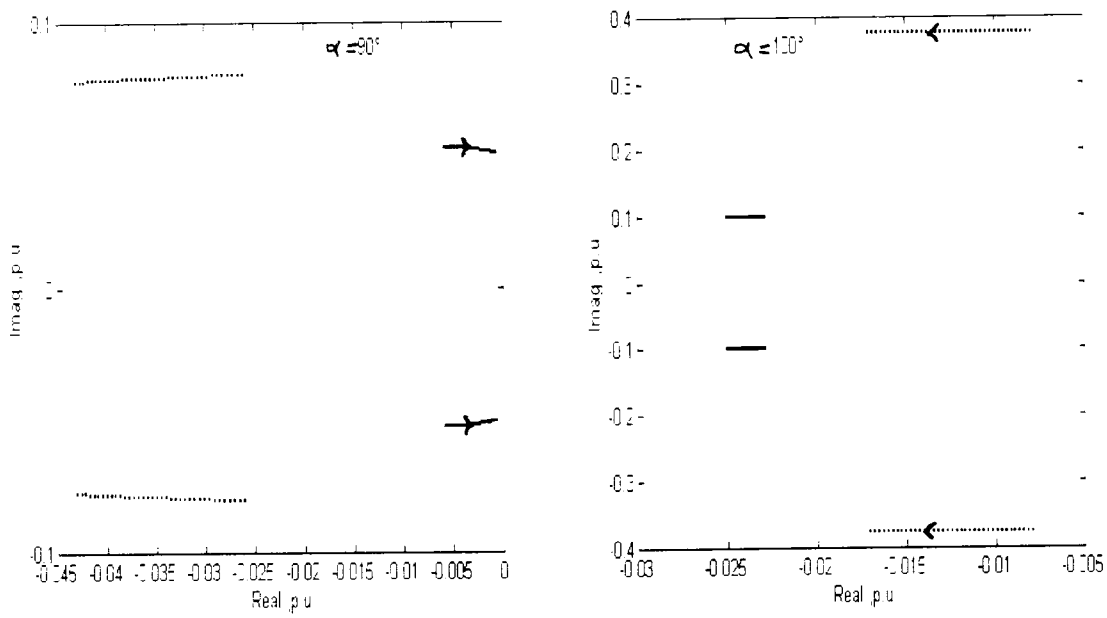

(a) (b)

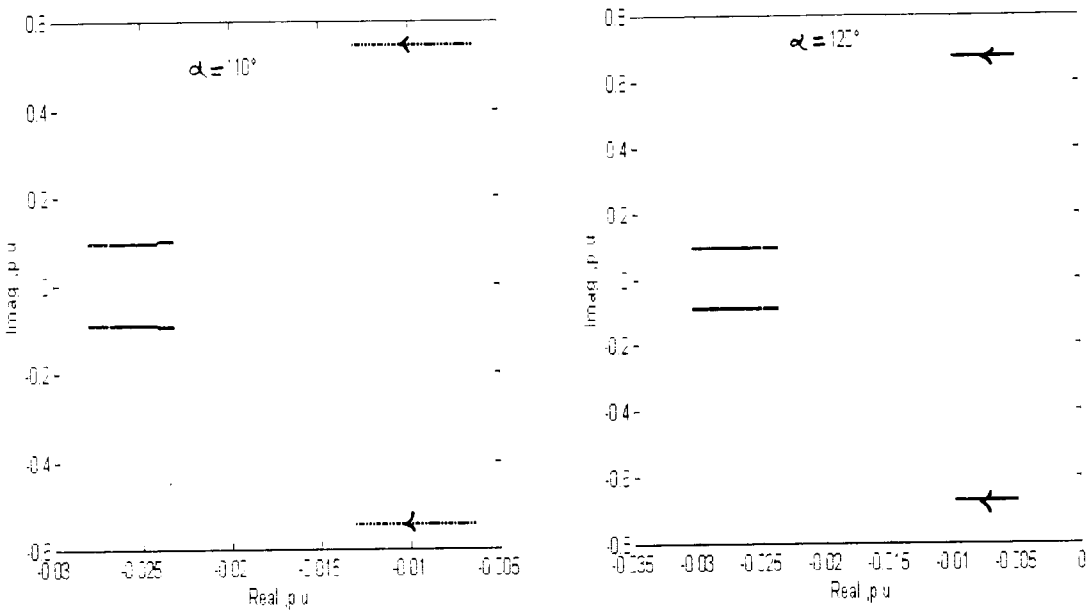

(c) (d)

Fig. 4.27 Eigenvalues loci for R_S variation (T_L = 0.1 p.u)

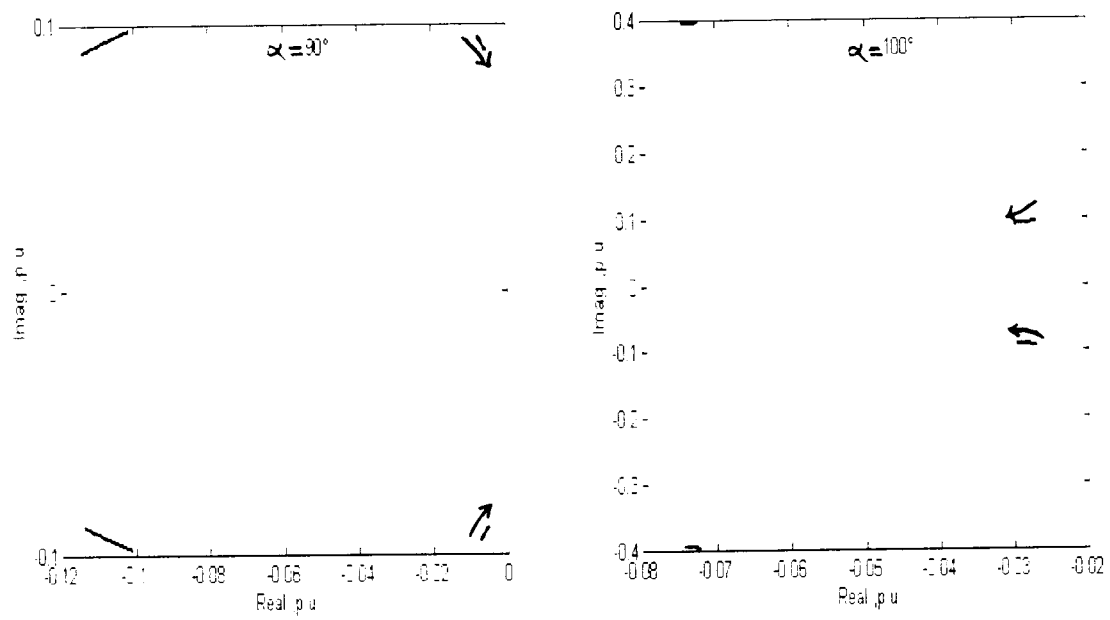

(a) (b)

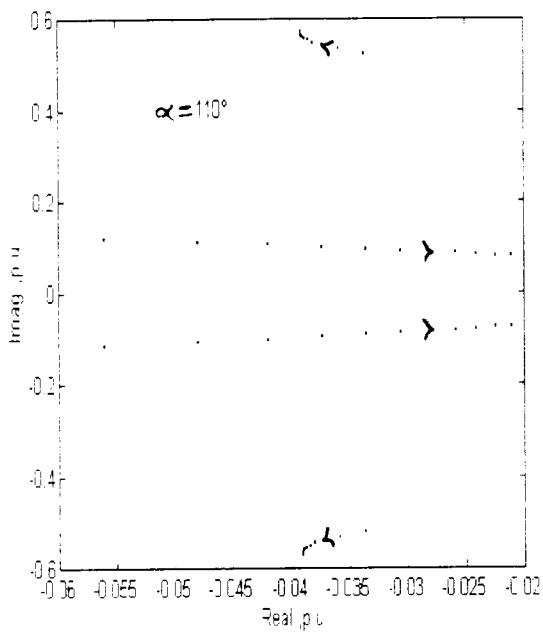

(c)

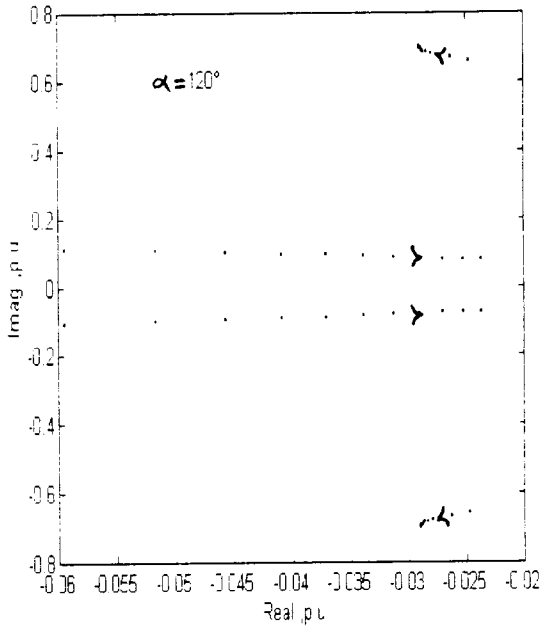

(d)

Fig. 4.25 Eigenvalues loci for X_d variation (T_L = 0.6 p.u)

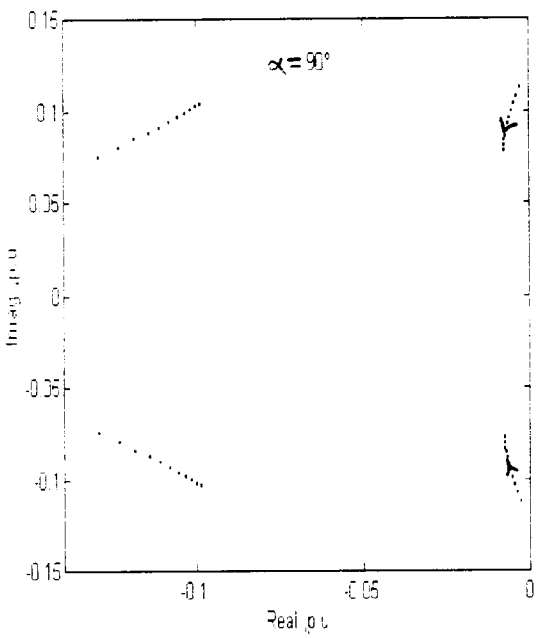

(a)

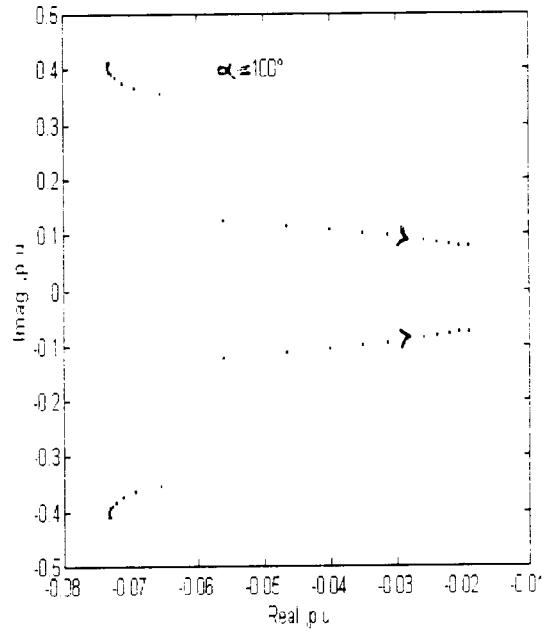

(b)

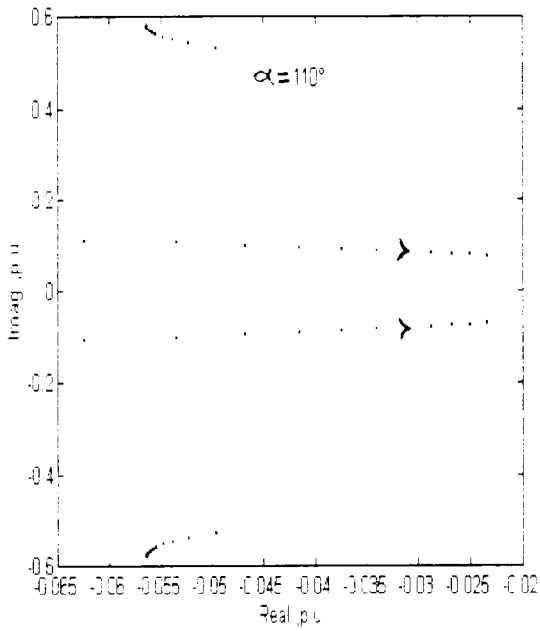

(c)

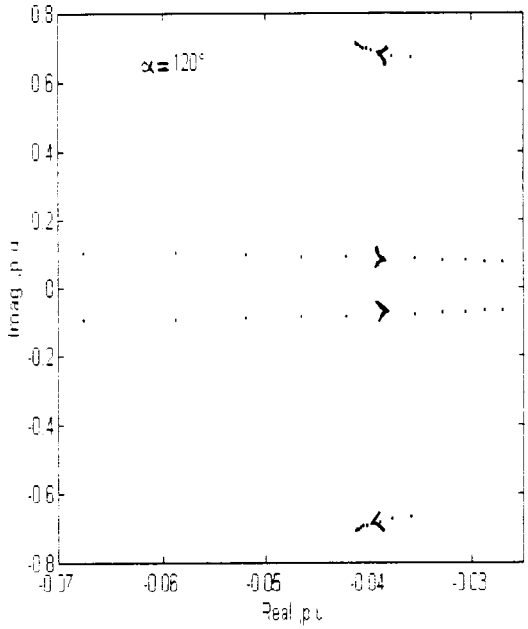

(d)

Fig. 4.26 Eigenvalues loci for X_d variation (T_L = 0.9 p.u)

At load torque T_L = 0.1 p.u :

For α = 90 °, The drive relative stability decreases as X_d is increased.
For the remaining firing angles the relative stability increases as X_d increases.

At T_L = 0.4 p.u :

For firing angle α = 90°, the system being initially unstable, becomes stable for values of X_d = 1.4 p.u and higher. For α = 100°, the relative stability decreases as X_d increases or decreases around 0.7 p.u.
For α = 110°, the relative stability is decreased if X_d is varied around 1.3 p.u. For α = 120°, any increase in X_d enhances the drive relative stability.

At T_L = 0.6 p.u :

For α = 90°, the system being unstable for X_d less than 0.7 p.u, it gains in relative stability for Xd greater or equal to 0.7 p.u. For α = 100°, the drive relative stability is decreased as X_d increases.

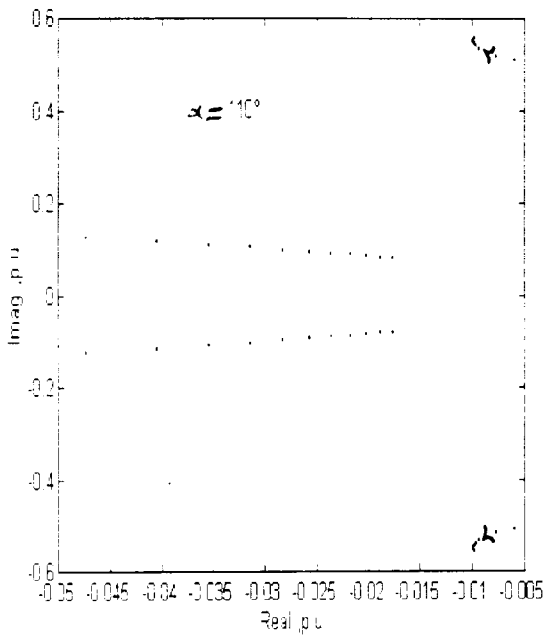

(c)

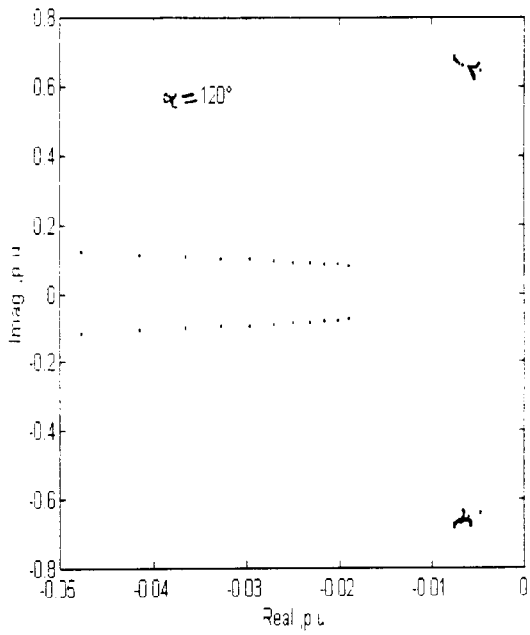

(d)

Fig. 4.23 Eigenvalues loci for X_d variation (T_L = 0.1 p.u)

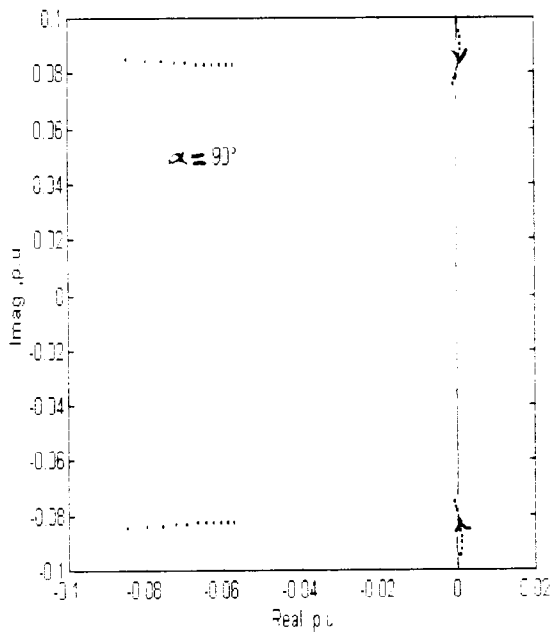

(a)

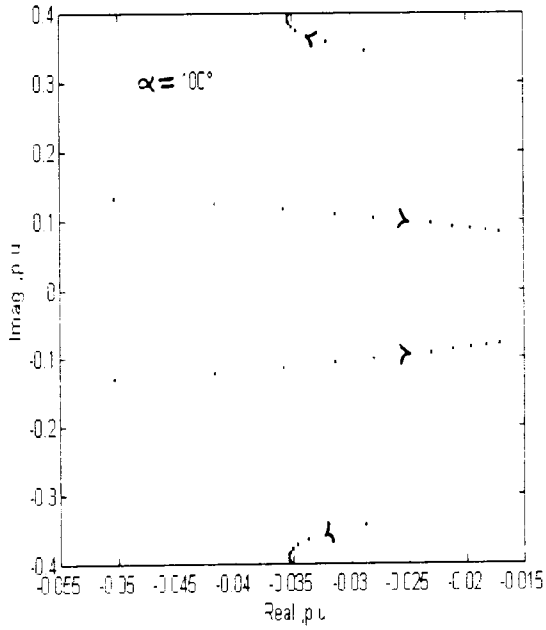

(b)

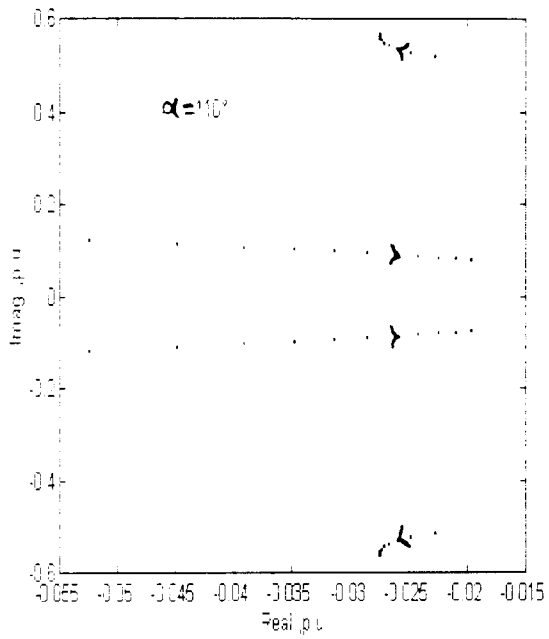

(c)

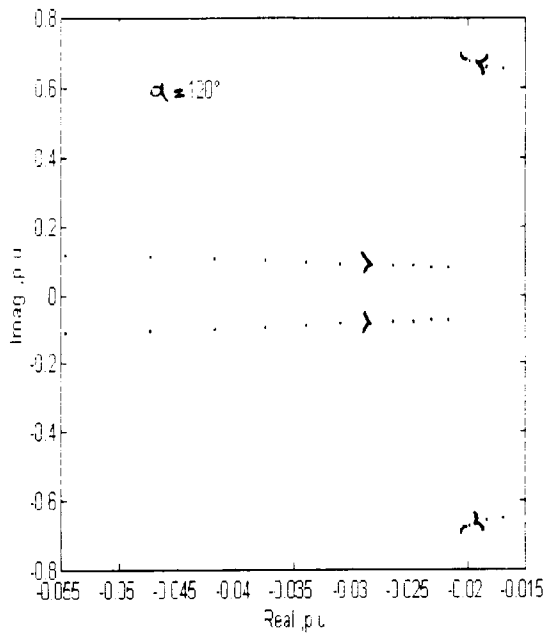

(d)

Fig. 4.24 Eigenvalues loci for X_d variation (T_L = 0.4 p.u)

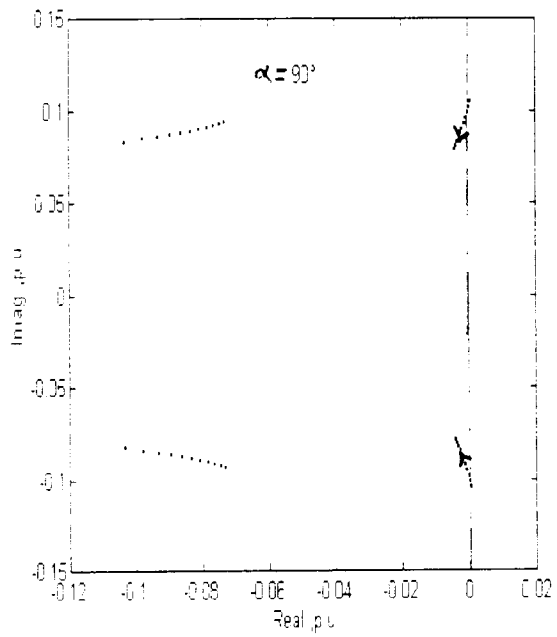

(a)

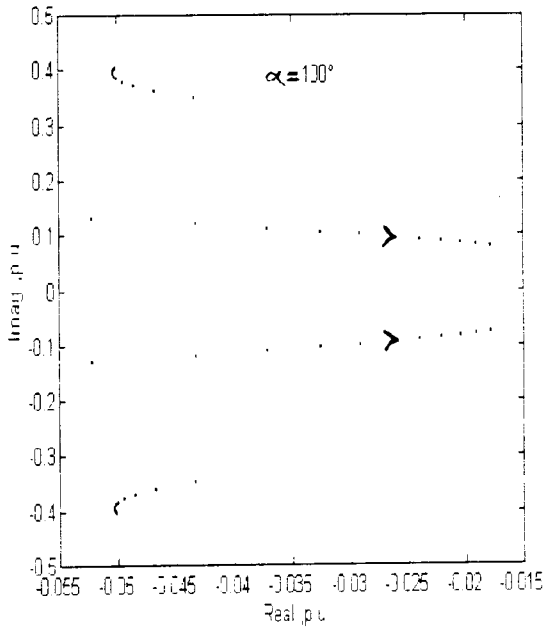

(b)

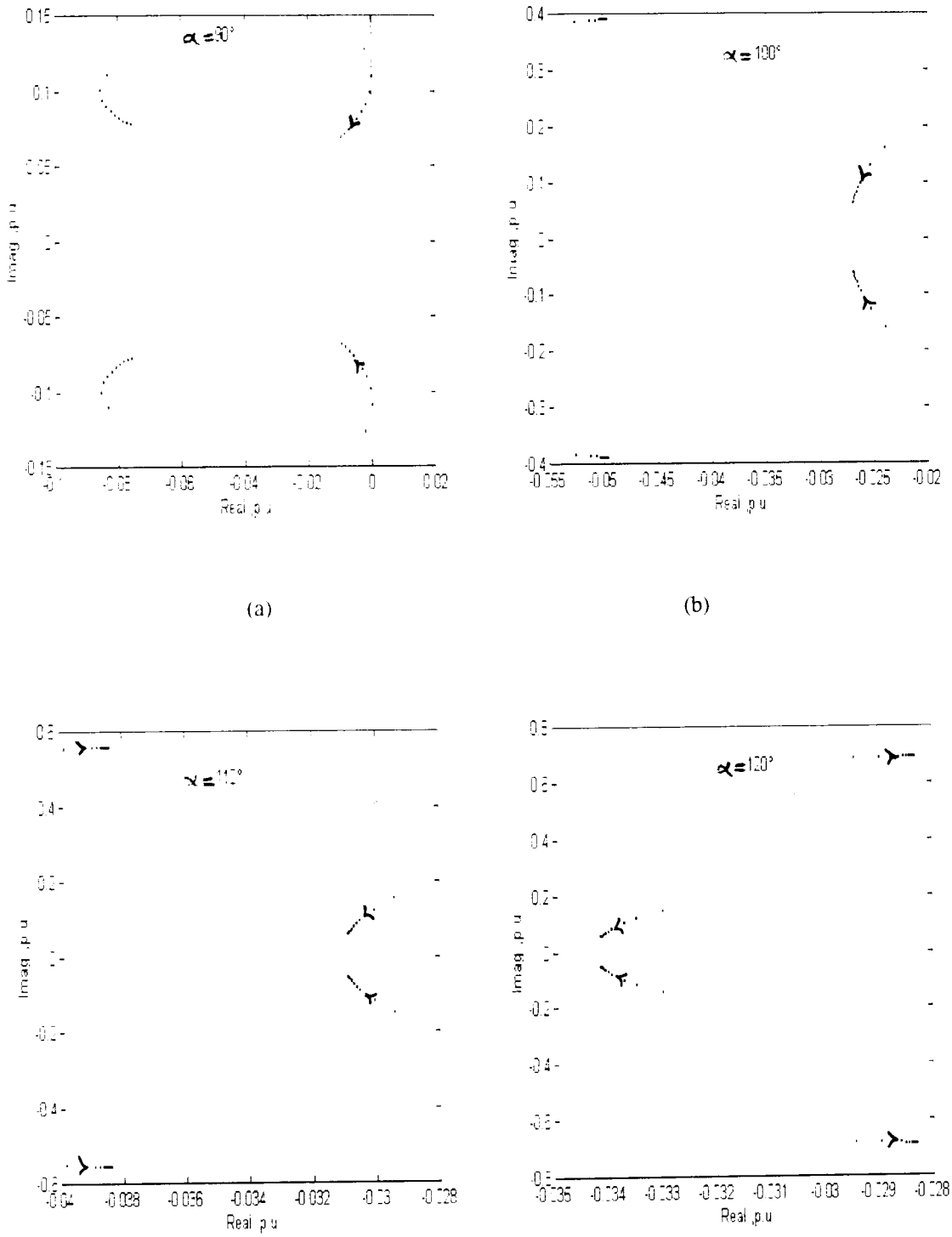

(a) (b)

(c) (d)

Fig. 4.21 Eigenvalues loci for H variation (T_L = 0.6 p.u)

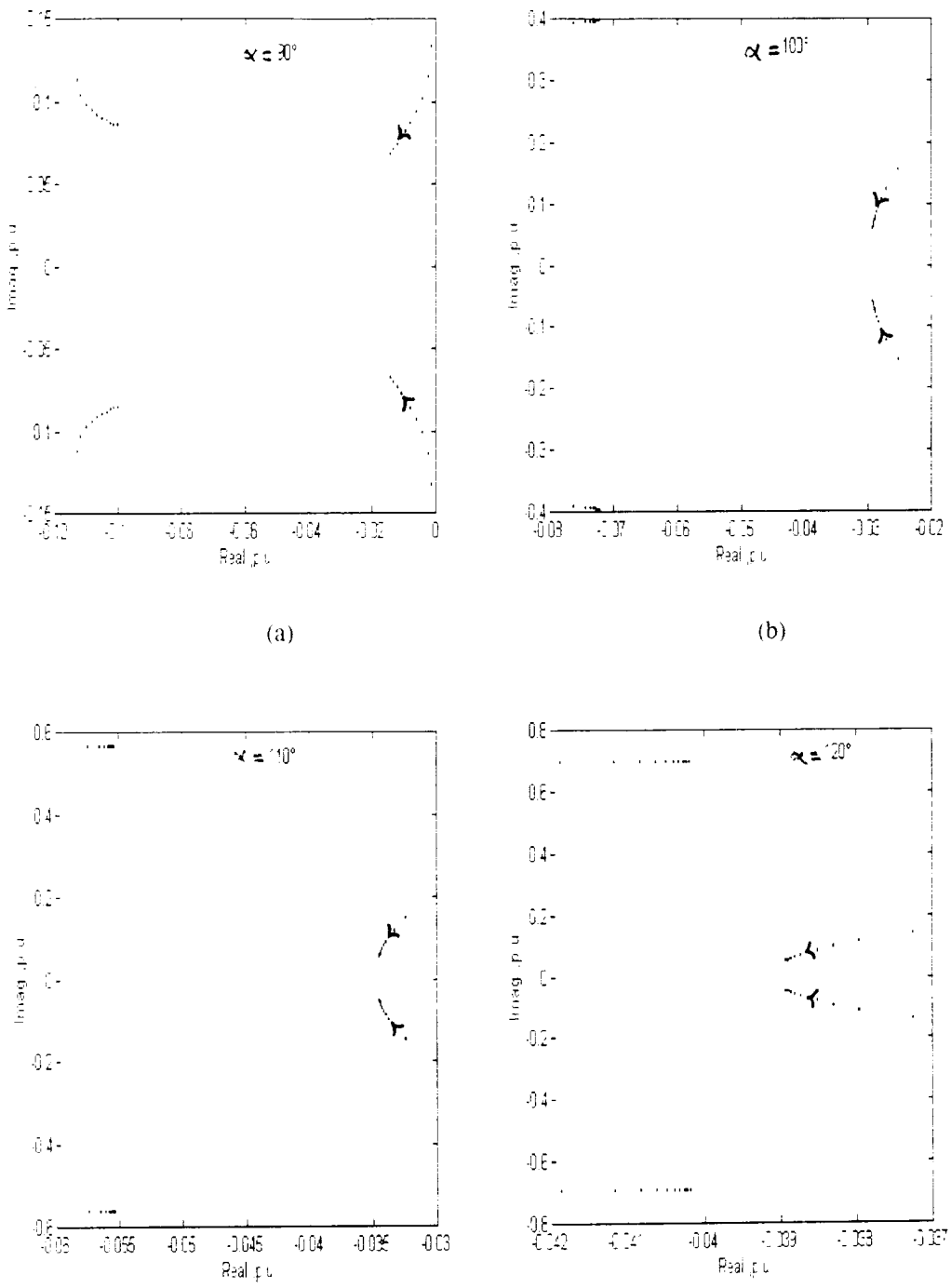

(a) (b)

(c) (d)

Fig. 4.22 Eigenvalues loci for H variation (T_L = 0.9 p.u)

At load torque T_L = 0.1 p.u :

For α = 90° if H varies from 0.1 s to 0.35 s the system relative stability decreases and for H > 0.36 s the drive is unstable.

For α = 100°, 110° and 120° an increase of H within the normal range of variation decreases the relative stability only very slightly.

At T_L = 0 .4 p.u :

For α = 90°, the relative stability decreases for H varying from 0.1 s to 0.15 s and the drive is unstable for H between 0.16 s and 0.32 s. Finally the relative stability increases from H = 0.33 s onwards. For α = 100° increase in H, increases the relative stability and for α = 110° and 120°, if H increases, the relative stability decreases very slightly.

At T_L = 0 .6 p.u :

For α = 90° the relative stability decreases for H varying from 0.1 s to 0.13 s. The drive is unstable from 0.13 s to 0.18 s and its relative stability improves for H greater or equal to 0.2 s. For α =100° and 110° the relative stability is enhanced as the inertia constant H is increased, but decreases for a firing angle α = 120°.

At T_L = 0 .9 p.u :

For all the firing angles the drive relative stability improves as the inertia constant H is increased.

4.5.1.2 Effect of filter reactance X_d variation :

The dc link filter reactance is varied by 50 % lower and higher than its nominal value, i.e., from 0.5 p.u to 1.5 p.u by a step of 0.1 p.u. The inertia constant H is equal to 0.26 s. The system eigenvalues loci are shown in Fig. 4.23, 4.24, 4.25 and 4.26.

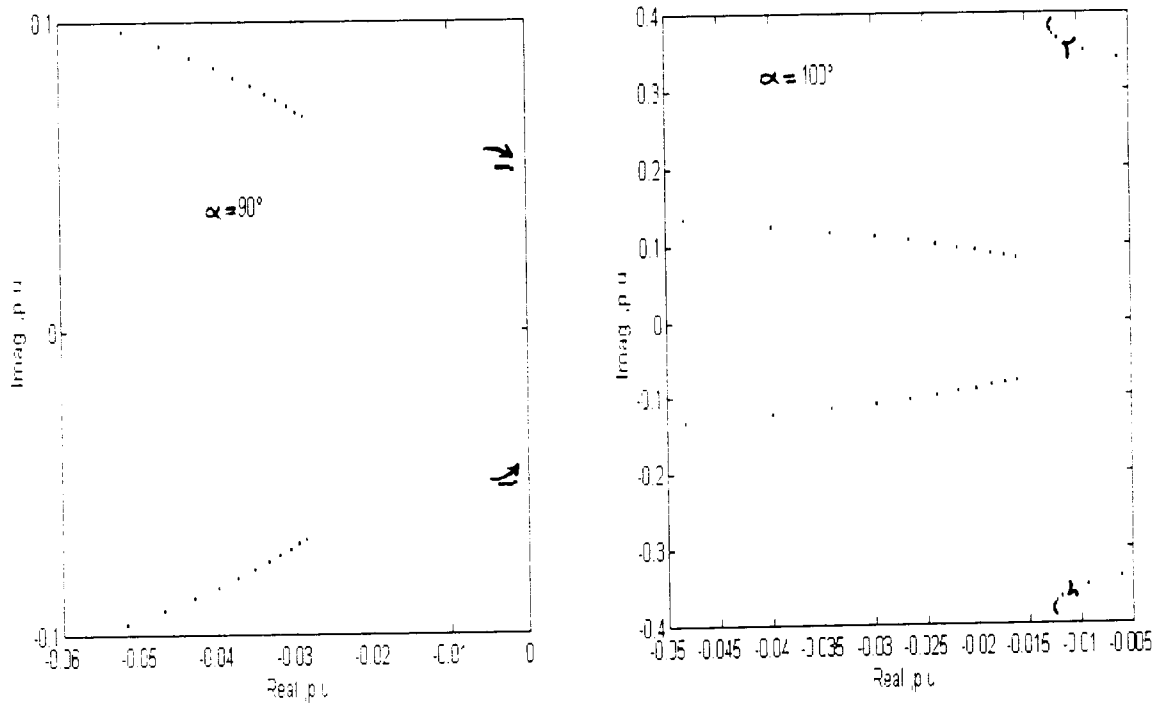

(a) (b)

Fig. 4.48 (a,b and c) show that any increase in the drive supply voltage will decrease system relative stability. One can notice from this figure that the dominant poles are shifted to the left as V_{ms} decreases, thus making the system more stable.

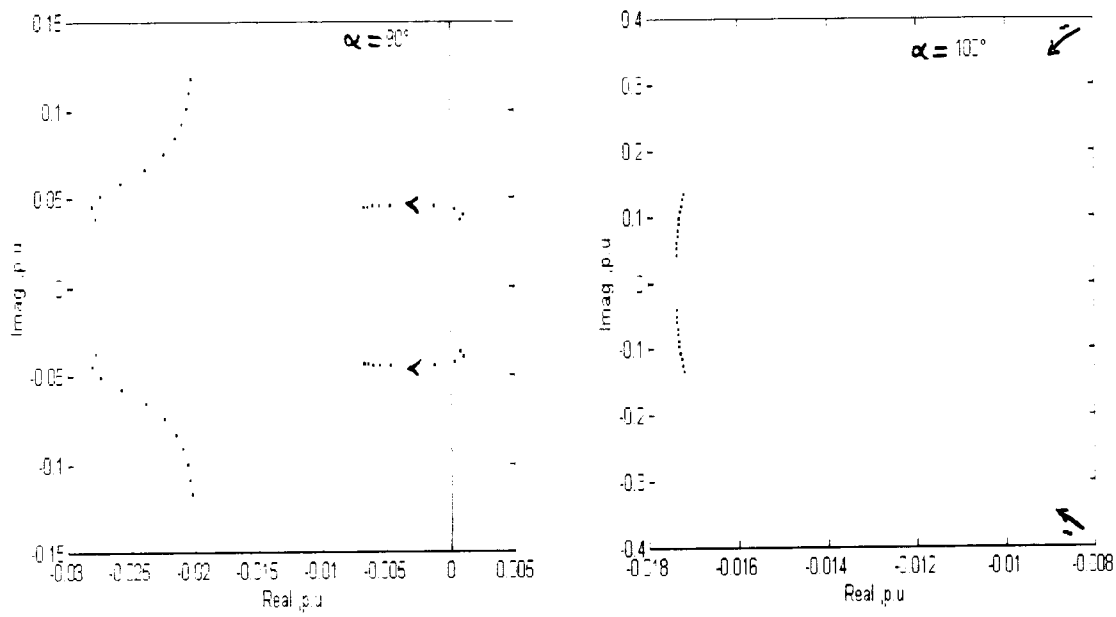

(a) (b)

Fig. 4.49 Eigenvalues loci for V_{ms} variation (T_L = 0.1 p.u)

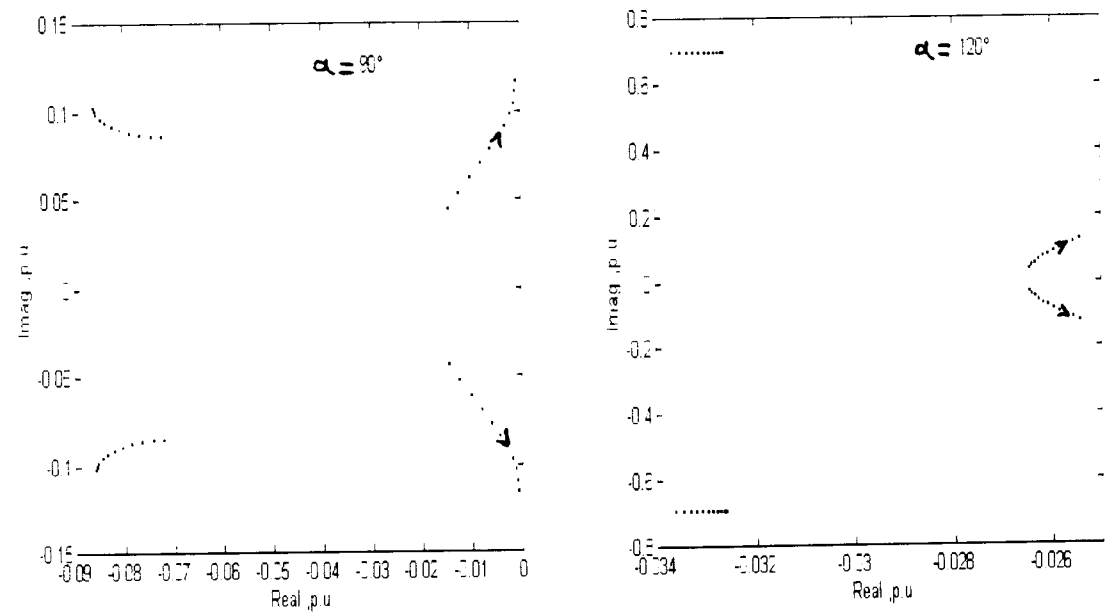

(a) (b)

Fig. 4.50 Eigenvalues loci for V_{ms} variation (T_L = 0.9 p.u)

The loci of the eigenvalues have also been investigated for V_{ms} varying in the range 0.5 p.u to 1.5 p.u. This is shown in Fig. 4.49 and 4.50. The plots show that any increase in the system supply voltage V_{ms} will :

- Increase the system relative stability at T_L = 0.1 p.u .
- Decrease the drive relative stability at T_L = 0.9 p.u .

4.6.2 TRANSIENT RESPONSES

Transient response plots showing the behaviour of the drive when subjected to any input step change of the load torque T_L are obtained by numerical integration of eqn. 2.29. This is shown in Fig. 4.51 and 4.52, for load torques T_L = 0.1 and 0.9 p.u, at firing angles α= 90°, 100° and 120°, for H = 0.1 s and 0.3 s .

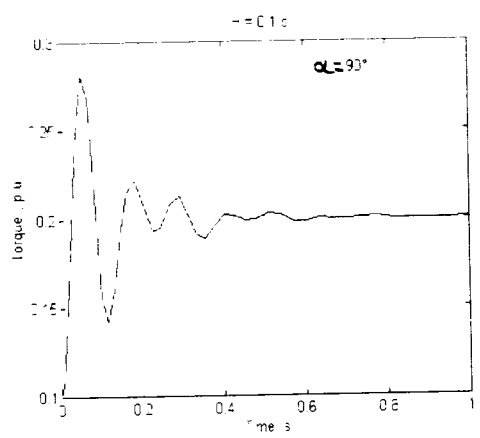

(a)

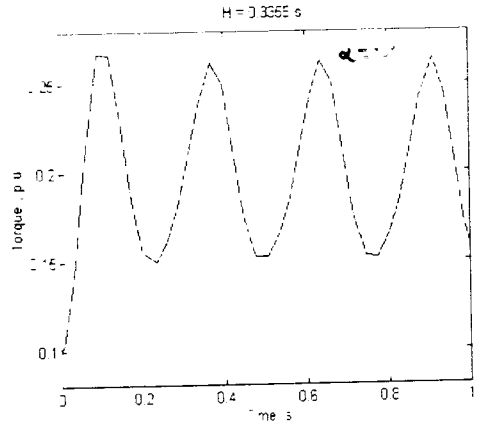

(b)

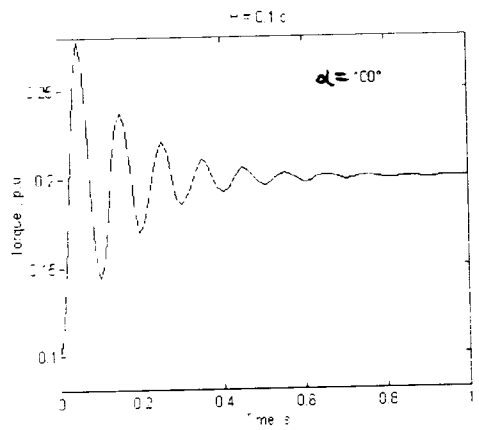

(c)

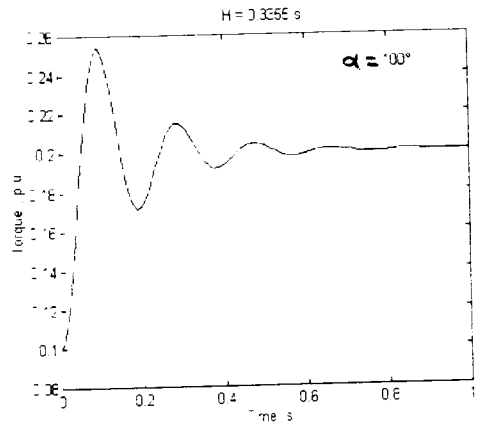

(d)

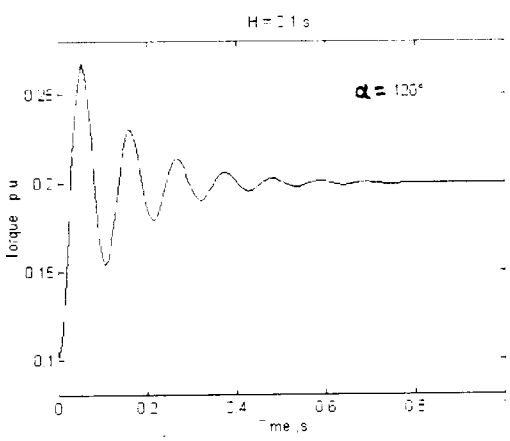

(e)

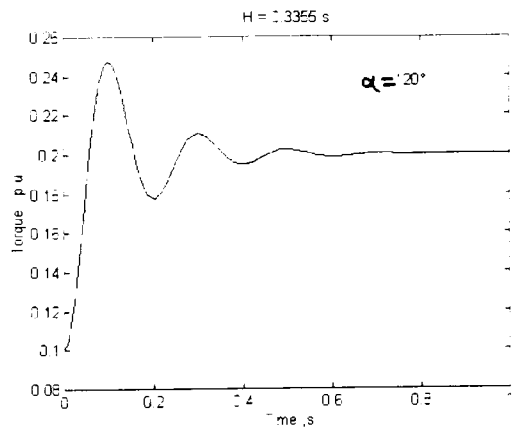

(f)

Fig. 4.51 Transient responses to step change in load torque ΔT_L = 0.1 p.u (Initial torque T_L = 0.1 p.u)

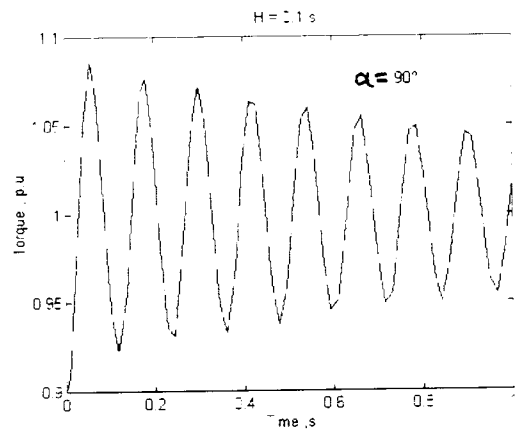

(a)

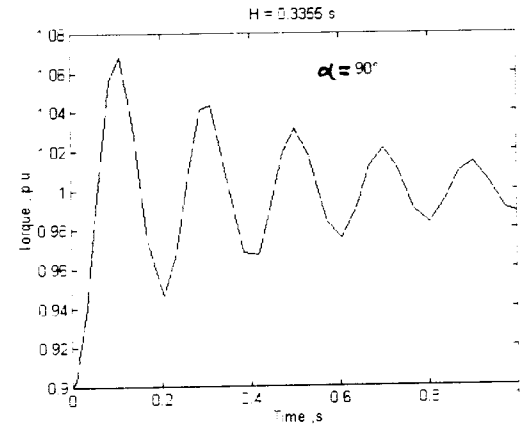

(b)

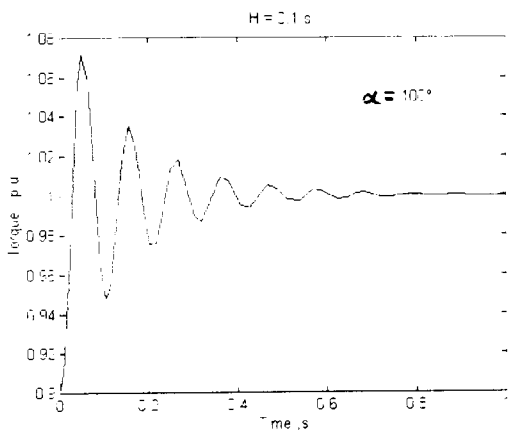

(c)

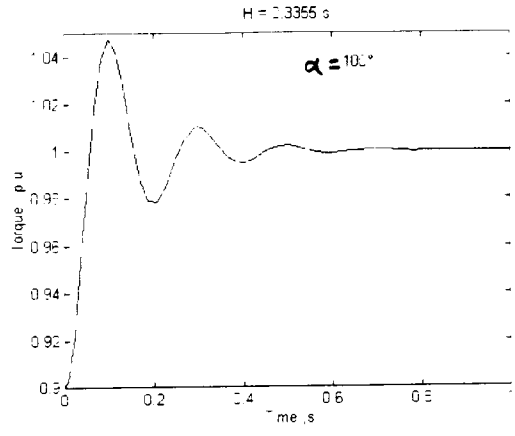

(d)

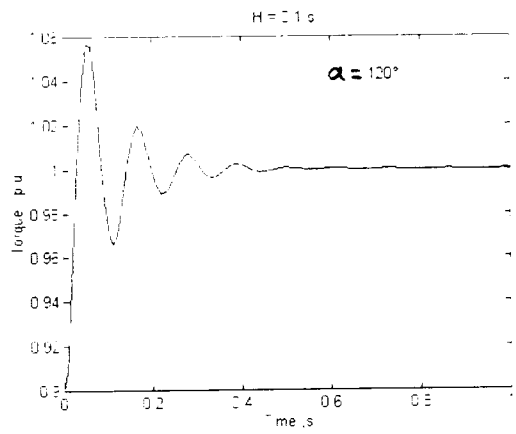

(e)

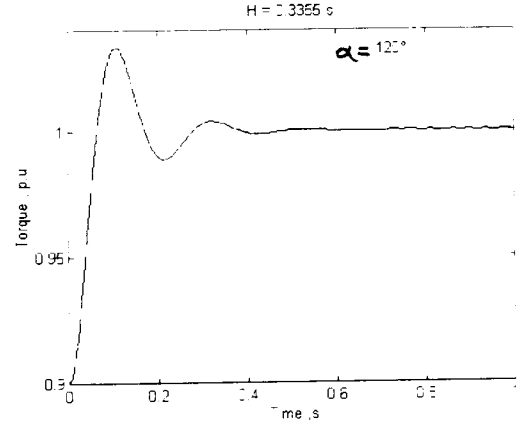

(f)

Fig. 4.52 Transient responses to step change in load torque ΔT_L = 0.1 p.u
(Initial torque T_L = 0.9 p.u)

The electromagnetic torque transient responses to step change in load torque of ΔT_L = 0.1 p.u is shown in Fig. 4.51 for an initial steady state load torque of T_L = 0.1 p.u, and in Fig. 4.52 for an initial steady state load torque of T_L = 0.9 p.u. The plots indicate that :

At T_L = 0.1 p.u :

The torque transient responses gets more oscillatory as the inertia constant H is increased, thus making the drive tend towards instability.

At T_L = 0.9 p.u :

The system becomes more stable as H is increased, the torque transient responses are shown to be more damped .

These observations support the previouseigenvalues loci investigation results.

4.6.3. STARTUP TRANSIENTS

The electromagnetic torque transients during start up of the drive for firing angles α = 90° and 120° from standstill to load torques T_L = 0.1 and 0.9 p.u are shown in Fig. 4.53 and Fig. 4.54 :

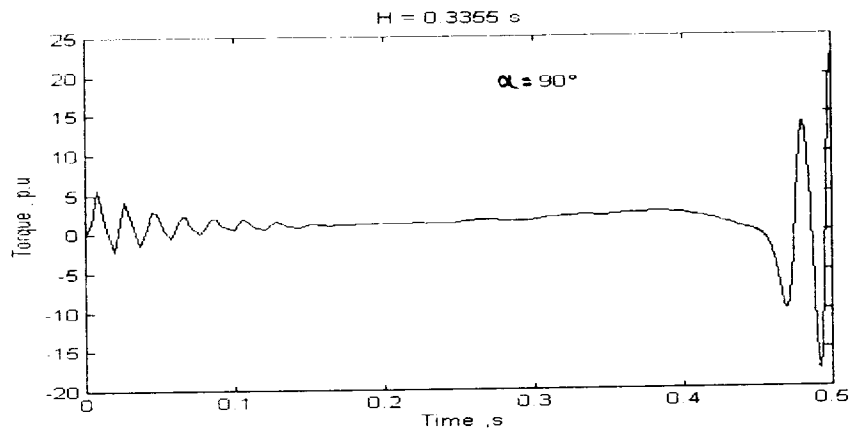

(a)

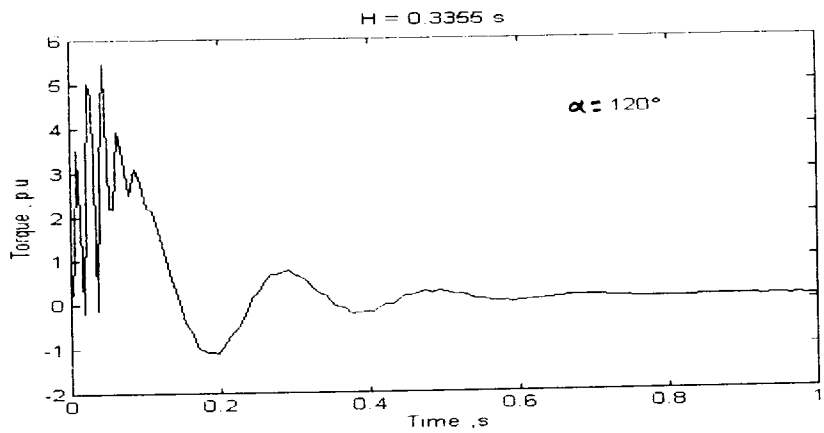

(b)

Fig. 4.53 Startup transients to T_L = 0.1 p.u

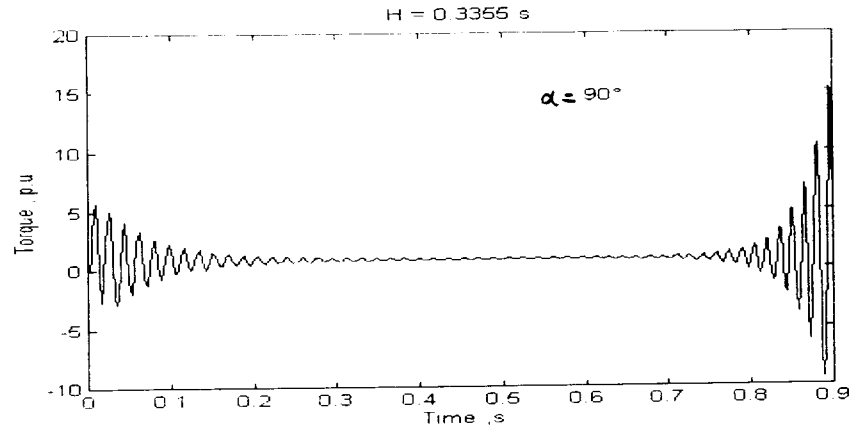

(a)

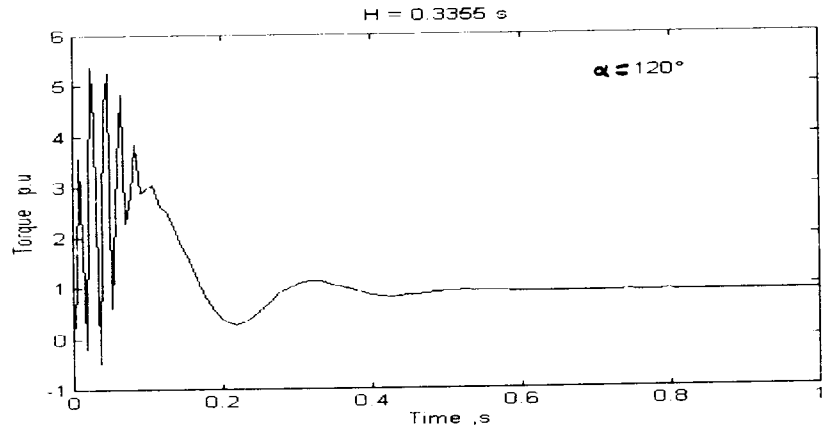

(b)

Fig. 4.54 Startup transients to T_L = 0.9 p.u

The effect of firing angle and load on transient torque consequent to switching has been shown in Fig. 4.53 and 4.54. The plots revealed the following :

- With an increase in the firing angle, the amplitude of the torque oscillations decreases whereas the run-up time increases.
- For a given firing angle α, torque oscillations becomes more oscillatory for an increase in load torque.
- The magnitude of the peaks are practically unaffected by a change in load torque.

One can notoce from Fig. 4.53(a)and 4.54 (a), that for α = 90°, the torque oscillations are negatively damped, hence instability occurs at start up.

Chapter 5

GENERAL CONCLUSION

The stability analysis of the static Kramer drive in its conventional form preceded by a detailed steady state analysis have been carried out in this present work.

The steady state behaviour of the system with particular emphasis on its electromagnetic , torque-speed characteristics has been studied using improved versions of DC and AC equivalent circuits together with a DQ model expressed in the synchronously rotating reference frame, with the objective of proving the erroneous character of a previously used model that has so far constituted the basis of a stability study of the drive.
The usefullness of the simple 2^{nd} order DC model of the drive has been extended by investigating the effects of system overall inertia constant H, the dc link inductance L_d and the commutation overlap in the diode bridge on system stability.

This study indicates that the drive relative stability is, as expected, reinforced as the inertia constant H is increased. In contrast, an increase in the system filter inductance L_d will decrease the system relative stability. Also commutation overlap effect when taken into account will improve the system stability. The system response to any step change in load torque is less oscillatory, that is more damped, than if it is neglected. In other words, the drive would actually be more stable than otherwise found, because of the damping effect of the overlap when included.
Thus according to the simple model, neglecting the effect of commutation overlap in the stability analysis of the drive will effectively correspond to the worst case condition, i.e., yield pessimistic predictions regarding system stability.

A higher order linearized model obtained from a non linear DQ model of the static Kramer drive was obtained using the small signal perturbation method, followed by extensive eigenvalue analysis applied to the linear model obtained for investigating drive stability for small perturbation around an operating point.
In support of the stability investigations, computer simulations of the system transient responses following step changes in load torque have been carried out by numerically solving the drive nonlinear DQ differential equations.

Furthermore, in view of arriving at credible and pertinent results, the present stability analysis was carried out on three drives of different power levels : a very low power drive of 5 hp, a medium one of 500 hp and a large drive of 2250 hp.
The effect of varying the drive parameters on system stability was investigated at several operating points corresponding to a load torque of T_L = 0.1 p.u, 0.4 p.u, 0.6 p.u and 0.9 p.u for firing angles α = 90°, 100° 110° and 120°.

For the 5 hp Drive, at medium and full load conditions, the relative stability is decreased by any increase in the inertia constant H, for all firing angles except when α = 90° where any variation around the nominal value of H will decrease the system relative stability.
Under light load conditions, the drive is unstable for α = 90° in the normal range of H for this particular drive power level. The relative stability is however enhanced for firing angles greater than 90°, when the inertia constant H is increased.
The increase of the filter reactance X_d improves the stability at light and medium loads, but decreases it at full load conditions.
As the stator resistance R_s is increased the relative stability of the drive is increased at light loads but decreased at full loads.
On the other hand, under all load conditions, any increase in the rotor resistance R_r decreases drive stability. This can be important when considering some design aspect of the induction machine to be used in the drive.

When supply voltage V_{ms} is increased , the system relative stability decreases at light loads. However , at full load for $\alpha = 90°$, any variation around the nominal value of V_{ms} decreases the system relative stability. For other firing angles, at full load, if V_{ms} decreases, stability deteriorates.
Voltage dips which usually occur in power systems can therefore have a negative effect on the drive stability.

For the 500 hp Drive, at light loads, the system stability is decreased by any increase of the inertia constant H. At $\alpha = 90°$ the system becomes unstable.
As loading is increased, the drive becomes more stable, that is at medium and full loads the drive relative stability is enhanced by any increase of H.
Increase in filter reactance X_d enhances the system realtive stability at light loads, except for $\alpha = 90°$ where the opposite happens. The stability decreases at full loads. At medium loads however, any variation around a certain value of X_d decreases the drive relative stability.
As the stator resistance R_s is increased, system stability is improved for firing angles greater than 90°, but worsens for $\alpha = 90°$. Any increase in the rotor resistance R_r decreases the drive stability at light loads and enhances it at full loads for all firing angles.
The effect of increasing the system supply voltage V_{ms} revealed that the drive stability is increased at light load conditions, but more importantly decreases at full loads.

For the 2250 hp Drive, the system relative stability is enhanced by any increase in the inertia constant H, except for $\alpha = 90°$ at medium loads where there exists certain ranges of instability and border line stability (limitedly stable).
The effect of the filter reactance X_d variation on the drive stability has also been investigated and revealed that it is enhanced at light loads.
But at medium and full loads, any variation of X_d around its nominal value decreases the drive relative stabilty for all firing angles.
As the stator resistance R_s is increased, the stability, for $\alpha = 90°$, is decreased and enhanced for the remaining firing angles. If the rotor

resistance R_r is increased the drive relative stability is decreased at light loads and enhanced at full loads.
Increase of the system supply voltage V_{ms} enhances the drive relative stability at light loads and decreases it at full loads.
System voltage fluctuations in terms of increase, can therefore have a negative effect on drive stability.

At medium and full loads, the 500 hp and 2250 hp drives stability is enhanced by any increase in the inertia constant H for firing angles greater than 90°.
For a given drive, whatever its power level, as the firing α is decreased approching its minimum value (90°), the system relative stability is decreased. This correspond to top speed with possible instability at α= 90°.
For the 5 hp drive, instability occurs at light load and minimum firing angle value. But for the 500 hp and 2250 hp drives, the system may go unstable at medium loads.
The electromagnetic torque transient responses to step change in load torque of ΔT_L = 0.1 p.u have been computed, by numerical inetgration of the drive dynamical differential equations and plotted. They effectively support the results obtained in the eigenvalues loci investigation with different values of the inertia constant H used. Results revealed that, For any increase in the firing angle α, the torque transients get less oscillatory thus the drive becomes more stable. The transient torque peak value is not affected by change in the initial steady state load torque.

Comparing the degree of relative stability of the three drives at the same operating point that is the same load torque T_L and firing angle α, revealed that the higher the drive power is, the more stable the system is.

We notice substantial differences in the stability of the three drives. It is affected by loading conditions on the one hand, and the power level of the drive on the other.

Subramanyam et al., who used incorrect assumptions in the drive model, concluded that the static Kramer drive can never become unstable under normal operation [12]. It is clear that this conclusion is open to question.

The present study indeed, reveals the existence of instability regions at operating points of practical relevance.
Further more, in the light of the above findings, the drive power level is an important factor in this study; a 5 hp drive has shown important differences regarding its stability in comparison with the 500 and 2250 hp which show essentially similar behaviour from a stability point of view.

Scope for further work :

The effect of commutation overlap, in the rotor diode bridge, is important and can not therefore be neglected. It can contribute to substantial additional reactive power [15]. According to the simple model (Chapter 3), commutation overlap effect will impart more damping to the system, i.e., stability will be improved. However, strictly speaking, the damping effect of overlap should be confirmed through the use of a higher order model which can properly represents the system. The present DQ model does not lend it self to the inclusion of the commutation overlap effect. A new, higher order model that would adequately take this effect into account is therefore suggested as further work.

BIBLIOGRAPHY

[1] B. L. JONES and J. E. BROWN, "Electrical variable speed drives", an IEE Review, IEE Proc., Vol.131, Pt.A, No. 7, Sept. 1984.

[2] R. M. OLOFSSON, K. ABERG, P. WITSTROM, " A new slip recovery system", 4th Int. Conf. on power Electronics and Variable Speed Drives, IEE Conf. Publication, No 324, pp. 17-19, July 1990.

[3] S. R. DORADLA, S. CHAKRAVORTY and K. E. HOLE, "A new slip power recovery system with improved supply power factor", 11th Annual IEEE Power Electronics Specialists Conf. Records, pp 188-94, 1985.

[4] L. REFOUFI and B.A. T AL ZAHAWI, " Improved version of a slip energy recovery drive", International conference on EMDC, 1990, Hungary.

[5] L. REFOUFI, P. PILLAY and M.R HARRIS, "A Step-Down Chopper-Controlled Slip Energy Recovery Induction Motor Drive", IEEE Transactions On Energy Conversion, Vol. 8, p. 396-403, Sept. 1993.

[6] V.N.MITTLE, K.VENKATESAN, and S.C.GUPTA :" Stability analysis of a constant torque static slip power recovery drive", IEEE Trans. Industry Applications Vol. 16, pp. 119 - 126, Jan. /Feb. 1980.

[7] D. W. NOVOTNY and J. H. WOUTERSE, "Induction Machine Transfer Functions and Dynamic Response by Means of Complex Time Variables", IEEE Trans. on Power Apparatus and Systems, Vol. PAS-95, No 4, pp.1325-1335.

[8] S. STERN and D. W. NOVOTNY, "A simplified Approach to the Determination of Induction Machine Dynamic Response", IEEE Trans. on Power Apparatus and Systems, Vol. PAS-97, No. 4, pp. 1430-1439, 1978.

[9] A. R. MILES and D. W. NOVOTNY, " Transfer Functions of the Slip-Controlled Induction Machine", IEEE Trans. on Industry Applications, Vol. IA-15, No.1, pp.54-62, 1979.

[10] B. LEQUESNE and A. R. MILES, "Generalized Root-Loci Theory for the Static Scherbius Drive", IEEE Trans. on Power Apparatus and Systems, Vol. PAS-103, No.6, June 1984.

[11] P. VAS , J. E. BROWN and J. W. FINCH, " Stability Analysis of Induction Machines with Rotor Circuit Control", 22nd Universities Power Engineering Conference (UPEC), SUNDERLAND POLYTECHNIC, England, 14th-16th, April 1987.

[12] V. SUBRAMANYAM and K. SURENDRAN : "On the stability of a static slip energy recovery drive", IEE PROCEEDINGS, Vol.134, Pt.B, No. 6, November 1987.

[13] P. C. KRAUSE, O. WASYNCZUK, M. S. HILDERBRANDT, " Reference frame analysis of a slip energy recovery system", IEEE Trans. on energy conversion, Vol .3, No.2, pp. 404 - 408, June 1988.

[14] B. A. T. AL ZAHAWI, B. L. JONES and W. DRURY, " Effect of Rotor Rectifier on Motor Performance in Slip Energy Drives", Canadian Electrical Engineering Journal, Vol. 12, No 1, 1987.

[15] BOSE, " Power Electronics and AC variable Speed Drives ", (Book), Prentice Hall , 1986.

[16] A. LAVI and R. J. POLGE, " Induction Motor Speed Control With Static Inverter in the Rotor ", IEEE Transaction on power apparatus and systems, Vol. PAS-85, pp. 76-84, Jan. 1966.

[17] P. C. SEN and K. H. J. MA, " Rotor Control for Induction Motor Drive : TRC Strategy ", IEEE Transaction on Industry Applications, Vol. IA-11, pp. 43-49, Jan./Feb. 1975.

[18] P. N. MILJANIC, " The Through-Pass Inverter and Its Application to the Speed Control of Wound rotor Induction Machines.", IEEE Transactions on Power Apparatus and Systems, Vol. PAS-87, No. 1, pp. 234-239, 1968.

[19] T. KRISHNAN and B. RAMASWAMI, " Slip Ring Induction Motor Speed Control Using Thyristor Inverter", Automatica, Vol. 11, pp. 419-424, Pergamon Press, Printed in Great Britain, 1975.

[20] "Introduction to Electronic Control Engineering", F. FROHR and F. ORTTENBURGER, (Book), Siemens, Aktiengesellschaft, Heyden & Son Ltd, 1982 London.

[21] G.J. ROGERS, "Linearised Analysis of Induction -Motor Transients", Proc. IEE, Vol. 112, No. 10, October 1965.

[22] T.A. LIPO, and P.C. KRAUSE, "Stability Analysis of a Rectifier-Inverter Induction Motor Drive", IEEE Trans. on Power Apparatus and Systems, Vol. PAS-88, No. 1, January 1969.

[23] P. PILLAY and L. REFOUFI, "Calculation of Slip Energy Recovery Induction Motor Drive Behaviour Using the Equivalent circuit", IEEE Transactions On Industry Applications, Vol. 30, p. 154-163, Jan-Feb. 1994.

[24] V. N. MITTLE, K. VENKATESAN, and S. C. GUPTA, " Switching Transients in Static Slip Energy Recovery Drive. ", IEEE, Transactions on Power Apparatus and Systems, Vol. PAS-98, No. 4, pp. 1315-1320, July/Aug 1979.

APPENDIX A

DRIVES PARAMETERS

A.1 Small drive : 5 hp drive

The drive has the following parameters:
Slip ring induction motor: 5 hp, 3-phase, 400 V, 50 Hz having the following p.u parameters :
$H = 0.25$ s , $X_{ss} = 3$, $X_{rr}' = 3$.
$X_m = 2.9$, $R_s = 0.058$, $R_r' = 0.072$.
The base impedance is 42.9 Ω . The base torque is 9.89 N.m .
The filter parameters in p.u :
$X_d' = 1.00$, $R_d' = 0.02$.

A.2 Medium drive : 500 hp

Slip ring induction motor : 500 hp , 3-phase , 2300 V, 50 Hz having the following parameters:
$H = 0.25$s , $X_{ss} = 55.226\ \Omega$, $X_{rr}' = 55.226\ \Omega$.
$X_m = 54.02\ \Omega$, $R_s = 0.262\ \Omega$, $R_r' = 0.187\ \Omega$.
The base impedance is 14.18 Ω . The base torque is 1980 N.m .
The filter parameters in p.u:
$X_d' = 1.00$, $R_d' = 0.02$.

A.3 Large drive : 2250 hp

In order to investigate the stability behaviour of a very big drive , an other system has been studied. It has the following parameters :
Slip ring induction motor : 2250 hp , 3-phase , 2300 V , 50 Hz .
$H = 0.33$ s , $X_{ss} = 13.266\ \Omega$, $X_{rr}' = 13.266\ \Omega$.
$X_m = 13.4\ \Omega$, $R_s = 0.029\ \Omega$, $R_r' = 0.022\ \Omega$.
The base impedance is 3.15 Ω . The base torque is 8900 N.m .
The filter parameters in p.u:
$X_d' = 1$, $R_d' = 0.002$.

APPENDIX B

WRITTEN PAPERS :

1. " Steady State Analysis of the Static Kramer Drive", M. Kesraoui and L. Refoufi, submitted to COMAEI ' 96 Tlemcen, ALGERIA.

2. " On the Stability of the Static Kramer Drive", M. Kesraoui and L. Refoufi, accepted for publication in the Proceedings of :

   - IEEE-SMC , CESA' 96, IMACS Multiconference, Computational Engineering in Systems Applications, July 9-12, 1996, Lille, FRANCE.

   - MMAR ' 96, Third International Symposium on Methods and Models in Automation and Robotics, Sept. 10-13, 1996, Miedzyzdroje, POLAND.

APPENDIX C :

The drive DQ non linear equations are given by :

$$\begin{cases} \left(\frac{1}{w}\right)pI_{qs} = X_m V_{ms}\cos\alpha + \frac{ZV_{qs}}{K} - \frac{ZR_s}{K}I_{qs} - \frac{(ZX_{ss} - sX^2{}_m)}{K}I_{ds} + \frac{RX_m}{K}I'_{qr} \\ \left(\frac{1}{w}\right)pI_{ds} = sI_{qs} + s\frac{X'_{rr}}{X_m}I'_{qr} \\ \left(\frac{1}{w}\right)pI'_{qr} = -\frac{X_{ss}V_{ms}\cos\alpha}{K} - \frac{X_m}{K}V_{qs} + \frac{R_s X_m}{K}I_{qs} + \frac{X_m X_{ss}(1-s)}{K}I_{ds} - \frac{RX_{ss}}{K}I'_{qr} \\ \left(\frac{1}{w}\right)p\left(\frac{w_r}{w}\right) = -\frac{X_m}{2wH}I_{ds}I'_{qr} - \frac{T_L}{2wH} \end{cases} \quad (1)$$

By replacing in equation (1) , each variable f_i by : $f_i + \Delta f_i$ we obtain :

$$\begin{cases} \left(\frac{1}{w}\right)p(I_{qs0}+\Delta I_{qs}) = X_m V_{ms}\cos\alpha + \frac{Z(V_{qs0}+\Delta V_{qs})}{K} - \frac{ZR_s}{K}(I_{qs0}+\Delta I_{qs}) - \frac{(ZX_{ss} - (1-\left(\frac{w_{r0}}{w} + \Delta\left(\frac{w_{r0}}{w}\right)\right)X^2{}_m)}{K}(I_{ds0}+\Delta I_{ds}) \\ \qquad + \frac{RX_m}{K}(I'_{qr0}+\Delta I'_{qr}) \\ \left(\frac{1}{w}\right)p(I_{ds0}+\Delta I_{ds}) = (1-\left(\frac{w_{r0}}{w} + \Delta\left(\frac{w_{r0}}{w}\right)\right)(I_{qs0}+\Delta I_{qs}) + (1-\left(\frac{w_{r0}}{w} + \Delta\left(\frac{w_{r0}}{w}\right)\right)\frac{X'_{rr}}{X_m}(I'_{qr0}+\Delta I'_{qr}) \\ \left(\frac{1}{w}\right)p(I'_{qr0}+\Delta I'_{qr}) = -\frac{X_{ss}V_{ms}\cos\alpha}{K} - \frac{X_m}{K}(V_{qs0}+\Delta V_{qs}) + \frac{R_s X_m}{K}(I_{qs0}+\Delta I_{qs}) + \frac{X_m X_{ss}\left(\frac{w_{r0}}{w} + \Delta\left(\frac{w_{r0}}{w}\right)\right)}{K}(I_{ds0}+\Delta I_{ds}) \\ \qquad - \frac{RX_{ss}}{K}(I'_{qr0}+\Delta I'_{qr}) \\ \left(\frac{1}{w}\right)p\left(\frac{w_{r0}}{w} + \Delta\left(\frac{w_{r0}}{w}\right)\right) = -\frac{X_m}{2wH}(I_{ds0}+\Delta I_{ds})(I'_{qr0}+\Delta I'_{qr}) - \frac{T_L}{2wH} \end{cases}$$

According to the small signal perturbation method rule , the steady state values are eliminated and the product of higher order incremental terms are neglected (to obtain a first order equation) . We obtain the following equation :

$$\begin{cases}
\left(\frac{1}{w}\right)p(\Delta I_{qs}) = X_m V_{ms}\cos\alpha + \frac{Z(\Delta V_{qs})}{K} - \frac{ZR_s}{K}(\Delta I_{qs}) - \frac{(ZX_{ss}\Delta I_{ds} - (1-\frac{w_{r0}}{w})X^2{}_m\Delta I_{ds} - X^2{}_m I_{ds0}\Delta\left(\frac{w_{r0}}{w}\right))}{K} \\
\qquad + \frac{RX_m}{K}(\Delta\Gamma_{qr}) \\
\left(\frac{1}{w}\right)p(\Delta I_{ds}) = (1-\frac{w_{r0}}{w})\Delta I_{qs} - I_{qs0}\Delta\left(\frac{w_{r0}}{w}\right) + (1-\frac{w_{r0}}{w})\frac{X'_{rr}}{X_m}\Delta\Gamma_{qr} - \frac{X'_{rr}}{X_m}\Gamma_{qr0}\Delta\left(\frac{w_{r0}}{w}\right) \\
\left(\frac{1}{w}\right)p(\Delta\Gamma_{qr}) = -\frac{X_{ss}V_{ms}\cos\alpha}{K} - \frac{X_m}{K}(\Delta V_{qs}) + \frac{R_s X_m}{K}(\Delta I_{qs}) + \frac{X_m X_{ss}\frac{w_{r0}}{w}\Delta I_{ds} + X_m X_{ss} I_{ds0}\Delta\left(\frac{w_{r0}}{w}\right)}{K} \\
\qquad - \frac{RX_{ss}}{K}(\Delta\Gamma_{qr}) \\
\left(\frac{1}{w}\right)p\left(\Delta\left(\frac{w_{r0}}{w}\right)\right) = -\frac{X_m}{2wH}(I_{ds0}\Delta\Gamma_{qr} + \Gamma_{qr0}\Delta I_{ds}) - \frac{T_L}{2wH}
\end{cases}$$

Then the following linear state space matrix equation is obtained :

$$\dot{X} = AX + BU$$

Where the state vector is :

$$X = \begin{pmatrix} \Delta I_{qs} \\ \Delta I_{ds} \\ \Delta I_{qr} \\ \Delta\frac{\omega_r}{\omega} \end{pmatrix}$$

And U the input scalar.

The matrix A and vector B are given by :

$$A = \begin{bmatrix} A_{11} & A_{12} & A_{13} & A_{14} \\ A_{21} & 0 & A_{23} & A_{24} \\ A_{31} & A_{32} & A_{33} & A_{34} \\ 0 & A_{42} & A_{43} & 0 \end{bmatrix} \tag{4.3}$$

$$B = \begin{bmatrix} 0 \\ 0 \\ 0 \\ -\dfrac{T_l}{2\omega H} \end{bmatrix} \tag{4.4}$$

With:

$$A_{11} = \frac{Z(b_0 - R_s)}{K} \quad ; \quad A_{12} = \frac{a_0 Z - Z X_{ss} + S_0 X_m{}^2}{K} \quad ; \quad A_{13} = \frac{Z c_0 + X_m R}{K} \quad ;$$

$$A_{14} = \frac{Z d_0 - X_m{}^2 I_{ds0}}{K}$$

$$A_{21} = S_0 \quad ; \quad A_{23} = \frac{S_0 X'_{rr}}{X_m} \quad ; \quad A_{24} = -\frac{I_{qs0} X_m + X'_{rr} I_{qr0}}{X_m} \quad ;$$

$$A_{31} = \frac{(R_s - b_0) X_m}{K} \quad ; \quad A_{32} = \frac{X_m X_{ss}(1 - S_0) - a_0 X_m}{K} \quad ; \quad A_{33} = -\frac{R X_{ss} + c_0 X_m}{K}$$

$$A_{34} = \frac{I_{ds0} X_m X_{ss} - d_0 X_m}{K}$$

$$A_{42} = -\frac{X_m I_{qr0}}{2\omega H} \quad ; A_{43} = -\frac{X_m I_{ds0}}{2\omega H}$$

$$m_0 = \frac{V_{ds0}}{V_{qs0}} \quad ; a_0 = -m_0 a \quad ; \quad b_0 = m_0 b \quad ; \quad c_0 = m_0 c \quad ; \quad d_0 = m_0 d \quad ;$$

$$a = R_s \quad ; \quad b = X_{ss}(S_0 - 1) \quad ; \quad c = \frac{S_0 X'_{rr} X_{ss} - X_m{}^2}{X_m} \quad ; \quad d = -\frac{X_{ss}(X_m I_{qs0} + X'_{rr} I_{qr0})}{X_m} \quad ;$$

$$S_0 = 1 - \frac{\omega_{r0}}{\omega}$$

A N N E X

Liste et composition du Jury en vue de la soutenance de mémoire de Magister en Ingenierie des Systemes Electroniques par ***Mr KESRAOUI Mohamed.***

PREIDENT/ *Dr N. LOUAM,* Maitre de Conference, E.N.P

RAPPORTEUR/ *Dr L. REFOUFI,* Maitre de Conference, I.N.E.L.E.C

MEMBRES/ *Dr K. HARICHE,* PhD, Chargé de Recherche, I.N.E.L.E.C
Dr H. ZEROUR, PhD, Chargé de Cours, U.S.T.H.B